To the Graduate Council:

I am submitting herewith a thesis written by William C. Sutherland entitled "The Practical Operational-Amplifier Gyrator Circuit for Inductorless Filter Synthesis." I recommend that it be accepted in partial fulfillment of the requirements for the degree of Master of Science, with a major in Electrical Engineering.

J. M. Googe, Major Professor

We have read this thesis and recommend its acceptance:

J. W. Walker

A. Samuel Jordan

Accepted for the Council:

Hilton A. Smith
Vice Chancellor
Graduate Studies and Research

THE PRACTICAL OPERATIONAL-AMPLIFIER GYRATOR CIRCUIT FOR INDUCTORLESS FILTER SYNTHESIS

A Thesis

Presented for the

Master of Science

Degree

The University of Tennessee, Knoxville

William C. Sutherland

March 1976

170161

ACKNOWLEDGMENTS

First, I wish to thank Dr. J. M. Googe for his guidance and helpfulness in performing this study. Also, thanks are extended to Professors J. W. Waller and G. S. Jordan for serving on my committee.

NASA's Marshall Space Flight Center provided the financial assistance that made this graduate study possible, and this is greatly appreciated.

I wish to thank Mrs. Margie Hooie, Miss Carol Bagley, and Mrs. Doris Hipp for typing the rough draft. Thanks are also extended to W. J. Ziak and the Technical Publications Division of MSFC for their assistance in preparing this manuscript in the final form.

I want to praise and give thanks to God for His abundant goodness without which none of this would ever have become a reality.

Lastly, I wish to express thanks to my wife Jewell for her patience and encouragement.

ABSTRACT

This study involves a search of the literature for gyrator circuits utilizing operational amplifiers as the active device. A gyrator is a two-port nonreciprocal device with the property that the input impedance is proportional to the reciprocal of the load impedance. Following an experimental study, the gyrator circuit with optimum properties was selected for additional testing. A theoretical analysis was performed and compared to the experimental results for excellent agreement.

Chapter 1 is a brief introduction to the gyrator with a description of the mathematical properties.

In Chapter 2 the results of the literature search are reported. The original author' s work is summarized briefly, and the reported findings of other authors dealing with each original circuit are included.

Chapter 3 summarizes the experimental test results of the gyrator circuits given in Chapter 2. From this, the modified Antoniou gyrator was selected on the basis of stability, Q-factor, bandwidth, and the number of components required for a more thorough experimental and theoretical analysis.

Chapter 4 gives the experimental test results of the circuit chosen in Chapter 3. A theoretical analysis is then performed and compared to the experimental results with excellent agreement.

Chapter 5 is a brief summary of the findings and results of this study.

TABLE OF CONTENTS

CHAPTER		PAGE
1.	INTRODUCTION TO THE GYRATOR	1
	1.1 Purpose of Study	1
	1.2 Background	1
	1.3 Ideal Gyrator	3
	1.4 Nonideal Gyrator	5
	1.5 Q-Factor	8
	1.6 Summary	15
	1.7 Preview	15
2.	OPERATIONAL AMPLIFIER GYRATORS	17
	2.1 Introduction	17
	2.2 Huelsman-Morse Gyrator	17
	2.3 Brugler Gyrator	21
	2.4 Hawley Gyrator	23
	2.5 Prescott Gyrator	26
	2.6 Deboo Gyrator	28
	2.7 Riordan Gyrator	31
	2.8 Antoniou Gyrator	34
	2.9 Riordan Circuits Modified by Antoniou	42

CHAPTER PAGE

2.10 Other Circuits Modified by Antoniou 45

2.11 Summary of Findings 47

3. COMPARISON OF EXPERIMENTAL DATA OF VARIOUS GYRATORS 52

3.1 Introduction 52

3.2 The Test Circuit 53

3.3 Description of Components Used to Construct Each Test Gyrator 54

3.4 Test Equipment 54

3.5 Description of Tests Performed 56

3.6 Preliminary Results 57

3.7 Individual Gyrator Performance Results 59

3.8 Summary of Results 67

4. RESULTS OF EXPERIMENTAL TESTS ON THE MODIFIED ANTONIOU GYRATOR 69

4.1 Introduction 69

4.2 Tests Performed 71

4.3 Test Results 72

4.4 Calculated Gyrator Z_{in} 76

CHAPTER PAGE

4.5 Synthesis of Z_{in} 80

4.6 Effects of Operational Amplifier Parameter Variations 84

4.7 Gyrator Implementation in a Filter 86

4.8 Conclusions 93

5. SUMMARY 95

LIST OF REFERENCES 99

APPENDIXES 103

A. DERIVATION OF THE GYRATOR INPUT IMPEDANCE FOR FIGURE 4-9 104

B. IMPORTANT DESIGN EQUATIONS 108

VITA 111

LIST OF TABLES

TABLE		PAGE
2-1.	Comparison of Operational Amplifier Gyrators	48
3-1.	Number of Components in Each Gyrator Tested	60
3-2.	Results of Test Two	61
3-3.	Gyrator Stability Results	64
4-1.	Effect of Operational Amplifier Parameters on Components of Figure 4-8	85

LIST OF FIGURES

FIGURE		PAGE
1.1	Symbol for an ideal gyrator	3
1-2.	Symbol for an active gyrator	6
1-3.	Symbol for a reactive gyrator	7
1-4.	Symbol for a nonideal gyrator	7
1-5.	First realization	9
1-6.	Second realization	9
1-7.	Log Q, R_{eq}, and L_{eq} versus ω	14
2-1.	Voltage controlled current source	18
2-2.	Huelsman-Morse VCCS gyrator model	19
2-3.	Huelsman-Morse gyrator	20
2-4.	Negative impedance inverter	21
2-5.	Current negative impedance converter	21
2-6.	Negative resistance realization	22
2-7.	Brugler gyrator	22
2-8.	Noninverting VCCS with emitter follower	24
2-9.	Inverting VCCS with emitter follower	25
2-10.	Hawley gyrator	26
2-11.	RC T-network and its equivalent circuit	27

FIGURE PAGE

2-12. Simplified Prescott gyrator 27

2-13. Prescott gyrator 28

2-14. Deboo gyrator 29

2-15. Deboo gyrator with port one grounded 29

2-16. Deboo gyrator with port two grounded 30

2-17. Basic Riordan gyrator circuit 32

2-18. Riordan gyrator, type 1 32

2-19. Riordan gyrator, type 2 32

2-20. Antoniou gyrator, circuit 1 35

2-21. Antoniou gyrator, circuit 2 36

2-22. Antoniou gyrator, circuit 3 37

2-23. Antoniou gyrator, circuit 4 38

2-24. Nullor equivalent circuit of Figure 2-20 39

2-25. Nullor equivalent circuit of Figure 2-22 40

2-26. New gyrator circuit obtained from Figure 2-24 40

2-27. New gyrator circuit obtained from Figure 2-25 41

2-28. Nullor equivalent of Riordan gyrator 43

2-29. Modified Riordan gyrator, type 1 43

2-30. Modified Riordan gyrator, type 2 44

FIGURE PAGE

2-31. Modified Brugler gyrator 46

2-32. Modified Deboo gyrator 47

3-1. Test circuit 53

3-2. Test setup 55

3-3. General equivalent circuit 65

3-4. Frequency response of Figure 2-27 to Test One 65

3-5. General equivalent circuit for Figures 2-29 and 2-30 66

3-6. Frequency response of Figure 2-29 to Test One 67

4-1. Modified Antoniou gyrator test circuit 70

4-2. Curves of Q versus frequency for R = 10 kΩ 73

4-3. Curves of Q versus frequency for R = 31.6 kΩ 74

4-4. Curves of Q versus frequency for R = 100 kΩ 75

4-5. Curves of Q versus frequency for R = 3.16 kΩ 76

4-6. Ideal inductor obtained when A approaches infinity 78

4-7. Network realized from Equation (4-3) 79

4-8. Network synthesized from Equation (4-8) 81

4-9. Gyrator circuit of Figure 4-1 showing R_i 83

4-10. Test filter network 86

4-11. Equivalent circuit of Figure 4-10 87

FIGURE PAGE

4-12. Frequency response of filter network 87

4-13. Expanded scale of Figure 4-12 bandpass 88

4-14. Calculated frequency response of transfer function 89

4-15. Expanded scale of calculated bandpass of Figure 4-14 89

4-16. Theoretical filter 91

4-17. Response of theoretical LC filter 91

4-18. Expanded scale of bandpass of the theoretical filter 92

5-1. One method of realizing a floating inductor 97

A-1. Gyrator circuit of Figure 4-9 with nodes numbered 104

B-1. Equivalent circuit model of a gyrator useful up to the self-resonant frequency 108

B-2. Antoniou gyrator circuit 110

CHAPTER 1

INTRODUCTION TO THE GYRATOR

1.1 Purpose of Study

The purpose of this study was to examine the characteristics of practical operational amplifier gyrators when used to simulate an inductor for use in filter synthesis. Of the 18 gyrators tested, one gyrator realization was selected on the basis of stability, Q-factor, and bandwidth to have the most promise for simulating an inductor.

A synthetic inductor to be used in filter networks must possess several important properties, which are as follows: (1) an inductance independent of frequency, (2) stability, (3) a high Q-factor, (4) wide bandwidth, and (5) an easily determined value of inductance. This study develops the mathematical model of a gyrator and compares the theoretical results from this model to experimental test results. A number of Q-factor versus frequency curves obtained from experimental test results are included also.

1.2 Background

Since B. D. H. Tellengen [1] introduced the gyrator as a new element in 1948, numerous papers have been written concerning the design and implementation of gyrators as network elements. A gyrator is one class of impedance inverter [2], the basic property of which is to invert the impedance at

port two into its reciprocal at port one. Thus, if a load impedance $Z_L = 1/sC$ is placed across port two, the input impedance $Z_{in} = sr^2C$ is obtained at port one, where r is the gyrator constant. The gyrator has been realized using vacuum tubes, transistors, operational amplifiers, and integrated circuits as the active element.

At first, the interest in gyrators was purely academic, a novelty to be investigated in the laboratory. Then, with the advent of microminiaturization, a new interest was created in the gyrator as a means of producing miniature inductors. However, it was only after the introduction of the integrated circuit operational amplifier that most of the practical work on gyrators was performed. High open loop gain, low dc drift, high input impedance, low output impedance, good bandwidth, small size, economical price, and availability were all factors contributing to the popularity of the integrated circuit operational amplifier for use in a large variety of circuits.

The gyrator was introduced as the fifth basic passive network element, the four other basic elements being the resistor, capacitor, inductor, and the ideal transformer. The gyrator is unique as a basic element in that it is the only one that violates the reciprocity relation.

In this chapter some of the properties of gyrators are discussed. The properties of an ideal gyrator are covered, and some of the ways that a nonideal gyrator and its properties differ from the ideal are developed. The Q-factor is defined and discussed in terms of the nonideal gyrator parameters.

1.3 Ideal Gyrator

The ideal gyrator [3] is defined by the two-port, open-circuit impedance parameters

$$z_{11} = z_{22} = 0$$

$$z_{12} = -r$$

$$z_{21} = r \quad , \tag{1-1}$$

where r is a positive real number known as the gyration resistance. This can also be written in matrix form as

$$[Z] = \begin{bmatrix} 0 & -r \\ r & 0 \end{bmatrix} \quad . \tag{1-2}$$

The symbol for an ideal gyrator is shown in Figure 1-1. The gyrator is a non-reciprocal two-port since $z_{12} \neq z_{21}$. Inspection of the previous matrix reveals another important feature of the ideal gyrator, i.e., zero input and output impedances.

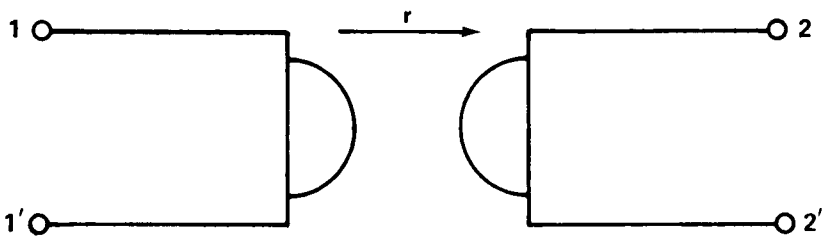


Figure 1-1. Symbol for an ideal gyrator.

The short circuit admittance matrix may be easily derived from Equation (1-2) and is given by

$$\begin{bmatrix} I_1 \\ I_2 \end{bmatrix} = \begin{bmatrix} 0 & g \\ -g & 0 \end{bmatrix} \begin{bmatrix} V_1 \\ V_2 \end{bmatrix} \quad , \tag{1-3}$$

where again the main diagonal terms are zero and the off-diagonal terms are known as gyration conductances. The admittance [4] matrix can be expressed as the sum of two Y-matrices as shown in Equation (1-4).

$$\begin{bmatrix} 0 & g \\ -g & 0 \end{bmatrix} = \begin{bmatrix} 0 & g \\ 0 & 0 \end{bmatrix} + \begin{bmatrix} 0 & 0 \\ -g & 0 \end{bmatrix} \quad . \tag{1-4}$$

This shows one method of realizing a gyrator by realizing each matrix separately and then connecting them in parallel. Observe that the two new matrices represent voltage controlled current sources, one with positive gain and the other with negative gain. If these two voltage controlled current sources are connected back-to-back in parallel, a gyrator will be realized.

Now, consider the case of an ideal gyrator with a capacitor as the load at port two. The expression for the input impedance of a loaded two-port network is given by

$$Z_{in} = z_{11} - \frac{z_{12}z_{21}}{z_{22} + Z_L} \quad . \tag{1-5}$$

By substituting the parameters of Equation (1-2) into Equation (1-5) and letting the load impedance $Z_L = 1/sC$, the result obtained is

$$Z_{in} = sr^2C \quad . \tag{1-6}$$

This result shows that the input impedance of an ideal gyrator loaded with a capacitor is an ideal inductance of r^2C henries. Therefore, a capacitor loaded gyrator could be used to replace a heavy and bulky inductor in a filter circuit. Also, since a capacitor usually has less loss than an inductor, the simulated inductor may have a higher Q than the actual inductor. The single most important application of gyrators is in their applications for RC network synthesis.

1.4 Nonideal Gyrator

Several circuits are available for the practical realization of a gyrator; however, a practical gyrator will not generally satisfy Equation (1-2), because of its nonzero input and output immittance. The properties of a practical gyrator will be discussed in the following paragraphs.

The first case of a nonideal [3] gyrator to be considered is a two-port network described by Equation (1-7),

$$\begin{aligned} z_{11} &= z_{22} = 0 \\ z_{12} &= -r_1 \\ z_{21} &= r_2 \quad . \end{aligned} \tag{1-7}$$

This network is known as an active gyrator and is represented by the symbol shown in Figure 1-2. It has ideal input and output characteristics, but has a different transfer parameter in each direction.

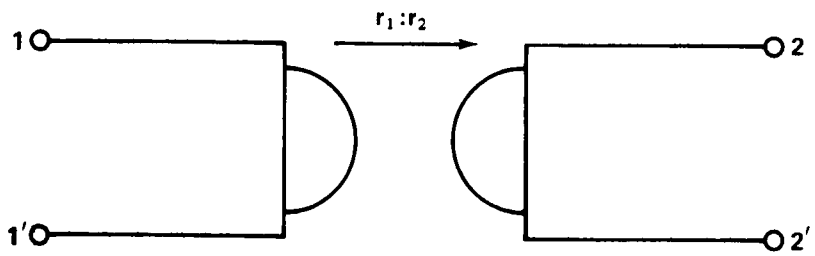


Figure 1-2. Symbol for an active gyrator.

A second type of nonideal gyrator behavior is obtained when the transfer parameters become frequency dependent. This type of gyrator is called a reactive gyrator and is defined by

$$V_1 = -\alpha(s) I_2$$

$$V_2 = \alpha(s) I_1 \quad , \tag{1-8}$$

where $\alpha(s)$ is a complex gyrator impedance. The symbol for a reactive gyrator is shown in Figure 1-3. Notice that where the ideal gyrator transfer parameters are independent of frequency, those of the reactive gyrator are not and therefore it is a potentially unstable device.

The more general and practical type of nonideal gyrator may depart from the ideal in many ways. It is described by

$$z_{11} \neq 0$$

$$z_{22} \neq 0$$

$$z_{12} \neq -z_{21} \quad . \tag{1-9}$$

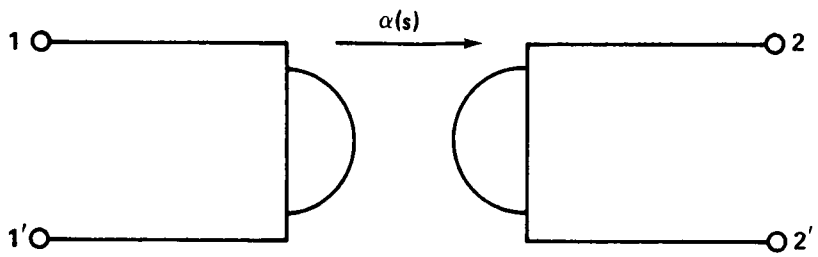


Figure 1-3. Symbol for a reactive gyrator.

The terms z_{11} and z_{22} usually have some small finite value and may be considered as parasitic impedances. The nonideal gyrator may be represented by the symbol shown in Figure 1-4. Some gyrator realizations compensate for the nonzero main diagonal terms by using negative resistances.

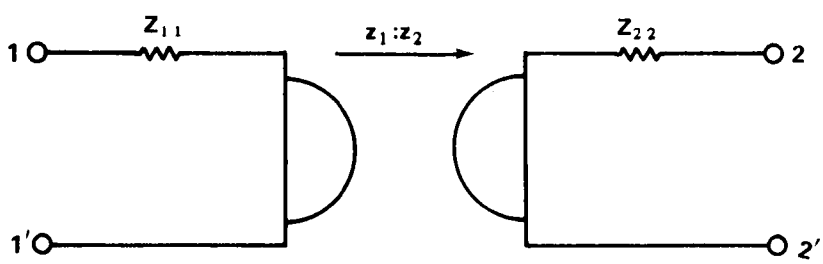


Figure 1-4. Symbol for a nonideal gyrator.

1.5 Q-Factor

With the increasing application of gyrator circuits to replace inductors in filter networks, it is useful to define the Q of the gyrator for comparison with the Q of a real inductor. A practical gyrator may be represented by the resistance matrix of Equation (1-10).

$$\begin{bmatrix} V_1 \\ V_2 \end{bmatrix} = \begin{bmatrix} R_1 & -R_2 \\ R_3 & R_4 \end{bmatrix} \begin{bmatrix} I_1 \\ I_2 \end{bmatrix} \quad . \tag{1-10}$$

Substituting the quantities of Equation (1-10) into Equation (1-5) and again letting the load $Z_L = 1/sC$, the input impedance is obtained as

$$Z_{in} = R_1 + \frac{R_2 R_3}{\left(R_4 + \frac{1}{sC}\right)} \quad . \tag{1-11}$$

This expression can be simplified and rewritten as

$$Z_{in} = \frac{[sC(R_1R_4 + R_2R_3) + R_1]}{(sR_4C + 1)} \quad . \tag{1-12}$$

To realize Equation (1-12) as a passive network, the techniques of modern network synthesis [5] may be applied to obtain either of the circuits shown in Figures 1-5 or 1-6. The values of the components are given by Equations (1-13) and (1-14), respectively, for Figures 1-5 and 1-6.

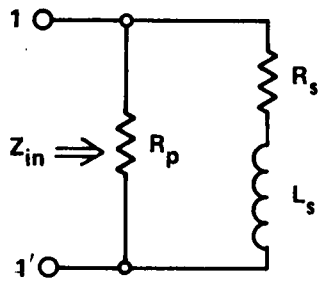


Figure 1-5. First realization.

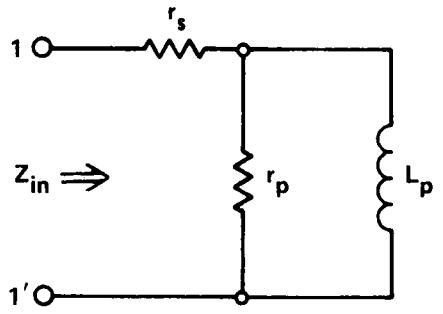


Figure 1-6. Second realization.

$$R_p = R_1 + \frac{R_2R_3}{R_4}$$

$$R_s = \frac{R_1(R_1R_4 + R_2R_3)}{R_2R_3}$$

$$L_s = \frac{C(R_1R_4 + R_2R_3)^2}{R_2R_3} \quad . \tag{1-13}$$

$$r_s = R_1$$

$$r_p = \frac{R_2R_3}{R_4}$$

$$L_p = R_2R_3C \quad . \tag{1-14}$$

Substituting $s = j\omega$ into Equation (1-12) and defining Q [6] as

$$Q = \frac{\mathrm{Im}[Z(j\omega)]}{\mathrm{Re}[Z(j\omega)]} \tag{1-15}$$

gives a value for Q of

$$Q = \frac{\omega R_2R_3C}{R_1 + \omega^2R_4C^2(R_1R_4 + R_2R_3)} \quad . \tag{1-16}$$

To find the frequency where Q is maximum, take the derivative $dQ/d\omega$ and set this quantity equal to zero to define the resonant frequency ω_0,

$$\omega_0 = \sqrt{\frac{R_1}{R_4C^2(R_1R_4 + R_2R_3)}} \quad . \tag{1-17}$$

Substituting this value of ω_0 given by Equation (1-17) into Equation (1-16) gives the value of Q_{max} as

$$Q_{max} = \frac{R_2R_3}{2\sqrt{R_1R_4(R_1R_4 + R_2R_3)}} \quad . \tag{1-18}$$

Define X as

$$X = \frac{R_2R_3}{R_1R_4} \tag{1-19}$$

and substitute this into Equations (1-16), (1-17), and (1-18) to obtain Equations (1-20), (1-21), and (1-22), respectively.

$$Q = \frac{\omega CR_4X}{1 + \omega^2R_4^2C^2(1 + X)} \quad . \tag{1-20}$$

$$\omega_0 = \frac{1}{R_4C\sqrt{1 + X}} \quad . \tag{1-21}$$

$$Q_{max} = \frac{X}{2\sqrt{1 + X}} \quad . \tag{1-22}$$

Generally $X >> 1$; therefore, Equation (1-21) becomes

$$\omega_0 = \frac{1}{R_4 C \sqrt{X}} \quad , \tag{1-23}$$

and Equation (1-22) becomes

$$Q_{max} = \frac{\sqrt{X}}{2} \quad . \tag{1-24}$$

The sensitivity [7] of Q relative to X is defined by the relation

$$S_X^Q = \left(\frac{dQ}{dX}\right)\left(\frac{X}{Q}\right) \quad . \tag{1-25}$$

Applying this equation to Equation (1-20) gives the sensitivity of Q to X as shown in Equation (1-26) where $F = \omega C R_4$.

$$S_X^Q = \frac{1}{1 + F^2 X} \quad . \tag{1-26}$$

From Equation (1-23), $F = 1/\sqrt{X}$ at resonance. Making this substitution into Equation (1-26) gives the important result that the sensitivity at resonance is equal to 1/2. This shows that at resonance, a fractional change in Q is linearly dependent upon a fractional change in X and is independent of frequency and capacitance. This is an important requirement of an inductor if it is to be used in a filter.

The preceding equations were all developed in terms of the general two-port parameters given by Equation (1-10) for the nonideal gyrator. They will now be rewritten in terms of the components shown in Figure 1-6 and defined by Equation (1-14). Making these substitutions, Equation (1-12) for the input impedance then becomes

$$Z_{in} = \frac{sL_p(r_p + r_s) + r_p r_s}{sL_p + r_p} \quad . \tag{1-27}$$

Equation (1-16) for Q then becomes

$$Q = \frac{\omega L_p r_p^2}{r_p^2 r_s + \omega^2 L_p^2 (r_p + r_s)} \quad . \tag{1-28}$$

If the assumption that $r_p >> r_s$ is made, and this ordinarily will be true, Equations (1-27) and (1-28) can be rewritten as follows:

$$Z_{in} = \frac{sL_p r_p + r_p r_s}{sL_p + r_p} \tag{1-29}$$

$$Q = \frac{\omega L_p r_p}{r_p r_s + \omega^2 L_p^2} \quad . \tag{1-30}$$

Likewise, ω_0 in Equation (1-17) may be written as

$$\omega_0 = \frac{\sqrt{r_p r_s}}{L_p} \quad . \tag{1-31}$$

The expression for X in Equation (1-18) then becomes

$$X = \frac{r_p}{r_s} \quad , \tag{1-32}$$

and Q_{max} in Equation (1-19) becomes

$$Q_{max} = \frac{1}{2}\sqrt{\frac{r_p}{r_s}} \quad . \tag{1-33}$$

The input impedance given by Equation (1-27) may be written as a function of frequency by making the substitution $s = j\omega$ and then clearing the denominator of irrational terms to obtain

$$Z_{in}(\omega) = R_{eq}(\omega) + j\omega L_{eq}(\omega) \quad . \tag{1-34}$$

Figure 1-7 is a plot of the Q-factor, equivalent inductance, and equivalent resistance derived from Equation (1-27). Figure 1-7 shows that Q peaks at a $Q_{max} = \frac{1}{2}\sqrt{r_p / r_s}$ at a frequency $\omega_0 = \sqrt{r_p r_s}/L_p$. The Q-curve has a slope of 20 dB per decade. The $R_{eq}(\omega)$ curve has two break frequencies, one at ω_0 and the other at ω_n given approximately by

$$\omega_n = \frac{r_p}{r_s} \quad . \tag{1-35}$$

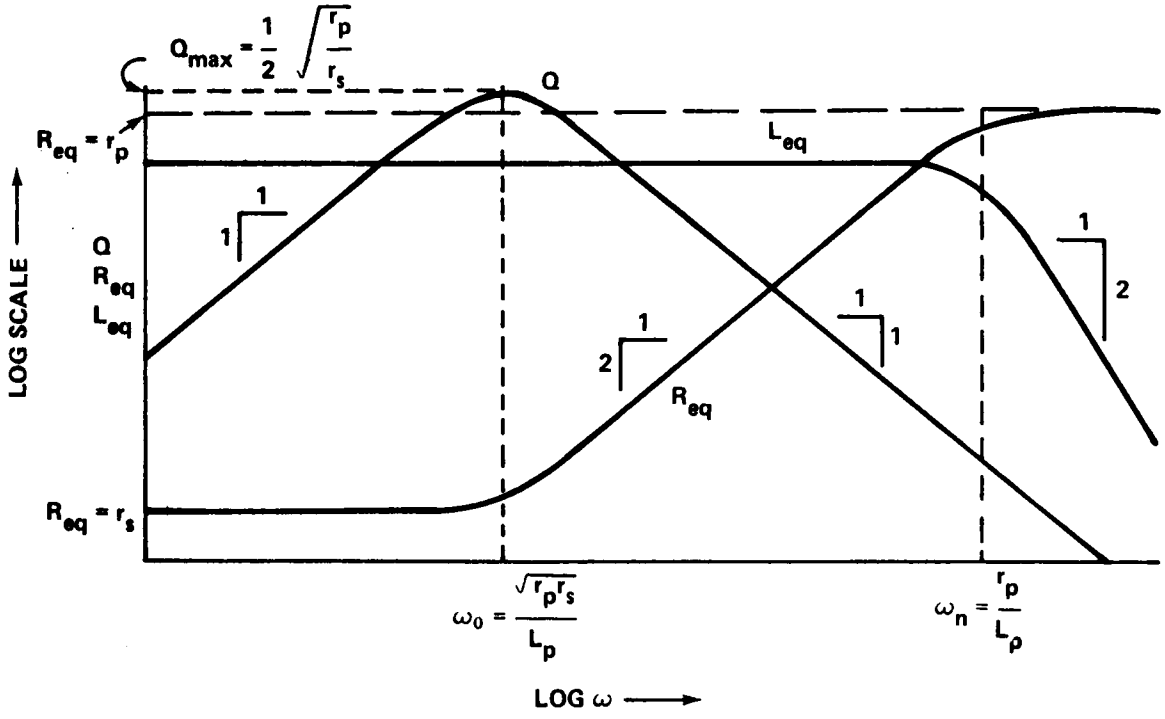


Figure 1-7. Log Q, R_{eq}, and L_{eq} versus ω.

At frequencies less than 0.3 ω_0, $R_{eq}(\omega)$ is approximately equal to r_s and at frequencies greater than $3\omega_n$, $R_{eq}(\omega)$ is very nearly equal to r_p. At frequencies between ω_0 and ω_n, the $R_{eq}(\omega)$ curve has a slope of 40 dB per decade. The $L_{eq}(\omega)$ curve is flat out to the break frequency ω_n, where it starts decreasing at the rate of 40 dB per decade. It can be shown that ω_n is related to ω_0 by the relation

$$\omega_n = 2\, Q_{max}\omega_0 \quad , \tag{1-36}$$

which also shows that the equivalent inductance is constant and independent of frequency out to frequencies much above the frequency of Q_{max}.

1.6 Summary

A brief background and an introduction to the fundamental properties of the gyrator were given in this chapter. The properties of both the ideal and nonideal gyrators were discussed. The equations for the Q-factor and the input impedance of a practical nonideal gyrator were developed. An equivalent network was synthesized using the methods described by Van Valkenburg. Then the equations for Z_{in}, Q, Q_{max}, and ω_0 were written in terms of the components in the equivalent network. The variation of the Q-factor, and the equivalent resistance and inductance were shown and discussed also.

1.7 Preview

For Chapter 2, a search of the technical literature was performed to obtain all the information possible on gyrator circuits using operational amplifiers. A brief summary of all the work found on each circuit is given along with a schematic of each.

Chapter 3 describes and summarizes the results of the preliminary experimental tests performed on the practical operational amplifier circuits given in Chapter 2. From these results, one circuit is selected for further testing in Chapter 4.

In Chapter 4, more experimental tests are performed on the gyrator circuit selected in Chapter 3. The results of these tests are used to draw the Q versus ω curves of the gyrator for different combinations of resistors and

capacitors. Also the equation for the input impedance is developed, and an equivalent network is synthesized from this.

Chapter 5 summarizes the findings of this study.

CHAPTER 2

OPERATIONAL AMPLIFIER GYRATORS

2.1 Introduction

The results of a search of the literature are reported in this chapter. The literature included various IEEE Transactions and other electronic publications, technical reports, and textbooks. The material found included not only those circuits utilizing operational amplifiers, but also those incorporating vacuum tubes, transistors, and integrated circuits. This material was then screened to select only the gyrator circuits that used operational amplifiers as the active element. This material was then further sorted according to the originator of each circuit.

This chapter is a summary of the published operational amplifier realizations found during the literature search. It is divided according to the originator of each circuit and contains a circuit schematic, the two-port parameters when available, and other theoretical and experimental information as available.

2.2 Huelsman-Morse Gyrator

Huelsman and Morse [8,9] developed a gyrator by using operational amplifiers in 1964. They used the voltage controlled current source (VCCS) method for their synthesis. Their VCCS's were constructed by using operational amplifiers as shown in Figure 2-1. The admittance matrix for

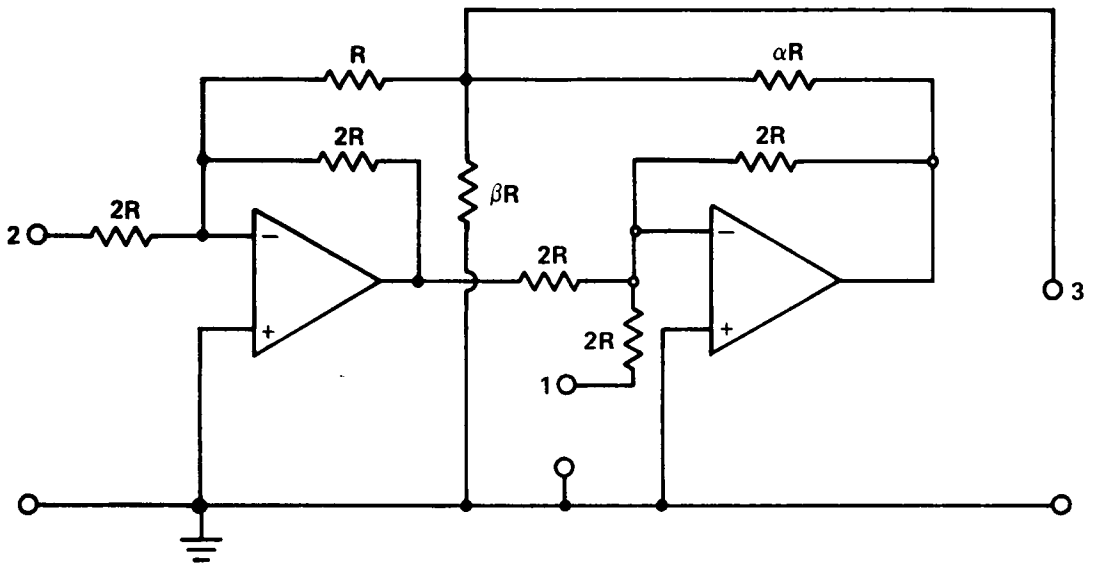


Figure 2-1. Voltage controlled current source.

Figure 2-1 is given by Equation (2-1) as

$$\begin{bmatrix} I_1 \\ I_2 \\ I_3 \end{bmatrix} = \begin{bmatrix} \frac{1}{2R} & 0 & 0 \\ 0 & \frac{1}{2R} & 0 \\ \frac{1}{\alpha R} & \frac{-1}{\alpha R} & \frac{1}{R_s} \end{bmatrix} \begin{bmatrix} V_1 \\ V_2 \\ V_3 \end{bmatrix} , \qquad (2\text{-}1)$$

where $R_s = \alpha\beta R/(\alpha\beta + \alpha - \beta)$. Shorting port two results in the following two-port admittance matrix:

$$\begin{bmatrix} I_1 \\ I_3 \end{bmatrix} = \begin{bmatrix} \frac{1}{2R} & 0 \\ \frac{1}{\alpha R} & \frac{1}{R_s} \end{bmatrix} \begin{bmatrix} V_1 \\ V_3 \end{bmatrix} . \qquad (2\text{-}2)$$

Similarly, shorting port one results in the admittance matrix

$$\begin{bmatrix} I_3 \\ I_2 \end{bmatrix} = \begin{bmatrix} \frac{1}{R_s} & \frac{-1}{\alpha R} \\ 0 & \frac{1}{2R} \end{bmatrix} \begin{bmatrix} V_3 \\ V_2 \end{bmatrix} . \qquad (2\text{-}3)$$

By connecting the two networks in parallel, the circuit shown in Figure 2-2 is obtained and the admittance matrix for this circuit is given by

$$\begin{bmatrix} I_1 \\ I_2 \end{bmatrix} = \begin{bmatrix} \frac{1}{R_s} + \frac{1}{2R} & \frac{-1}{\alpha R} \\ \frac{1}{\alpha R} & \frac{1}{R_s} + \frac{1}{2R} \end{bmatrix} \begin{bmatrix} V_1 \\ V_2 \end{bmatrix} . \qquad (2\text{-}4)$$

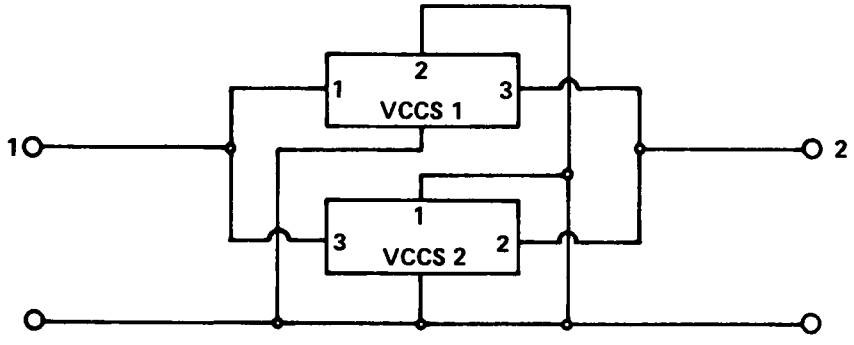


Figure 2-2. Huelsman-Morse VCCS gyrator model.

By defining the gyrator admittance as

$$G = \frac{1}{\alpha R} \qquad (2\text{-}5)$$

and equating the main diagonal terms of Equation (2-4) to zero, an ideal gyrator will be realized. Performing this operation results in

$$\frac{1}{R_s} + \frac{1}{2R} = \frac{\frac{3}{2}\alpha\beta + \alpha - \beta}{\alpha\beta R} = 0 \quad . \tag{2-6}$$

This condition is satisfied if

$$\alpha = \frac{\beta}{\frac{3}{2}\beta + 1} \quad . \tag{2-7}$$

The Huelsman-Morse gyrator is shown in Figure 2-3 with $\alpha = 0.1$ and $\beta = 0.11765$. No experimental results were published with this circuit. Since perfectly matched resistors are required to satisfy Equation (2-6), this circuit will have a low Q-factor because of the critical matching required to reduce the main diagonal terms to zero.

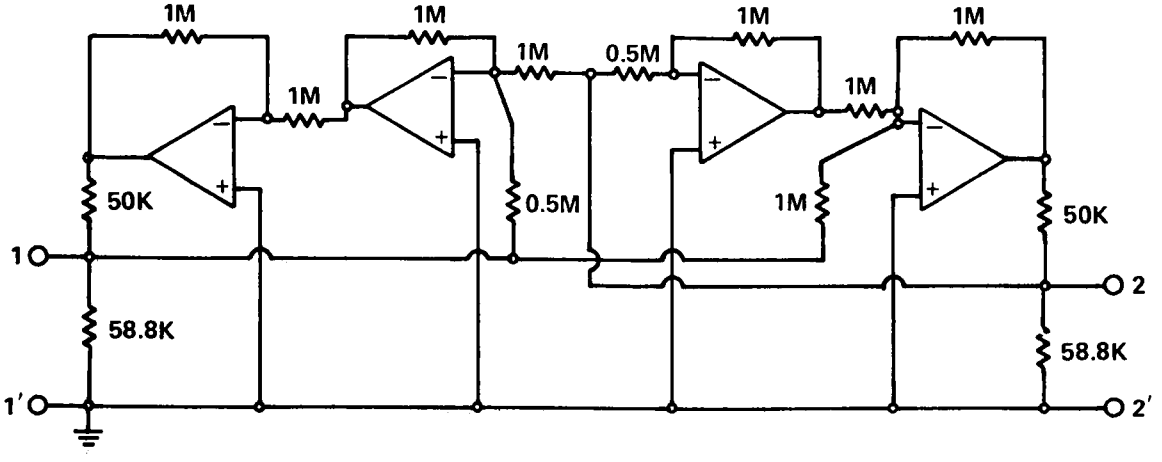


Figure 2-3. Huelsman-Morse gyrator.

2.3 Brugler Gyrator

Brugler [10] made a gyrator by using a negative impedance inverter (NIV) in series with a current negative impedance converter (INIC). The circuits for the NIV and INIC are shown in Figures 2-4 and 2-5, respectively.

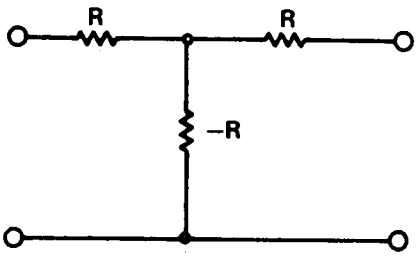


Figure 2-4. Negative impedance inverter.

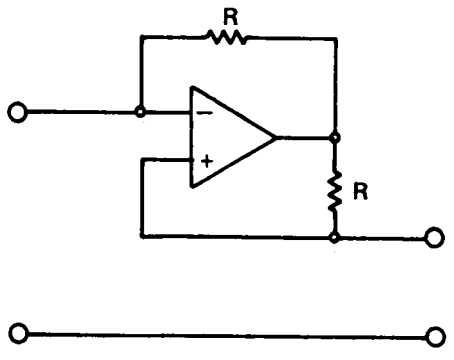


Figure 2-5. Current negative impedance converter.

The matrix for each figure is as follows. For the NIV,

$$[Z] = \begin{bmatrix} 0 & -R \\ -R & 0 \end{bmatrix} \tag{2-8}$$

and for the INIC,

$$[H] = \begin{bmatrix} 0 & 1 \\ 1 & 0 \end{bmatrix} . \tag{2-9}$$

In order to realize the negative resistance of the NIV, another NIC circuit must be used. This is shown in Figure 2-6. When Figure 2-6 is loaded with

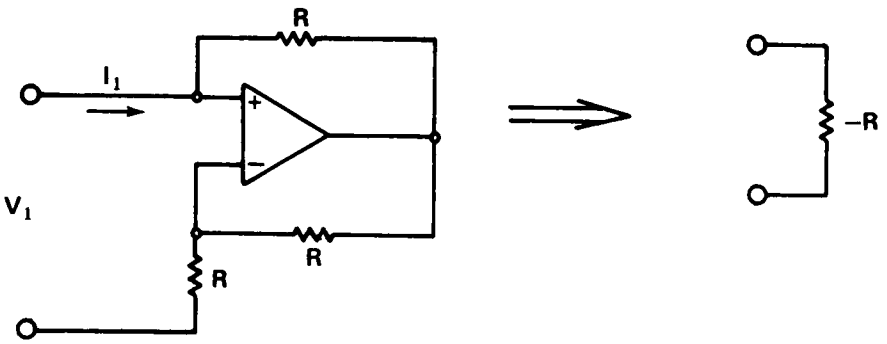


Figure 2-6. Negative resistance realization.

R resistance, the input is -R as shown by

$$\frac{V_1}{I_1} = -R \quad . \tag{2-10}$$

Brugler' s gyrator is obtained when the above circuits are all combined as shown in Figure 2-7, and the impedance [11] matrix parameters can be derived to obtain Equation (2-11).

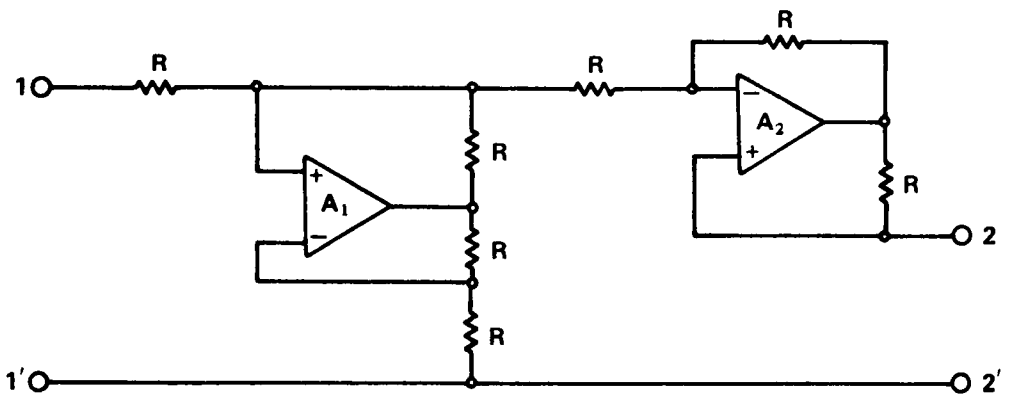


Figure 2-7. Brugler gyrator.

$$z_{11} = \frac{R(A_1 - 4A_2 + 10)}{D}$$

$$z_{12} = \frac{RA_2(A_1 + 2)}{D}$$

$$z_{21} = \frac{-RA_2(A_1 + 2)}{D}$$

$$z_{22} = \frac{R(4A_2 - A_1 + 6)}{D} \quad , \tag{2-11}$$

where $D = A_1A_2 - A_1 - 2A_2 + 6$. If it is assumed that the gains of the operational amplifiers approach infinity, Equation (2-11) reduces to give the ideal gyrator impedance parameters,

$$[Z] = \begin{bmatrix} 0 & +R \\ -R & 0 \end{bmatrix} \quad . \tag{2-12}$$

Antoniou [11] found that this circuit could attain low frequency unstable modes of operation. Also, since this circuit requires resistance cancellation, low Q-factors can be expected. No experimental data was published.

2.4 Hawley Gyrator

Hawley [12] also used the VCCS method to synthesize a gyrator. A Sheingold [13] type VCCS, as suggested by Morse and Huelsman [8], was used here in the inverting and noninverting configuration.

A noninverting VCCS realized with an operational amplifier and with a simple transistor emitter follower input is shown in Figure 2-8. The admittance matrix is given as

$$\begin{bmatrix} I_1 \\ I_2 \end{bmatrix} = \begin{bmatrix} \frac{1}{\beta R} & -\frac{1}{\beta R} \\ -\frac{1}{R} & 0 \end{bmatrix} \begin{bmatrix} V_1 \\ V_2 \end{bmatrix} , \qquad (2\text{-}13)$$

where β is the current gain of the transistor.

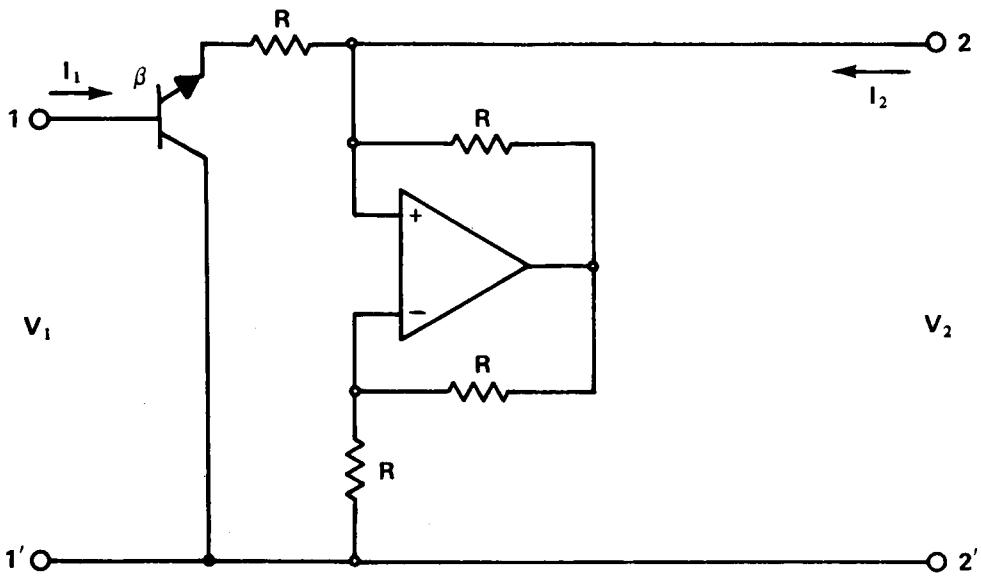


Figure 2-8. Noninverting VCCS with emitter follower.

The inverting VCCS is shown in Figure 2-9 and its admittance matrix is given as

$$\begin{bmatrix} I_1 \\ I_2 \end{bmatrix} = \begin{bmatrix} 0 & \frac{1}{R} \\ -\frac{1}{\beta R} & \frac{1}{\beta R} \end{bmatrix} \begin{bmatrix} V_1 \\ V_2 \end{bmatrix} . \qquad (2\text{-}14)$$

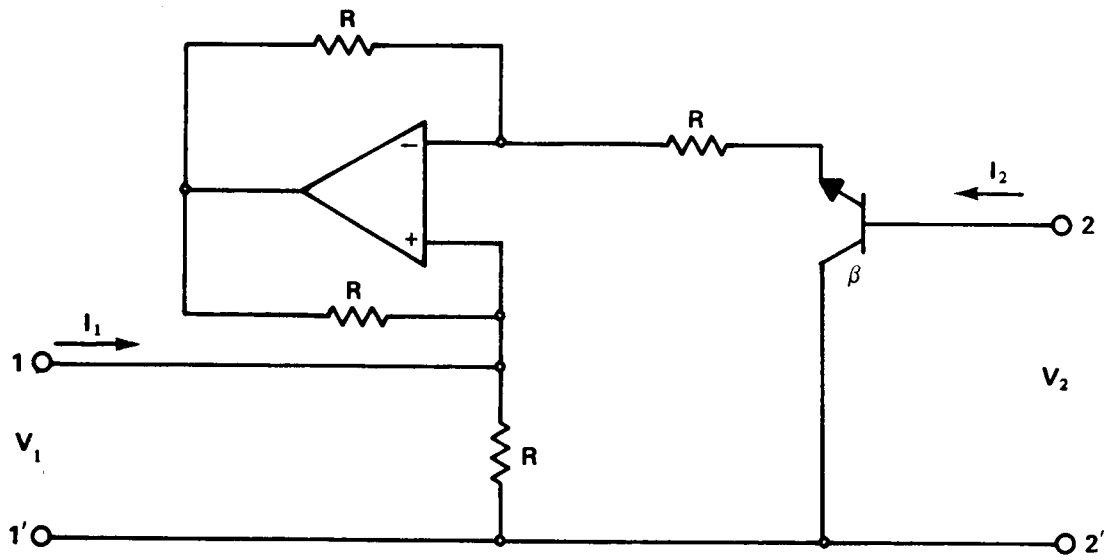


Figure 2-9. Inverting VCCS with emitter follower.

The gyrator shown in Figure 2-10 is realized when the VCCS' s are connected in parallel giving the admittance matrix of Equation (2-15). This matrix is obtained by adding the matrices of Equations (2-13) and (2-14).

$$\begin{bmatrix} I_1 \\ I_2 \end{bmatrix} = \begin{bmatrix} \frac{1}{\beta R} & \frac{1}{R} - \frac{1}{\beta R} \\ -\frac{1}{R} - \frac{1}{\beta R} & \frac{1}{\beta R} \end{bmatrix} \begin{bmatrix} V_1 \\ V_2 \end{bmatrix} . \qquad (2\text{-}15)$$

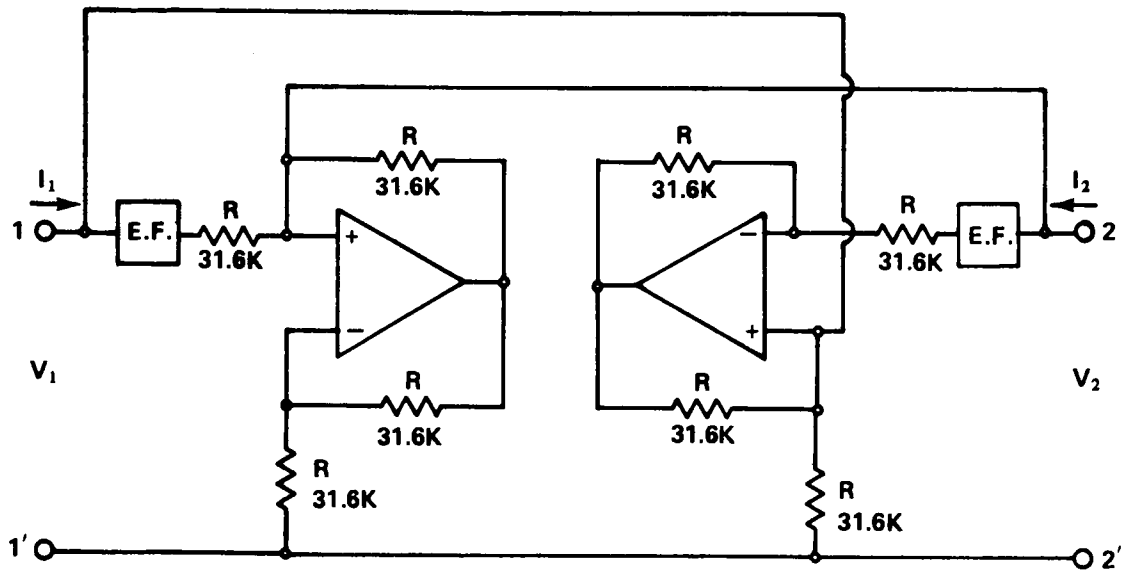


Figure 2-10. Hawley gyrator.

As the β of the transistor increases, the parameters in Equation (2-15) approach those of an ideal gyrator. Hawley used a gyration resistance of 31.6 kΩ for the experimental circuit and a 1000 pF capacitor loaded the gyrator. The operational amplifiers used here were discrete components, rather than integrated circuits. A peak resonant frequency of 21 kHz was obtained with an approximate Q-factor of 38. One serious disadvantage is that all terms in Equation (2-15) are dependent on the β of the emitter follower transistor, which means that the Q-factor will be temperature sensitive.

2.5 Prescott Gyrator

Prescott [14] developed a gyrator circuit by using an RC T-network with feedback from a unity gain operational amplifier. This circuit is shown in Figure 2-11 along with its equivalent circuit. This circuit requires a

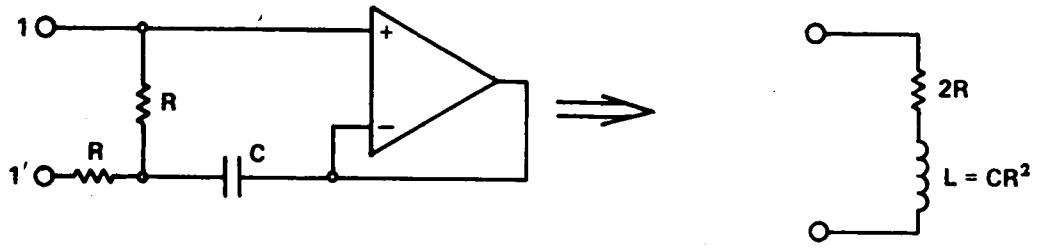


Figure 2-11. RC T-network and its equivalent circuit.

negative resistance in parallel with C to cancel the effective series resistance. The circuit for Prescott' s gyrator is shown in Figure 2-12. From this figure it can be seen that if $2R = R^2/R_1$ or $R_1 = R/2$, the resistors cancel exactly leaving an ideal inductor. The complete Prescott gyrator is shown in Figure 2-13 with the voltage negative impedance converter (VNIC) shown in dashed lines. Since this gyrator uses negative resistance for cancellation, a low Q-factor can be expected.

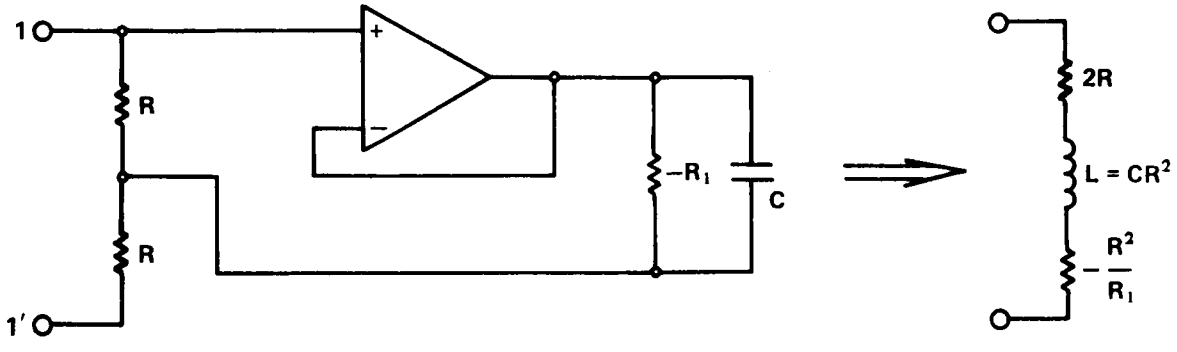


Figure 2-12. Simplified Prescott gyrator.

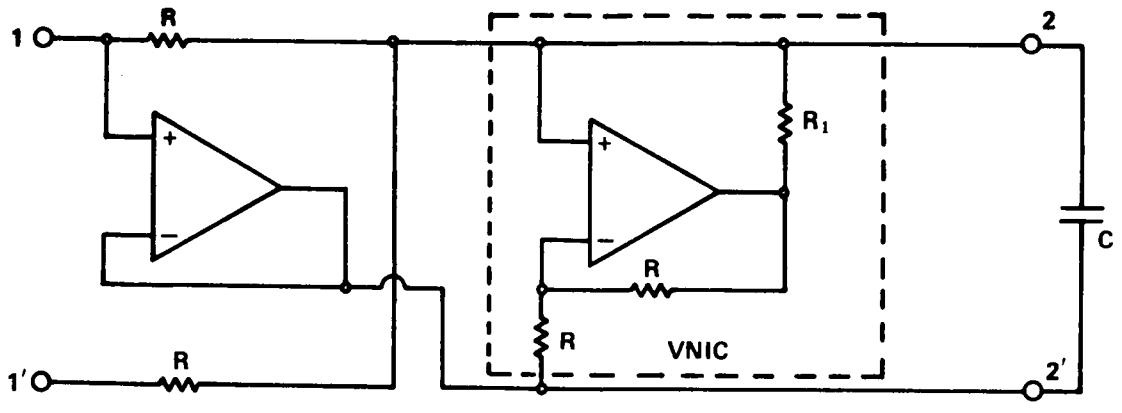


Figure 2-13. Prescott gyrator.

2.6 Deboo Gyrator

Deboo [15] constructed a three-terminal gyrator using operational amplifiers as shown in Figure 2-14 to realize ungrounded inductors. Assuming ideal amplifiers are used in this circuit, the parameters are defined by

$$\begin{bmatrix} I_1 \\ I_2 \\ I_3 \end{bmatrix} = \begin{bmatrix} 0 & 0 & -G \\ 0 & 0 & G \\ G & -G & 0 \end{bmatrix} \begin{bmatrix} V_1 \\ V_2 \\ V_3 \end{bmatrix} . \qquad (2\text{-}16)$$

If the terminals of port one are short-circuited to ground, the circuit reduces to the two-port circuit shown in Figure 2-15 and described by Equation (2-17) if ideal amplifiers are used.

$$\begin{bmatrix} I_2 \\ I_3 \end{bmatrix} = \begin{bmatrix} 0 & G \\ -G & 0 \end{bmatrix} \begin{bmatrix} V_2 \\ V_3 \end{bmatrix} . \qquad (2\text{-}17)$$

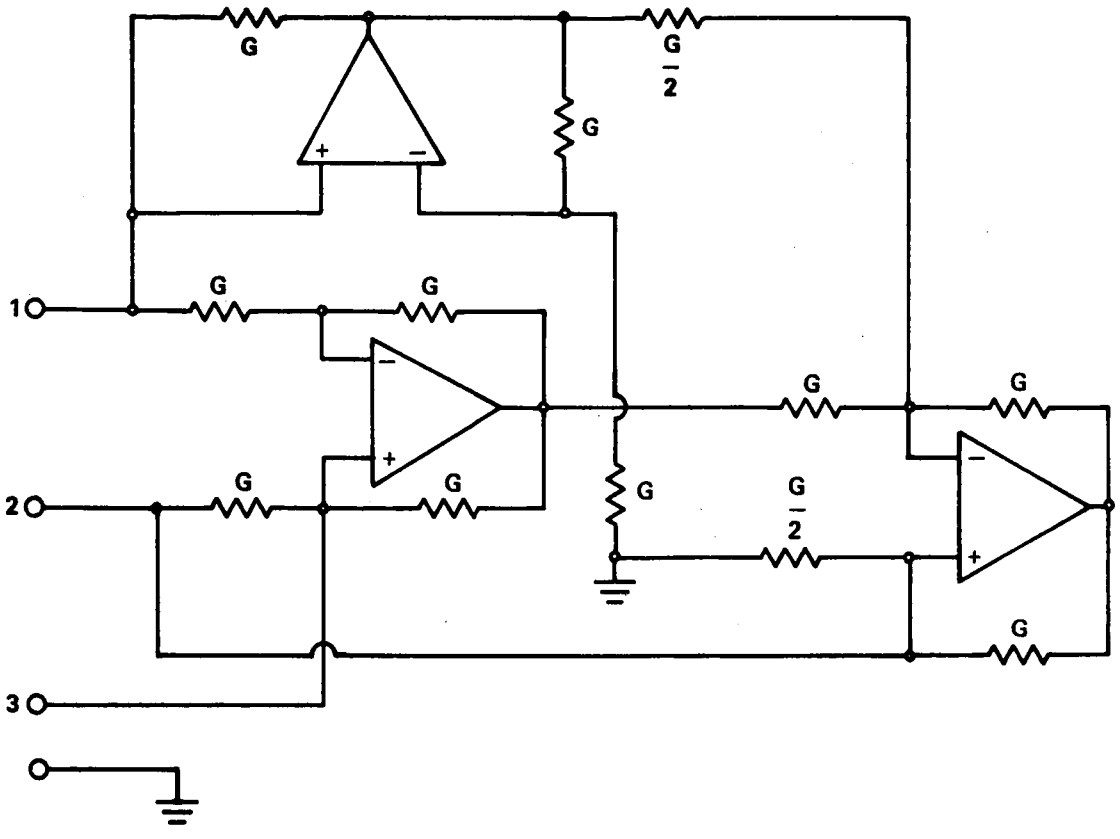


Figure 2-14. Deboo gyrator.

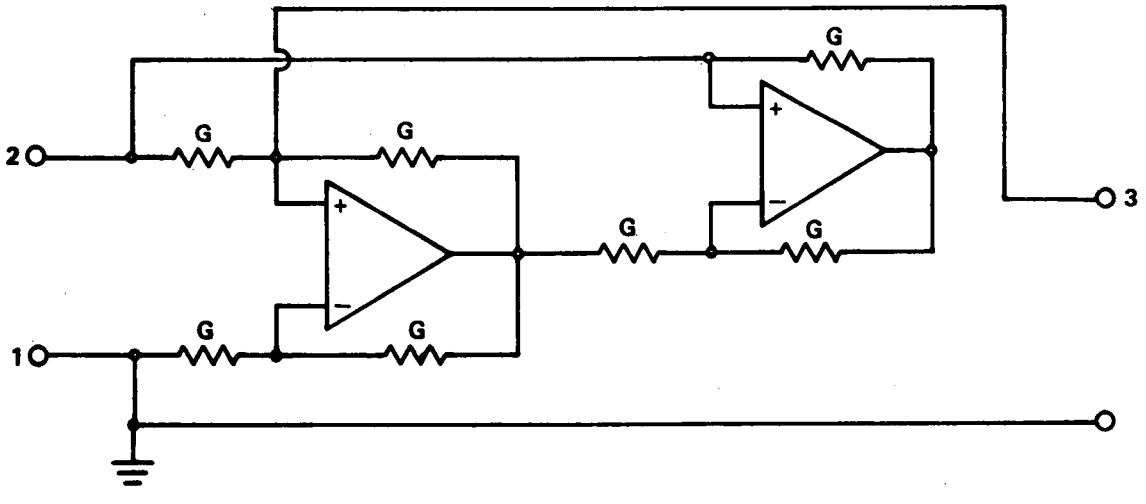


Figure 2-15. Deboo gyrator with port one grounded.

Alternately, if the terminal of port two is short-circuited to ground, then Figure 2-14 reduces to Figure 2-16 and is described by the equation

$$\begin{bmatrix} I_1 \\ I_3 \end{bmatrix} = \begin{bmatrix} 0 & -G \\ G & 0 \end{bmatrix} \begin{bmatrix} V_1 \\ V_3 \end{bmatrix} \quad . \tag{2-18}$$

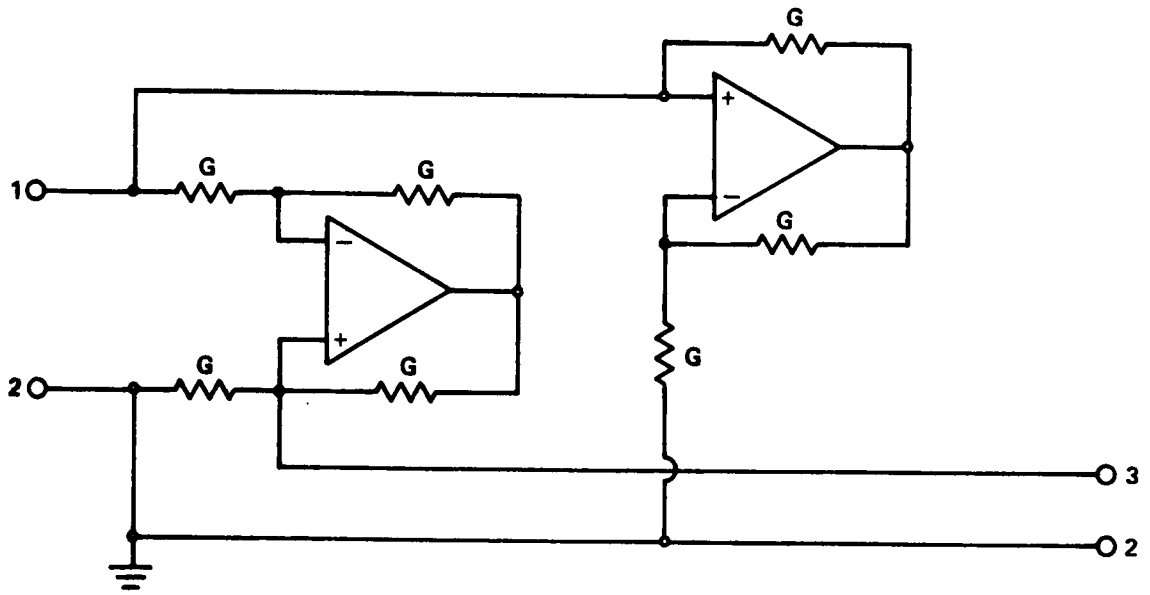


Figure 2-16. Deboo gyrator with port two grounded.

Figures 2-15 and 2-16 are realized with a Sheingold [13] VCCS with a shunt negative conductance to reduce the input conductance.

The circuit shown in Figure 2-16 has the impedance parameters [11] given by Equation (2-19).

$$z_{11} = \frac{4R(A_1 + 2)}{D}$$

$$z_{12} = \frac{A_2R(A_1 + 2)}{D}$$

$$z_{21} = \frac{-A_2R(A_1 + 2)}{D}$$

$$z_{22} = \frac{R(4A_2 - A_1 + 6)}{D} \quad , \qquad (2\text{-}19)$$

where $D = A_1A_2 - 2A_1 + 2A_2 + 12$ and $R = 1/G$. No experimental test data is given for these circuits; however, Antoniou has shown that Figure 2-16 can attain low frequency unstable modes. Also, since a negative resistance is required, the circuits will be low Q and very sensitive to resistance variations.

2.7 Riordan Gyrator

Riordan [16] developed a gyrator that does not require the cancellation of resistances and with a Q-factor apparently limited only by the losses in the capacitors used. This circuit used feedback between two operational amplifiers as shown in Figure 2-17.

Now, assuming that A_1 and A_2 both approach infinity, then

$$Z_{in} = \frac{E_1}{i_1} = \frac{Z_1Z_3Z_5}{Z_2Z_4} \quad . \qquad (2\text{-}20)$$

If either Z_2 or Z_4 is a capacitor C and all the other Z's are resistors R, then $Z_{in} = j\omega CR^2$. The circuit then will look as shown in Figure 2-18 or 2-19 according to the location of the capacitor.

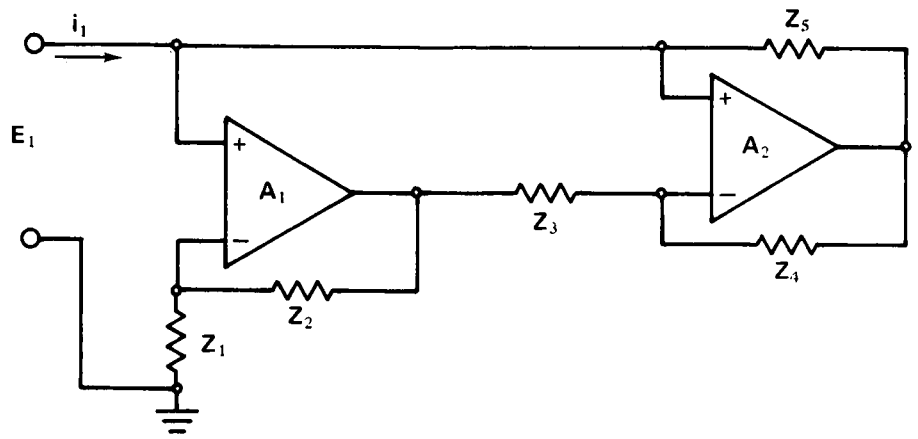


Figure 2-17. Basic Riordan gyrator circuit.

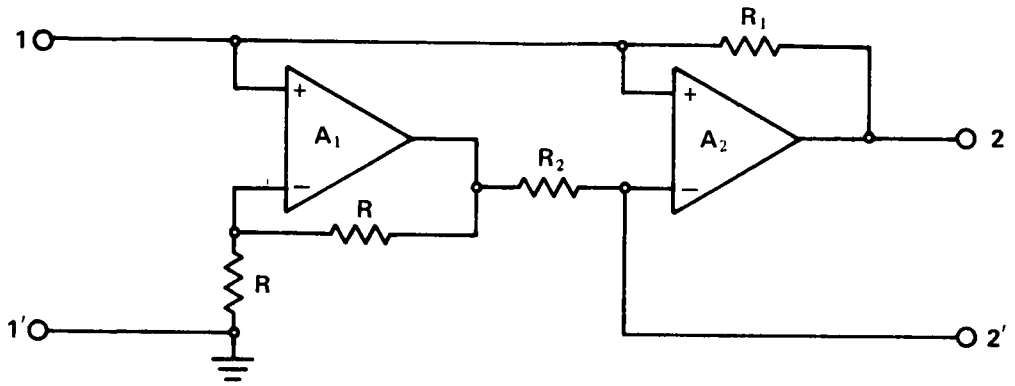


Figure 2-18. Riordan gyrator, type 1.

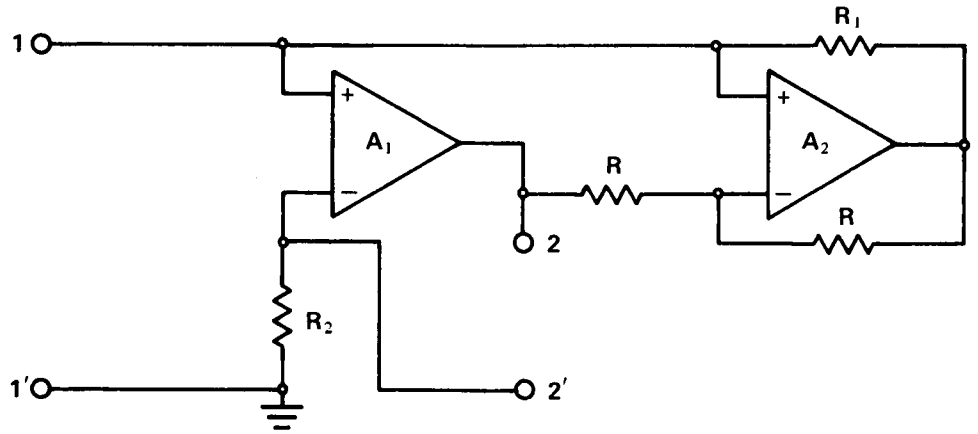


Figure 2-19. Riordan gyrator, type 2.

The Z-parameters [17] for each type of Riordan's circuits are given by the following equations. For the circuit in Figure 2-18,

$$z_{11} = \frac{R_1(A_1 + 2)}{D_1}$$

$$z_{12} = \frac{-R_2A_2(A_1 + 2)}{D_1}$$

$$z_{21} = \frac{R_1[A_1A_2 + 2(A_1 - A_2)]}{D_1}$$

$$z_{22} = \frac{R_2(A_1 + 2)}{D_1} \quad , \tag{2-21}$$

where $D_1 = A_1A_2 + A_1 - 2A_2 + 2$. For the circuit in Figure 2-19,

$$z_{11} = \frac{R_1(A_2 + 2)}{D_2}$$

$$z_{12} = \frac{-R_2A_1A_2}{D_2}$$

$$z_{21} = \frac{R_1A_1(A_2 + 2)}{D_2}$$

$$z_{22} = \frac{R_2(2A_1 - A_2 + 2)}{D_2} \quad , \tag{2-22}$$

where $D_2 = A_1A_2 - A_2 + 2$.

An inspection of these two equations shows that both equations reduce to those of an ideal gyrator if the amplifier gains are assumed to be infinite. However, Antoniou [17] has shown from the Llewellyn [18] stability equations that both circuits are subject to low frequency unstable modes of operation.

Riordan tested both circuits using both discrete components and Fairchild μA709C operational amplifiers and found the performance to be similar. Some experimental results were given for various load capacitors and gyration resistances. The results obtained ranged from a peak Q of 250 at 55 kHz to a peak Q of 2000 at 8 Hz. However, these circuits had a strong tendency to lock up in an abnormal mode of operation. Antoniou [17] found that the lockup mode of operation could be prevented by connecting two parallel diodes back-to-back across each port; however, the diodes severely reduce the voltage handling capacity of the circuits.

2.8 Antoniou Gyrator

Antoniou [19] synthesized four gyrators using negative impedance inverters (NIV) and negative impedance converters (NIC). The NIV's and NIC's in turn were realized by using operational amplifiers.

Antoniou's first circuit is shown in Figure 2-20. The NIC's and NIV's are shown by dotted lines. Letting A_1 and A_2 be the gains of the two operational amplifiers, this circuit can best be described by its Y-matrix as follows:

$$[Y] = \begin{bmatrix} \dfrac{1}{R_1(A_1+1)} & \dfrac{-A_1}{R_1(A_1+1)} \\ \dfrac{k_2 A_1}{R_2(A_1+1)} & -\dfrac{k_2}{R_2(A_1+1)} \end{bmatrix} , \qquad (2\text{-}23)$$

where $k_2 = \dfrac{A_2 - \dfrac{R_2+R}{R}}{A_2 + \dfrac{R_2+R}{R_2}}$.

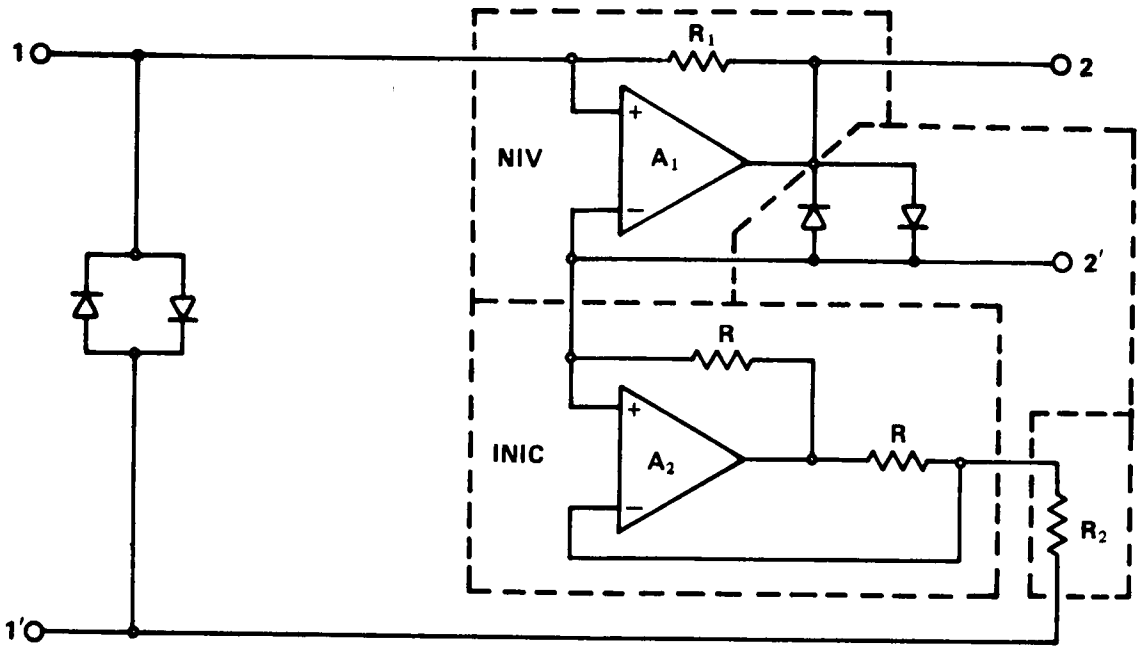


Figure 2-20. Antoniou gyrator, circuit 1.

To obtain the second circuit, the positive and negative inputs to each operational amplifier have to be interchanged. This circuit is shown in Figure 2-21 and can best be described by its Z-matrix which is

$$[Z] = \begin{bmatrix} \frac{R_1}{A_1 + 1} & \frac{k_1 A_1 R_2}{A_1 + 1} \\ -\frac{A_1 R_1}{A_1 + 1} & -\frac{k_1 R_2}{A_1 + 1} \end{bmatrix} , \qquad (2\text{-}24)$$

where $k_1 = \dfrac{A_2 - \dfrac{R_2 + R}{R_2}}{A_2 + \dfrac{R_2 + R}{R}}$.

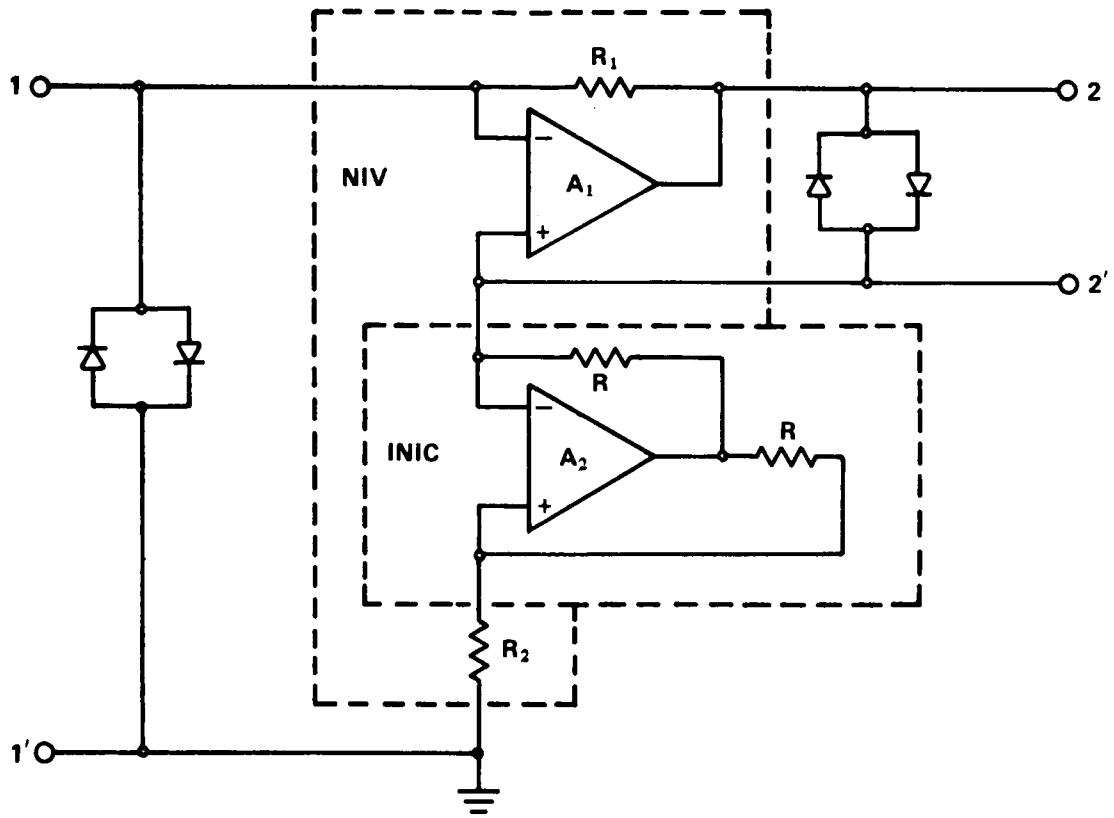


Figure 2-21. Antoniou gyrator, circuit 2.

Two other circuits can be obtained by interchanging the differential input connections of A_1 first in circuit 1 and then in circuit 2; however, analysis [19] has shown that these two are always unstable and so will not be considered.

The third circuit can be obtained by taking circuit 1 and switching the relative locations of the NIV and INIC as shown in Figure 2-22. This circuit also will be described by its Y-matrix parameters,

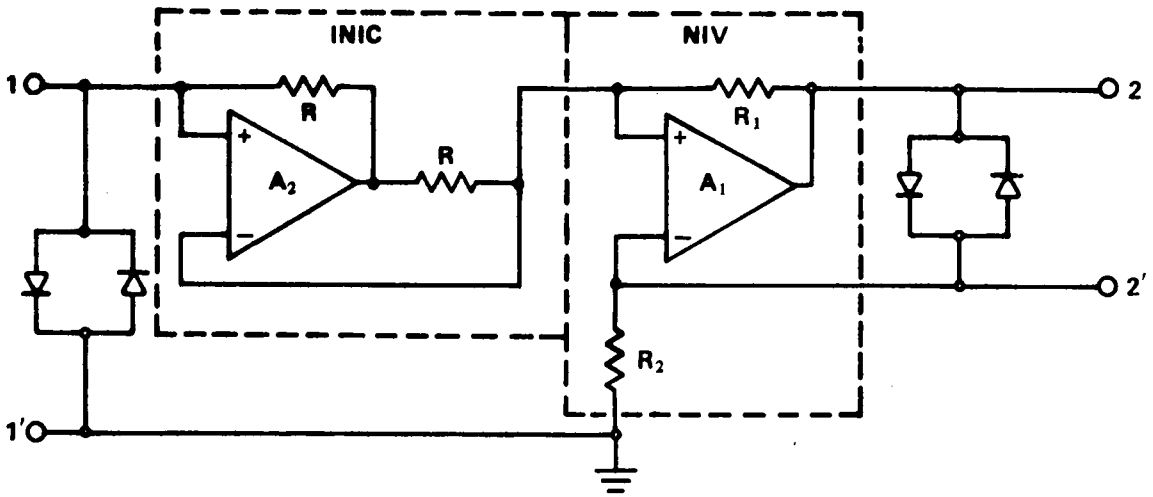


Figure 2-22. Antoniou gyrator, circuit 3.

$$y_{11} = \frac{R_1(A_1 + 1) - R(A_2 - 1)}{D_2 R}$$

$$y_{12} = \frac{A_1 A_2}{D_2}$$

$$y_{21} = \frac{-R_1 A_1 A_2}{D_2 R_2}$$

$$y_{22} = \frac{R_1(A_2 + 1) - R(A_1 - 1)}{D_2 R_2} \quad , \qquad (2\text{-}25)$$

where $D_2 = R_1(A_2 + 1)(A_1 + 1) + R$.

Circuit 4 can be obtained from circuit 3 by interchanging the positive and negative inputs to both operational amplifiers as shown in Figure 2-23. This circuit can best be described by its Z-matrix as given by Equation (2-26).

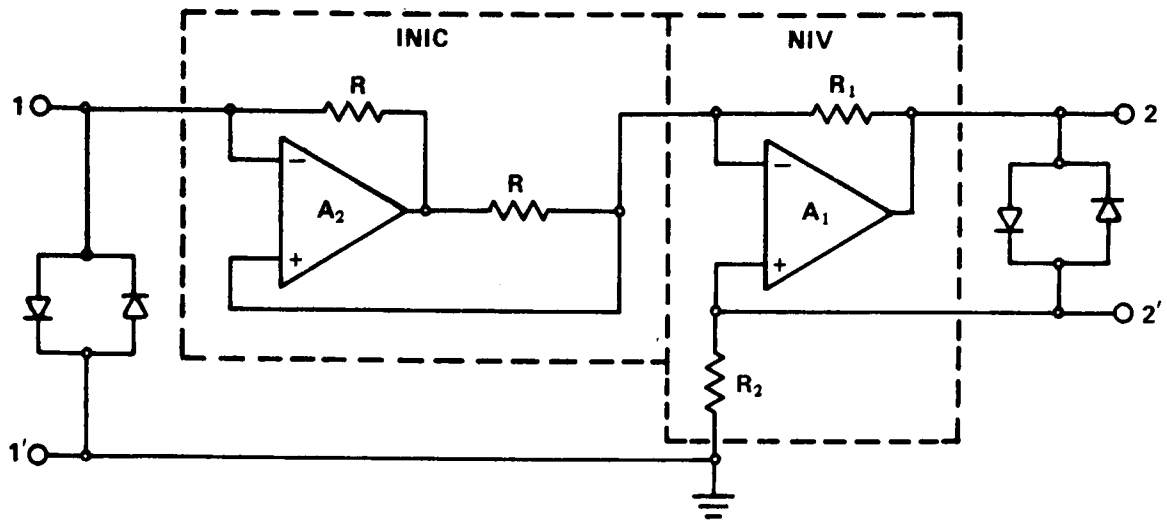


Figure 2-23. Antoniou gyrator, circuit 4.

$$z_{11} = \frac{RR_1(1 - A_2) + R^2(A_1 + 1)}{D_1}$$

$$z_{12} = \frac{-RR_2A_1A_2}{D_1}$$

$$z_{21} = \frac{RR_1A_1A_2}{D_1}$$

$$z_{22} = \frac{R_1R_2(1 - A_1) + RR_2(A_2 + 1)}{D_1} \quad , \qquad (2\text{-}26)$$

where $D_1 = R(A_1 + 1)(A_2 + 1) + R_1$.

Two other circuits can be obtained from circuits 3 and 4 just as they could from circuits 1 and 2, and they are always unstable also.

Antoniou constructed these circuits using Fairchild integrated operational amplifiers, type μA709C, and with $R_1 = R_2 = R = 1$ kΩ. He found that circuits 1 and 3 became unstable for large Z_{L2} (Z_{L2} is the load impedance on port 22') and circuits 2 and 4 became unstable for small Z_{L2}.

The only test data given was for circuit 3 and consisted of the input impedance measured at frequencies of 300 Hz, 1 kHz, 3 kHz, and 10 kHz and with C' s of 0.01 μF, 0.1 μF and 1.0 μF. The measured input impedance in each case is very close to the expected theoretical value.

Antoniou [20] later used the nullor concept to synthesize two additional gyrators using operational amplifiers. By replacing the operational amplifiers with nullors in his earlier gyrators [19], the nullor equivalent circuits were obtained as shown in Figures 2-24 and 2-25.

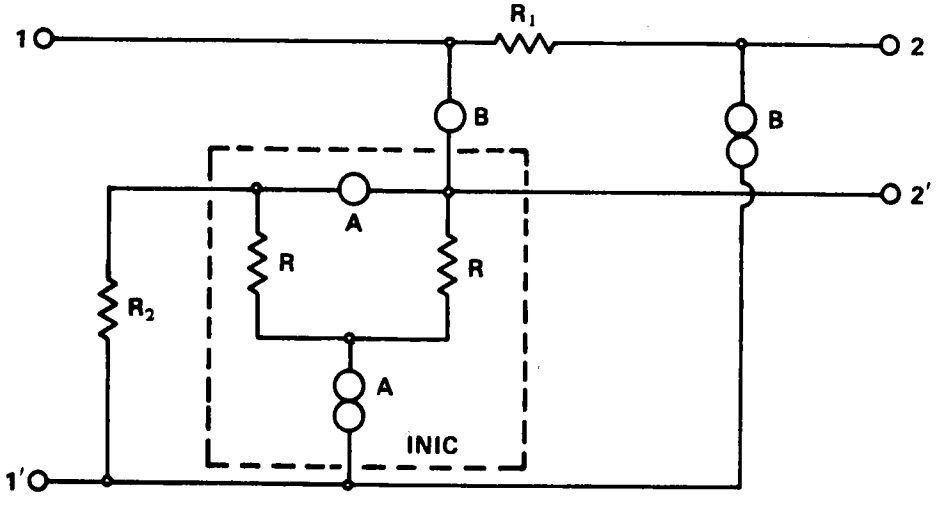


Figure 2-24. Nullor equivalent circuit of Figure 2-20 (page 35).

If nullators A and B are paired with norators B and A instead of A to A and B to B, the two new circuits are obtained. Four different circuits can be obtained for each nullor circuit because of various ways of interconnecting the terminals of each device; however, since negative feedback is required around

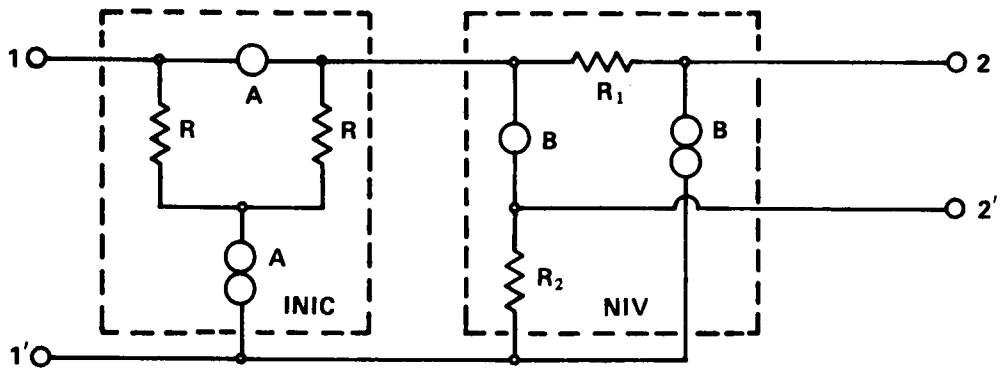


Figure 2-25. Nullor equivalent circuit of Figure 2-22 (page 37).

each operational amplifier for stability, only one new circuit is obtained for each of Figures 2-24 and 2-25. The two new circuits are shown in Figures 2-26 and 2-27.

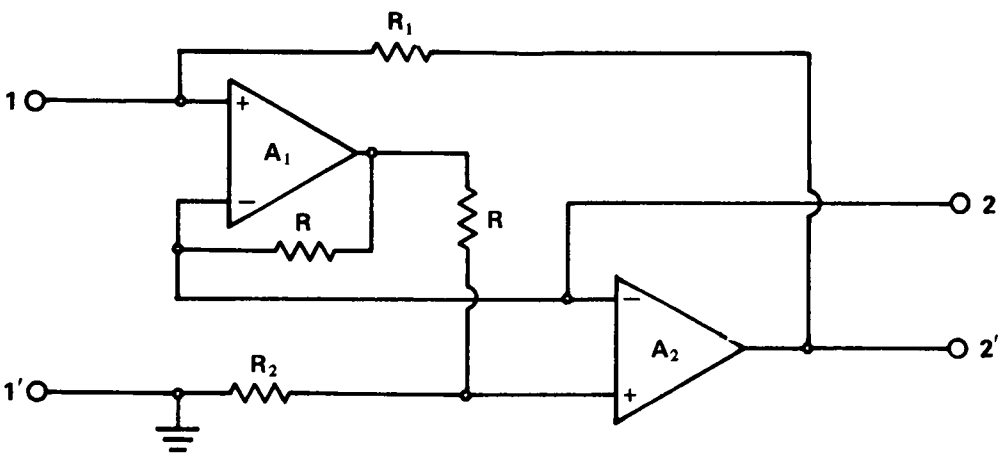


Figure 2-26. New gyrator circuit obtained from Figure 2-24.

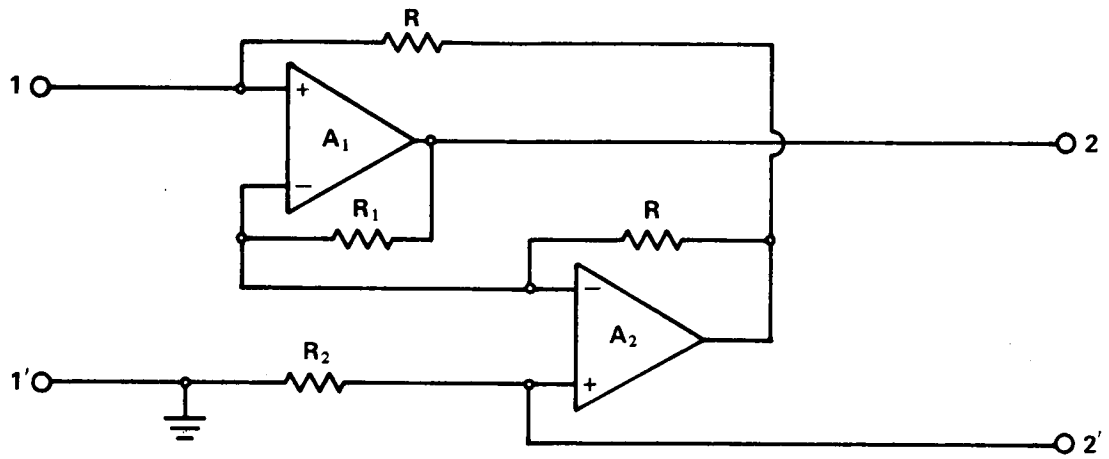


Figure 2-27. New gyrator circuit obtained from Figure 2-25.

The circuit in Figure 2-26 has Z-matrix parameters as follows:

$$z_{11} = \frac{R_1(A_1 + 1)(R + R_2)}{D_1}$$

$$z_{12} = \frac{-RA_2[R + R_2(A_1 + 1)]}{D_1}$$

$$z_{21} = \frac{R_1A_1[R_2 + R(A_2 + 1)]}{D_1}$$

$$z_{22} = \frac{R(R + R_2)(A_2 + 1)}{D_1} \quad , \qquad (2\text{-}27)$$

where $D_1 = (A_1 + 1)(R + R_2) + A_1A_2R$.

The circuit in Figure 2-27 has the following Z-matrix parameters.

$$z_{11} = \frac{R[R_1(A_2 + 1) + R(A_1 + 1)]}{D_2}$$

$$z_{12} = \frac{-A_2R_2[R_1 + R(A_1 + 1)]}{D_2}$$

$$z_{21} = \frac{RA_1[R + R_1(A_2 + 1)]}{D_2}$$

$$z_{22} = \frac{R_2[R_1(A_2 + 1) + R(A_1 + 1)]}{D_2} \quad , \qquad (2\text{-}28)$$

where $D_2 = R_1(A_2 + 1) + R(A_1 + 1) + A_1A_2R$.

These two circuits were found to be free from the low frequency unstable modes found in the earlier circuits during the time when the amplifiers are rising from zero voltage to full voltage gain. Therefore, the limiting diodes required in the original circuits are not required in these two new circuits. These circuits were constructed using Philbrick type P85AU operational amplifiers; however, no test data is given other than a Q of 2000 was measured at 200 Hz.

2.9 Riordan Circuits Modified by Antoniou

Antoniou [17] applied the nullor concept to the Riordan gyrator of Figure 2-17 (page 32) to obtain a new circuit. The nullor equivalent circuit is shown in Figure 2-28. When Antoniou paired nullators P and Q with norators Q and P, instead of P with P and Q with Q, another nullor equivalent circuit was obtained. When these nullors are replaced with operational amplifiers, the circuits shown in Figures 2-29 and 2-30 are obtained depending on whether Z_4 or Z_2 is to be replaced by a capacitor. The differential input terminals of each amplifier then must be connected to yield overall negative feedback to each amplifier.

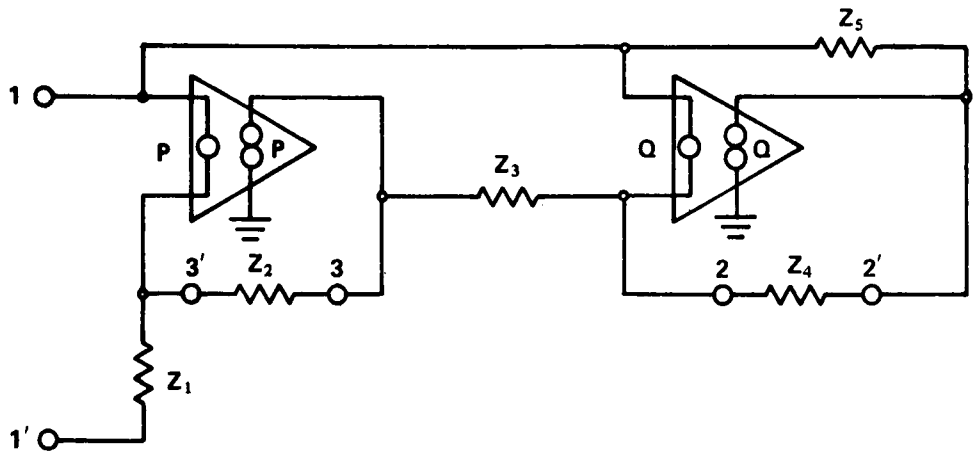


Figure 2-28. Nullor equivalent of Riordan gyrator.

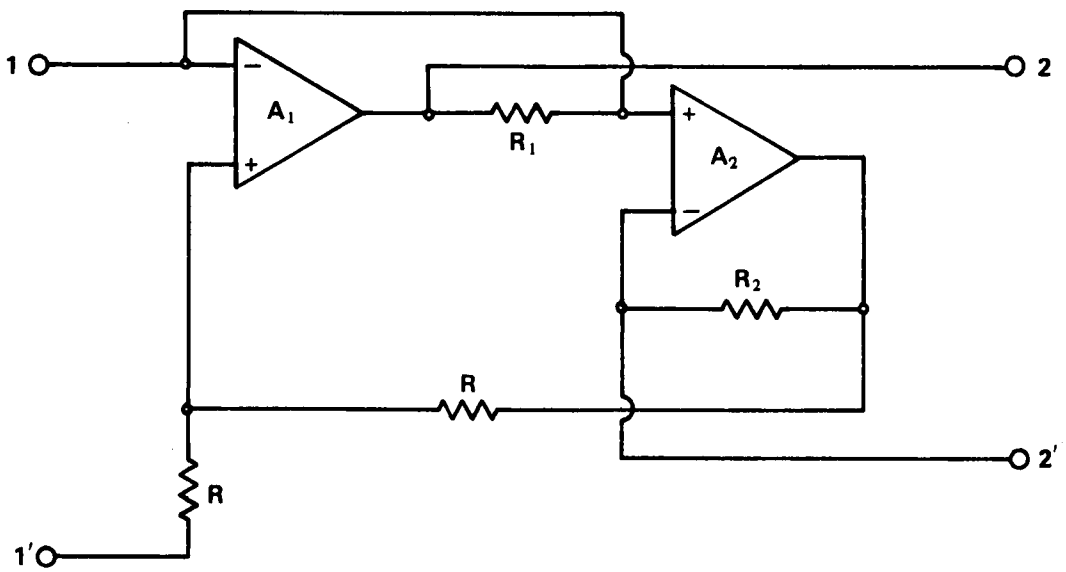


Figure 2-29. Modified Riordan gyrator, type 1.

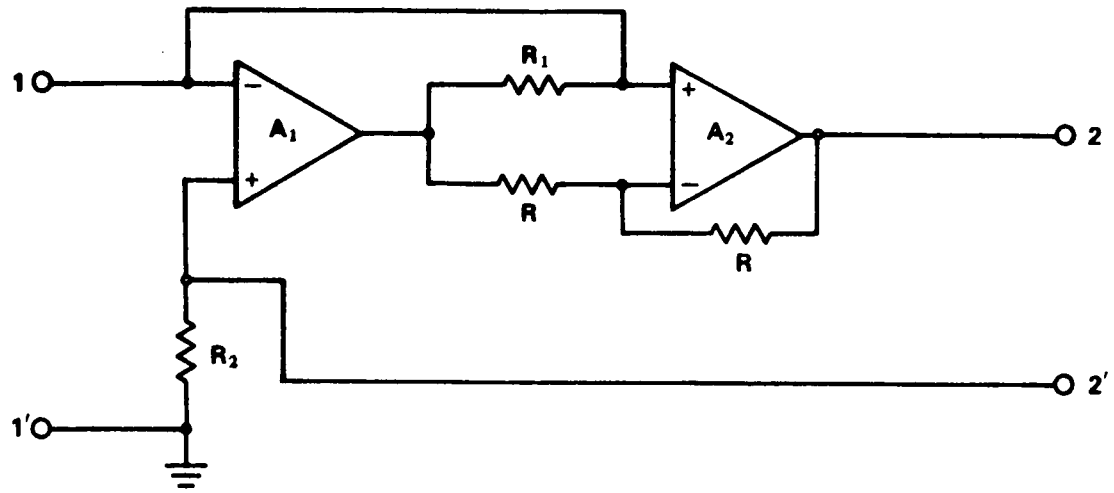


Figure 2-30. Modified Riordan gyrator, type 2.

The component values of Figure 2-28 are made as follows for Figure 2-29.

$$Z_1 = Z_2 = R$$

$$Z_3 = R_2$$

$$Z_4 = \infty$$

$$Z_5 = R_1 \quad . \tag{2-29}$$

This circuit then can be described by the open-circuit impedance matrix parameters

$$z_{11} = \frac{2R_1(A_2 + 1)}{D_1}$$

$$z_{12} = \frac{-R_2A_1A_2}{D_1}$$

$$z_{21} = \frac{R_1[A_1A_2 + 2(A_1 + A_2)]}{D_1}$$

$$z_{22} = \frac{2R_2(A_1 + 1)}{D_1} \quad , \tag{2-30}$$

where $D_1 = A_1A_2 + 2(A_1 + A_2) + 2$.

The modified Riordan circuit, type 2, is shown in Figure 2-30 and is described by the Z-matrix parameters as follows:

$$z_{11} = \frac{R_1(A_2 + 2)}{D_2}$$

$$z_{12} = \frac{-R_2A_1(A_2 + 2)}{D_2}$$

$$z_{21} = \frac{R_1A_2(A_1 + 2)}{D_2}$$

$$z_{22} = \frac{R_2(2A_1 + A_2 + 2)}{D_2} \quad , \qquad (2\text{-}31)$$

where $D_2 = (A_1 + 1)(A_2 + 2)$.

These two modified Riordan gyrator circuits were found to be free of the low frequency unstable modes of operation that could be attained in the original circuits. No test results were given for these two circuits.

2.10 Other Circuits Modified by Antoniou

Antoniou [11] also applied the nullor concept to the Brugler gyrator to obtain a new gyrator circuit. The modified Brugler circuit is shown in Figure 2-31. It can best be described by its Z-matrix parameters as follows:

$$z_{11} = \frac{2R(A_1 + A_2 + 5)}{D_3}$$

$$z_{12} = \frac{RA_2(A_1 + 4)}{D_3}$$

$$z_{21} = \frac{-RA_1(A_2 + 4)}{D_3}$$

$$z_{22} = \frac{2R(A_1 + A_2 + 3)}{D_3} \quad , \tag{2-32}$$

where $D_3 = A_1A_2 + 2(A_1 + A_2) + 6$.

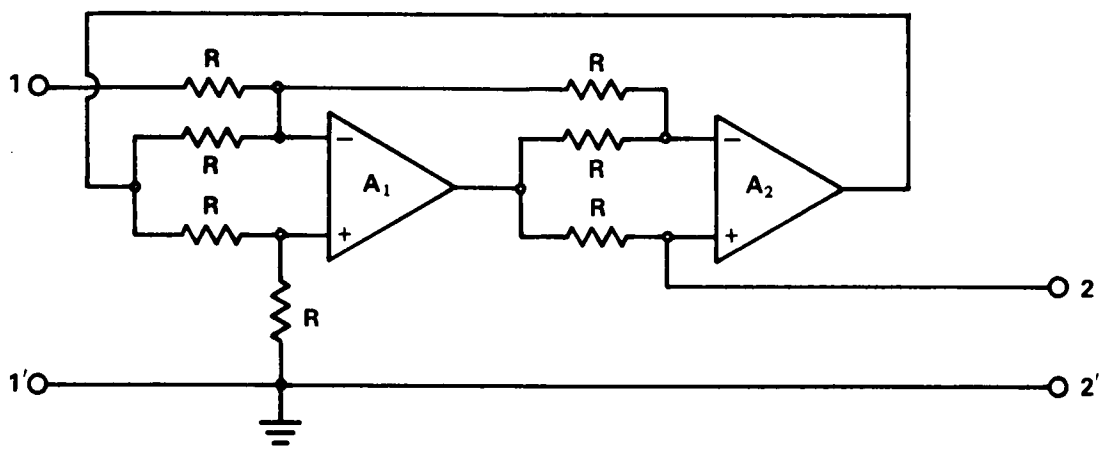


Figure 2-31. Modified Brugler gyrator.

If the series input resistor of the Brugler gyrator is removed and placed across the output terminals, the Deboo gyrator is realized. Likewise, if the series input resistor of the modified Brugler gyrator is removed and placed across the output terminals, the modified Deboo gyrator is realized as shown in Figure 2-32. This circuit has the Z-matrix parameters as given by Equation (2-33).

$$z_{11} = \frac{8R}{D_4}$$

$$z_{12} = \frac{RA_2(A_1 + 4)}{D_4}$$

$$z_{21} = \frac{-RA_1(A_2 + 4)}{D_4}$$

$$z_{22} = \frac{2R(A_1 + A_2 + 3)}{D_4} \quad , \qquad (2\text{-}33)$$

where $D_4 = A_1A_2 + 4(A_1 + A_2) + 12$.

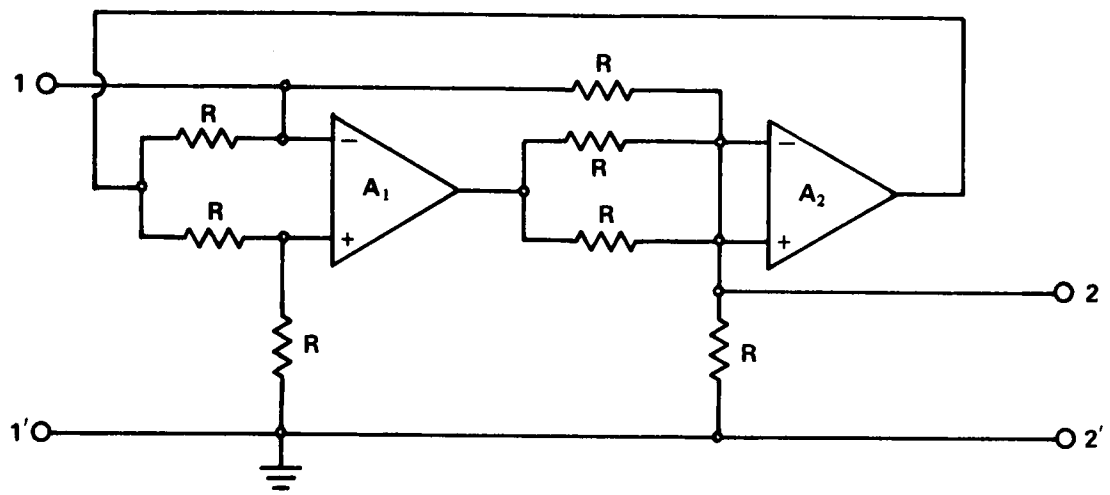


Figure 2-32. Modified Deboo gyrator.

Neither of these two modified circuits was found to suffer from the low frequency unstable modes of the original circuits; however, no test data was given for either of these modified circuits.

2.11 Summary of Findings

Eighteen different operational amplifier gyrator circuits were found in the literature search. The circuit schematic and a brief discussion of the properties of each circuit were given in this chapter. Table 2-1 presents the

Table 2-1. Comparison of Operational Amplifier Gyrators

Gyrator Name	Figure	Parts	Type Circuit	Stability	Q	Experimental Data
Huelsman-Morse	2-3 (page 20)	18	VCCS	-	Low	No
Brugler	2-7 (page 22)	9	NIV, INIC, VNIC	LFU	Low	No
Hawley	2-10 (page 26)	12	VCCS	-	Q=38 21 kHz	Yes
Prescott	2-13 (page 28)	7	VNIC	-	Low	No
Deboo	2-15 (page 29) 2-16 (page 30)	9	VCCS VNIC	LFU	Low	No
Riordan	2-18 (page 32) 2-19 (page 32)	6	-	LFU	Q=250 55 kHz	Yes
Antoniou	2-20 (page 35) 2-22 (page 37)	10	NIV INIC	ULZ	-	No
Antoniou	2-21 (page 36) 2-23 (page 38)	10	NIV INIC	USZ	-	No

Table 2-1. (Continued)

Gyrator Name	Figure	Parts	Type Circuit	Stability	Q	Experimental Data
Modified Antoniou	2-26 (page 40) 2-27 (page 41)	6	-	Stable	Q=2000 200 Hz	Yes
Modified Riordan	2-29 (page 43) 2-30 (page 44)	6	-	Stable	-	No
Modified Brugler	2-31 (page 46)	9	-	Stable	-	No
Modified Deboo	2-32 (page 47)	9	-	Stable	-	No

Abbreviations: VCCS — Voltage controlled current source
NIV — Negative impedance inverter
INIC — Current negative impedance converter
VNIC — Voltage negative impedance converter
LFU — Low frequency unstable
ULZ — Unstable with large Z_L
USZ — Unstable with small Z_L

important properties of each of these gyrators in tabular form for ease of comparison.

Table 2-1 shows that the Huelsman-Morse gyrator has the largest component count of the gyrators surveyed. In part 2.2 it was stated that because of the high degree of matching required for the resistors to reduce the matrix main diagonal terms to near zero, this gyrator will necessarily be a low-Q device.

Most of the original gyrator circuits were realized from some combination of two or more of the VCCS, NIV, INIC, or VNIC subnetworks. The only exception to this is the Riordan gyrator. All of the modified gyrator circuits were realized by Antoniou, who applied the nullor concept to the original circuit; however, none of these can be broken down into the subnetworks mentioned above.

Antoniou applied the Llewellyn stability equations to Figures 2-7 (page 22), 2-15 (page 29), 2-16 (page 30), 2-18 (page 32), and 2-19 (page 32) and found them to have low frequency unstable modes of operation. He also found Figures 2-20 (page 35), 2-21 (page 36), 2-22 (page 37), and 2-23 (page 38) to be potentially unstable depending upon the value of the load impedance Z_L. Antoniou also reported that some of the circuits had a tendency to lock up in an abnormal mode with power turn-on. Also, Antoniou applied the stability equations to each of the modified circuits and found all of them to be free of the stability problems.

Figures 2-7 (page 22), 2-13 (page 28), 2-15 (page 29), and 2-16 (page 30) were observed to be low Q-factor devices because they depend on negative resistors for resistance cancellation to reduce the matrix main diagonal terms to near zero.

CHAPTER 3

COMPARISON OF EXPERIMENTAL DATA OF VARIOUS GYRATORS

3.1 Introduction

In this chapter several gyrator circuits are tested to determine the stability, Q-factor, and the bandwidth of each. Stability is of prime importance, without which the gyrator is useless. The Q-factor and the bandwidth are additional important properties of a gyrator that affect its usefulness in a filter network.

All of the gyrators summarized in Chapter 2 were constructed and tested except the Huelsman-Morse circuit shown in Figure 2-3 (page 20). This gyrator was not constructed because of the high degree of resistor matching required by Equation (2-6), which would require the use of expensive precision resistors. Further, this gyrator requires 4 operational amplifiers and 14 resistors, a larger complement than any of the other circuits surveyed.

Gyrators tests were performed and data collected so that the following properties could be determined.

1. Stability.
2. The self-resonant frequency (SRF).

3. The Q-factor at the SRF.

4. The frequency response.

5. The equivalent resistance, inductance, and capacitance at the SRF.

These properties were then used as a basis for the comparison of each of the gyrator circuits. From this comparison, the gyrator having optimum performance was selected for further evaluation. The Q-factor and bandwidth were given primary consideration in evaluating performance.

3.2 The Test Circuit

Each gyrator was constructed and tested using the circuit shown in Figure 3-1. This circuit was tested with resistor R equal to 5 kΩ ± 1% and then with R equal to 200 kΩ ± 1%. The test data from each of these tests was compared to determine overall performance and bandwidth. Data from the test with R equal to 200 kΩ ± 1% provided information for determining the self-resonant frequency and the Q. Also, an approximate equivalent circuit can

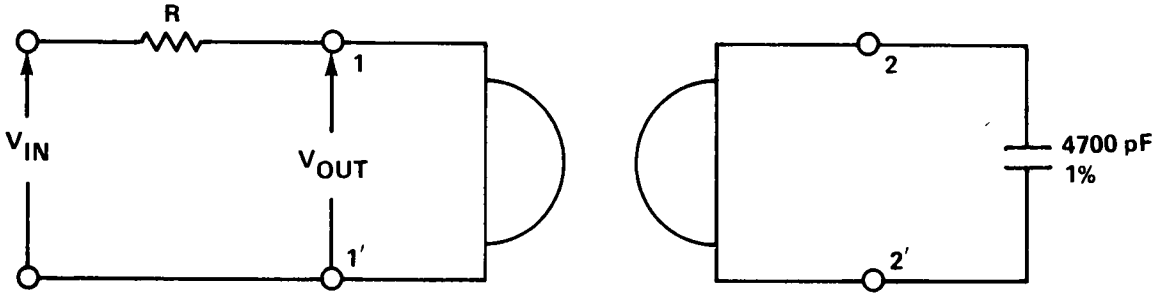


Figure 3-1. Test circuit.

be obtained by examining the test data. The results of each test are summarized in the following paragraphs.

3.3 Description of Components Used to Construct Each Test Gyrator

Gyrator test circuits were constructed using RCA type CA741 integrated circuit operational amplifiers and 10 kΩ ± 1% RN55 resistors. The load selected was a 4700 pF ± 1% Corning Electronics glass capacitor. Using these components, the gyrator circuits shown in Chapter 2 were constructed with the following variations:

1. In the Hawley gyrator of Figure 2-10 (page 26), the two transistor emitter followers were replaced with two operational amplifiers connected in the unity-gain voltage follower configuration.

2. In the Prescott gyrator of Figure 2-13 (page 28), the value of resistor R_1 was made 5 kΩ ± 1% as required for resistance cancellation.

3. In the Antoniou gyrators of Figures 2-20 (page 35), 2-21 (page 36), 2-22 (page 37), and 2-23 (page 38), the two pairs of back-to-back diodes were omitted since they severely limited the voltage amplitude capability and made comparison more difficult. This is discussed in more detail later.

3.4 Test Equipment

The test equipment was connected to the circuit as shown in Figure 3-2. The block labeled buffer was an operational amplifier used

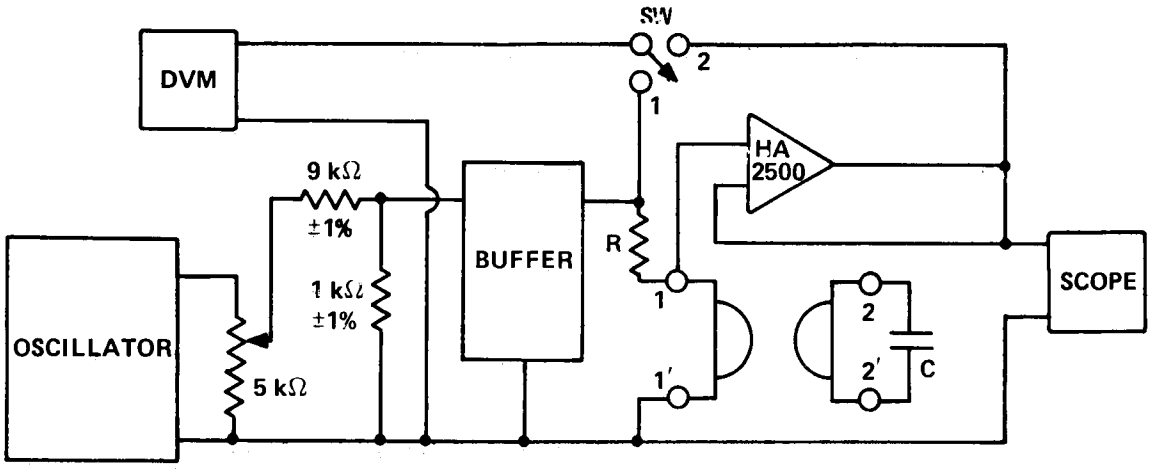


Figure 3-2. Test setup.

to prevent the DVM from loading the signal into the test circuit. The test equipment used is shown in the following list.

1. Spectral Dynamics oscillator, Model SD104A-5
2. Wavetek function generator, Model 103
3. Intercontinental Instruments pulse generator, Model PG-32
4. Tektronix oscilloscope, Model 555
5. Hewlett-Packard oscilloscope, Model 181A
6. Dana digital voltmeter, Model 5640
7. Hewlett-Packard frequency counter, Model 5233L

The Harris Semiconductor HA2500 operational amplifier was used as a buffer for the DVM and oscilloscope at the output. Tests on this buffer reveal that

the input impedance is 1250 MΩ shunted by 5.1 pF. The use of the buffer allows much higher frequency data to be taken than would otherwise be possible with the load presented by the DVM or oscilloscope.

3.5 Description of Tests Performed

Two tests were performed on each gyrator circuit and they can be described as follows:

1. Test One — R = 5 kΩ. This test was performed first with resistor R of Figure 3-2 equal to 5 kΩ ± 1% and the DVM connected as shown by switch position one. The oscillator output was adjusted at each different frequency for a reading of 1.000 V rms on the DVM. The DVM was then connected in switch position two and the output voltage read and recorded. These readings were taken over a frequency range of several decades so that a broad frequency response profile would be obtained. The overall purpose of Test One with R = 5 kΩ was to obtain the frequency response of each gyrator to use as one basis for comparing their performance. Hereafter this test will be referred to as Test One.

2. Test Two — R = 200 kΩ. In this test, the gyrators were tested as before except that resistor R in Figure 3-2 was equal to 200 kΩ ± 1%. The purpose of Test Two with R = 200 kΩ was to obtain test data so that the self-resonant frequency and the Q-factor at this frequency could be determined.

The Q-factor is a measure of how near a real inductor approximates the ideal. The self-resonant frequency is an indication of the upper frequency limit at which an inductor can effectively be used. From this data, the equivalent shunt values of inductance, resistance, and capacitance can be calculated.

Then, lastly, the gyrator output at port one was monitored on the oscilloscope with the port floating. The purpose was to determine the stability of the gyrator as the source impedance was increased to infinity.

3.6 Preliminary Results

The data taken during Test One indicates how well the gyrator performed in a simple high-pass RL filter circuit. A comparison of the data from each test indicates that the performance of all the gyrators was within ±2% of the best median up to about 30 kHz. Above this frequency, however, the performance varied widely and gave information useful in determining an approximate equivalent circuit. Three of the circuits tested did not simulate an inductor but instead acted like a simple voltage divider as would be expected of very low Q-factor devices. These circuits were checked for wiring errors and found to be correct. No further efforts were made with these circuits.

The Brugler gyrator in Figure 2-7 (page 22), the Antoniou gyrator in Figure 2-22 (page 37), and the modified Deboo gyrator of Figure 2-32 (page 47) did not operate properly. One reason for this may have been a very low

Q-factor. Also, two of Antoniou' s gyrators, Figures 2-21 and 2-23 (pages 36 and 38), were unstable in this test circuit; however, Antoniou had already noted the possibility of instability.

The data taken during Test Two were used to determine the equivalent shunt inductance, resistance, and capacitance of the simulated inductor at the self-resonant frequency. From this, the Q-factor at resonance could be calculated. Several of the gyrator circuits were unstable in this test which prevented the calculations. The gyrators shown in Figures 2-18 (page 32), 2-20 (page 35), 2-21, 2-22 (page 37), and 2-23 all oscillated in Test Two. Several of the gyrators had an output greater than the input in this test indicating that as the resistor R in Figure 3-1 (page 53) becomes very large, these circuits would become unstable. This conclusion was further confirmed when the resistor R in Figure 3-2 (page 55) was disconnected from the oscillator and left floating, because then all of these gyrator circuits either oscillated or went into saturation. The gyrators shown in Figures 2-7 (page 22), 2-10 (page 26), 2-15 (page 29), 2-16 (page 30), and 2-19 (page 32) are conditionally stable requiring a low driving source resistance. Good test data was obtained from Figures 2-13 (page 28), 2-26 (page 40), 2-27 (page 41), 2-29 (page 43), 2-30 (page 44), 2-31 (page 46), and 2-32 (page 47).

3.7 Individual Gyrator Performance Results

Each gyrator was tested as described earlier in this chapter, and the performance characteristics peculiar to each circuit described in the following paragraphs.

The Brugler gyrator, Figure 2-7 (page 22), simulated a very poor quality inductor with resistor R of Figure 3-1 (page 53) equal to 5 kΩ. The gyrator then oscillated when R was increased to 200 kΩ.

The Hawley gyrator, Figure 2-10 (page 26), had good performance in Test One with the small value of resistor R in Figure 3-1, however, as this resistor value was increased up to an open circuit, the gyrator became unstable and oscillated. As shown in Table 3-1 this gyrator had the most components of any circuit tested.

The Prescott gyrator, Figure 2-13 (page 28), simulated a poor quality inductor with a Q-factor of only 6.5 as shown in Table 3-2. This gyrator required resistor R_1 in Figure 2-13 to be 5 kΩ for resistance cancellation; however, the Q-factor is still low.

The Deboo gyrators, Figures 2-15 and 2-16 (pages 29 and 30), have several shortcomings. First, there is a tendency to lock up in a saturation mode with power turn-on as noted by Antoniou. However; switching the power supply off and back on several times caused the circuit to turn on normally. These circuits also became unstable and oscillated as the resistor R in Figure 3-1 was increased.

Table 3-1. Number of Components in Each Gyrator Tested

Type Gyrator	Figure	Number of Components		
		Operational Amplifiers	Resistors	Diodes
Brugler	2-7 (page 22)	2	7	
Hawley	2-10 (page 26)	4	8	
Prescott	2-13 (page 28)	2	5	
Deboo	2-15 & 2-16 (pages 29 & 30)	2	7	
Riordan	2-18 & 2-19 (page 32)	2	4	
Antoniou	2-20, 2-21, 2-22, & 2-23 (pages 35, 36, 37, & 38)	2	4	4
Antoniou	2-26 & 2-27 (pages 40 & 41)	2	4	
Modified Riordan	2-29 & 2-30 (pages 43 & 44)	2	4	
Modified Brugler	2-31 (page 46)	2	7	
Modified Deboo	2-32 (page 47)	2	7	

Table 3-2. Results of Test Two

Gyrator	Figure	Self Resonant Frequency	Q	L	C	R_p
Prescott	2-13 (page 28)	45 kHz	6.5	0.4838 H	20.8 pF	896 kΩ
Antoniou	2-26 (page 40)	35 kHz	75	0.4743 H	38.5 pF	7.85 MΩ
Antoniou	2-27 (page 41)	39 kHz	139	0.4711 H	30.3 pF	16.0 MΩ
Modified Riordan	2-29 (page 43)	30 kHz	9.4	0.4759 H	54.1 pF	843 kΩ
Modified Riordan	2-30 (page 44)	29 kHz	14.1	0.4730 H	58.6 pF	1.22 MΩ
Modified Brugler	2-31 (page 46)	25.5 kHz	14.5	0.4756 H	76.8 pF	1.1 MΩ
Modified Deboo	2-32 (page 47)	26.5 kHz	5.1	0.4679 H	72 pF	396 kΩ

The Riordan gyrators, Figures 2-18 and 2-19 (page 32), were also found to have the shortcomings as noted by Antoniou. Both tend to become unstable as the resistor R in Figure 3-1 (page 53) is increased and go to the saturation level with the input open-circuited.

The Antoniou gyrators, Figures 2-20 (page 35), 2-21 (page 36), 2-22 (page 37), and 2-23 (page 38), were constructed without the diodes as previously noted. The gyrator circuits of Figures 2-21 and 2-23 oscillated regardless of the value of resistor R. The circuit of Figure 2-22, had a

rather large dc offset and did not simulate a good quality inductor. The gyrator of Figure 2-20 (page 35) had a tendency to lock up in a saturation mode with power turn-on; however, repeatedly switching the power off and on caused the circuit to operate normally so that test data could be obtained. The circuit functioned properly with resistor R in Figure 3-1 (page 53) equal to 5 kΩ. When this resistor was changed to 200 kΩ, the circuit broke into uncontrolled oscillation as the input frequency was increased from 30 kHz to 35 kHz. Adding the diodes as shown in Figure 2-20 prevented oscillation but limited the maximum signal level to about 0.18 V rms. Performance of this circuit was degraded compared to some of the other gyrator circuits.

Antoniou's gyrators, Figures 2-26 and 2-27 (pages 40 and 41), were obtained from the nullor equivalent circuits of his previous gyrators and performed better than any of the other gyrators constructed and tested. From Table 3-1 it can be seen that these two gyrators are among the group with the lowest component count. Both of these gyrators performed well in both Test One and Test Two with no indication of oscillations when the input was open-circuited. Figure 2-27 had a slightly higher bandwidth and a higher Q-factor as shown in Table 3-2.

The modified Riordan gyrators, Figures 2-29 and 2-30 (pages 43 and 44), did not suffer from any of the shortcomings of the original circuits; however, they have a low Q-factor as seen in Table 3-2.

The modified Brugler gyrator, Figure 2-31 (page 46), likewise did not suffer from the shortcomings of the original circuit; however, the self-resonant frequency was the lowest of any tested. The Q-factor was low also.

The modified Deboo gyrator, Figure 2-32 (page 47), was free of the shortcomings of the original circuit; however, it had the lowest Q-factor of any of the circuits tested. The self-resonant frequency was only slightly higher than for the modified Brugler gyrator. The very low Q-factor may be the reason the test data taken with resistor R in Figure 3-1 (page 53) equal to 5 kΩ looked similar to that of a voltage divider instead of an inductor.

The results of the stability test are summarized in Table 3-3.

Upon examination of the data taken in Test One, it may be observed that an equivalent circuit for all the gyrators tested except for Figures 2-29 and 2-30 (pages 43 and 44) might look as shown in Figure 3-3. A passive network such as this would give the same response as obtained from the tests. As an example, the response of Figure 2-27 (page 41) is shown in Figure 3-4.

To analyze the circuit of Figure 3-3, first assume that resistor R_s is very small, which is ordinarily the case. This resistor could also be placed in series with L and represents the small nonzero resistance that would be measured at dc. This resistor will only have a major effect on the response at very low frequencies where the inductive reactance of L has the same order of magnitude. At these low frequencies, the Q-factor is primarily determined by R_s.

Table 3-3. Gyrator Stability Results

Gyrator	Figure	Stability
Brugler	2-7 (page 22)	Note 1 Oscillates
Hawley	2-10 (page 26)	Note 1 Oscillates
Prescott	2-13 (page 28)	Stable
Deboo	2-15 & 2-16 (pages 29 & 30)	Note 1 and Note 2
Riordan	2-18 & 2-19 (page 32)	Note 1 and Note 2
Antoniou	2-20 & 2-21 (pages 35 & 36) 2-22 & 2-23 (pages 37 & 38)	Note 3
Modified Antoniou	2-26 & 2-27 (pages 40 & 41)	Stable
Modified Riordan	2-29 & 2-30 (pages 43 & 44)	Stable
Modified Brugler	2-31 (page 46)	Stable
Modified Deboo	2-32 (page 47)	Stable

Note 1: Potentially unstable for large source impedance.

Note 2: Lockup in saturation mode with power turn-on.

Note 3: Stable only when diodes used. Without diodes Notes 1 and 2 apply.

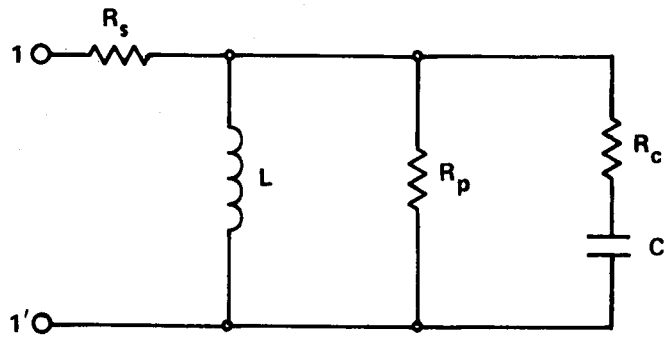


Figure 3-3. General equivalent circuit.

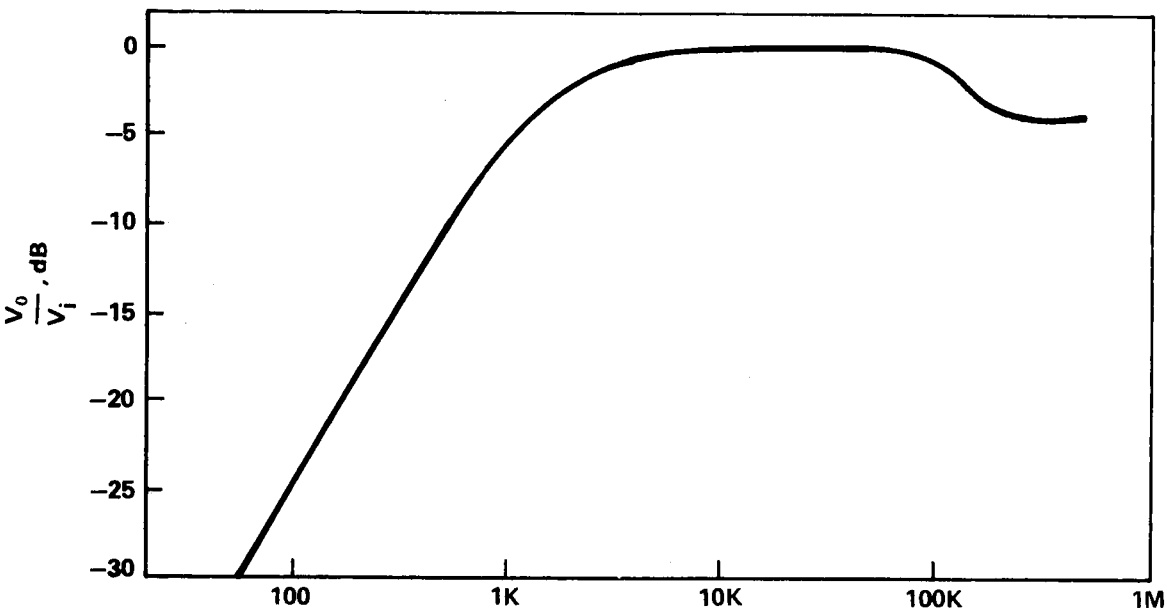


Figure 3-4. Frequency response of Figure 2-27 (page 41) to Test One.

The resistor R_p ordinarily has a large value and affects the Q-factor in the mid-frequency band. When this resistor is large compared to the source resistance, the shunting effect will be negligible.

Ordinarily the capacitor C is very small, so that this branch only has an effect at high frequencies. At frequencies where the capacitive reactance is

of the same order of magnitude as the resistor R_p, the R_c - C branch has the effect of shunting R_p to reduce the Q-factor even more. At frequencies where the capacitive reactance of C is of the same order of magnitude or less than R_c and R_c is of the same order of magnitude as the source resistance, the effect is comparable to a voltage divider. This effect is seen in the high frequency response in Figure 3-4.

The response of the gyrators in Figures 2-29 and 2-30 (pages 43 and 44), however, is such as to indicate another shunt leg could be added to the above network consisting of a series RLC circuit. This is shown in Figure 3-5. A network such as this would have a response similar to that obtained during Test One. The response of Figure 2-29 is shown in Figure 3-6.

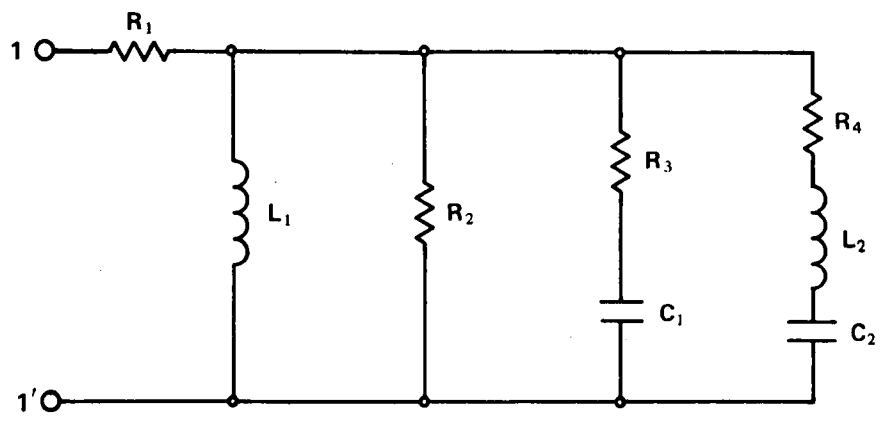


Figure 3-5. General equivalent circuit for Figures 2-29 and 2-30.

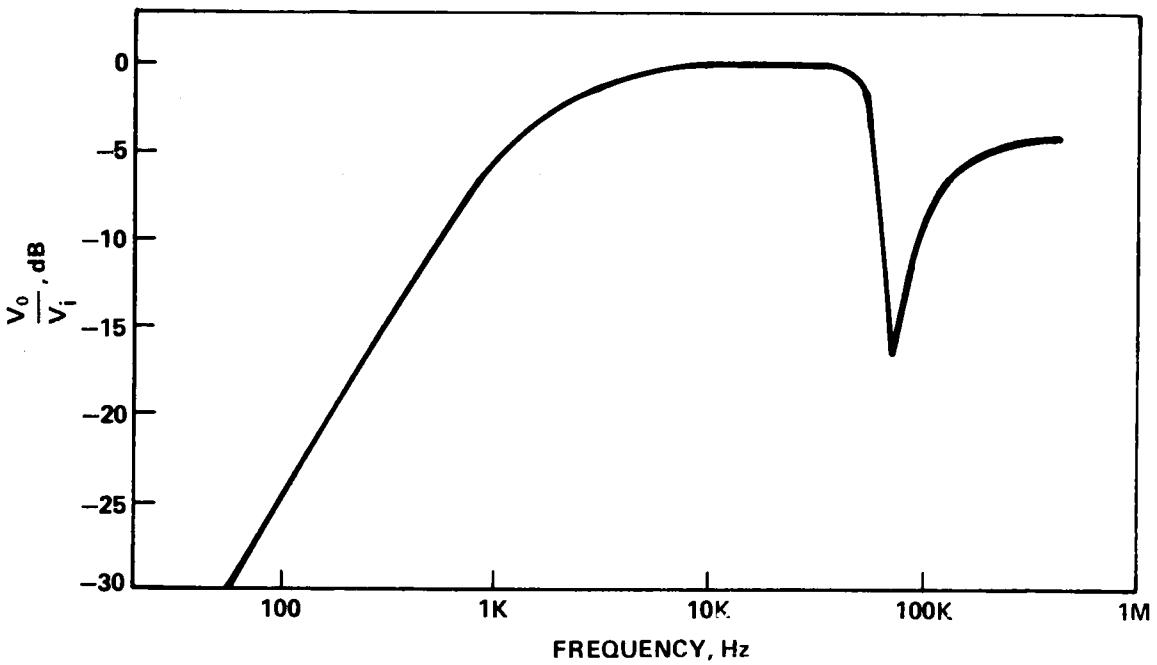


Figure 3-6. Frequency response of Figure 2-29 (page 43) to Test One.

The response of Figure 3-5 is similar to that of Figure 3-3 except that a null occurs in the response of Figure 3-5 because of the series RLC branch. The null occurs at the resonant frequency of the L_2C_2 combination with the depth dependent on the relation between the source resistance and resistor R_4.

These gyrator equivalent circuits illustrate the type of circuit that would have a response similar to that shown and are by no means unique.

3.8 Summary of Results

As mentioned earlier, each gyrator was constructed with the same components so that the basis for comparison would be the same. The performance and test results of each of the above gyrator circuits were carefully

examined and compared to each of the others to select the gyrator circuit that would simulate the highest quality inductor.

Several of the gyrator circuits tested were either completely unstable or were conditionally stable. The conditionally stable circuits were stable when the source or series resistor R in Figure 3-1 (page 53) was small. The stability of each gyrator is shown in tabular form in Table 3-3 (page 64).

Of the circuits remaining, a brief look at Table 3-2 (page 61) shows that many are low Q-factor devices and would be unacceptable in many applications. Since the self-resonant frequency spread of this group is relatively small, the highest Q-factor will be the prime basis of comparison for selecting one circuit.

Based on this performance evaluation, the Antoniou gyrator, Figure 2-27 (page 41), was selected as having the greatest potential as a substitute for a high quality inductor. A discussion of more extensive tests performed on this gyrator is presented in Chapter 4. Also of interest is the fact that the Antoniou gyrator, Figure 2-26 (page 40), was very similar in performance to the one selected and only somewhat lower in the quality of inductor simulated.

CHAPTER 4

RESULTS OF EXPERIMENTAL TESTS ON THE MODIFIED ANTONIOU GYRATOR

4.1 Introduction

After the results of the tests described in Chapter 3 were evaluated, the modified Antoniou gyrator circuit of Figure 2-27 (page 41) was selected as having the best performance characteristics of all the operational amplifier gyrators tested.

In this chapter a complete evaluation, that includes both experimental testing and a theoretical analysis, will be reported on the modified Antoniou gyrator. A breadboard of the gyrator circuit of Figure 2-27 was first constructed with the resistors $R_1 = R_2 = R$ as shown in Figure 4-1. A series of tests were performed on the breadboard using various combinations of resistors R and capacitors C to simulate a wide range of inductance values.

The method of performing the tests on the experimental gyrator is described briefly. This includes a description of the test data taken and how it is used to obtain the Q-factor. The results of the tests are discussed and the curves of Q-factor versus frequency for the various combinations of values of R and C are plotted.

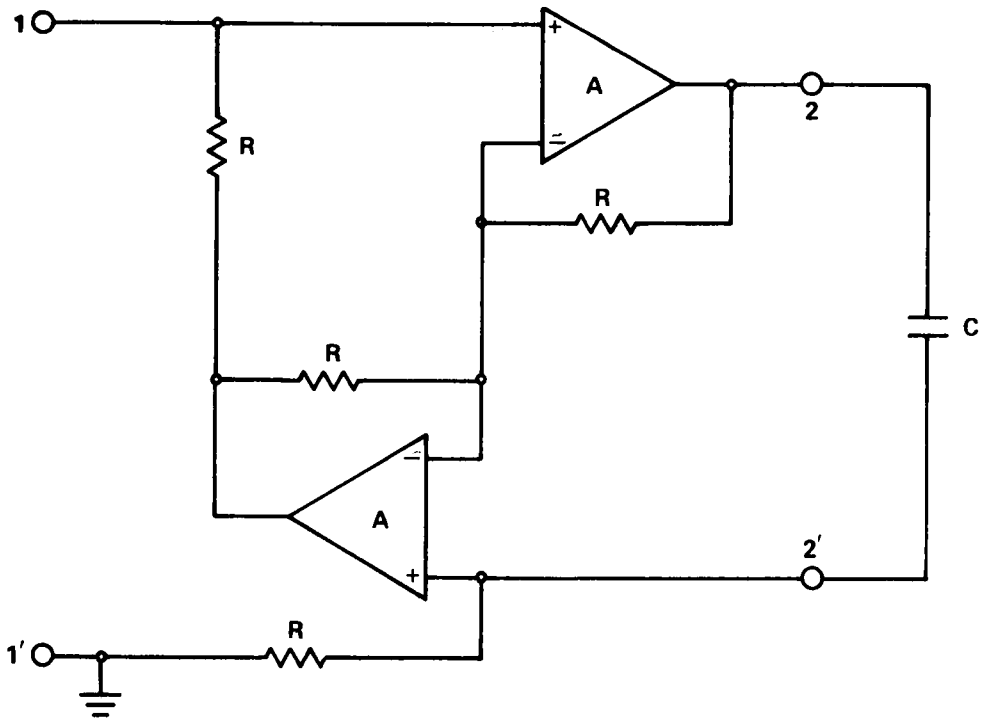


Figure 4-1. Modified Antoniou gyrator test circuit.

In the next part, the two-port impedance parameters are used to develop an equation for the input impedance Z_{in} of the gyrator shown in Figure 4-1. This equation is then extended to include the effects of the finite input resistance R_i of the operational amplifiers. Next, this equation is used to synthesize an equivalent circuit model of the gyrator.

The effects of the operational amplifier parameter variations on the element values of the circuit model are discussed and demonstrated. Lastly, the use of this gyrator in a narrow bandpass filter is described with both the experimental test results and the theoretical analysis presented for comparison.

4.2 Tests Performed

Each test consisted of operating the gyrator circuit with a certain resistor value R and a particular load capacitor C across port two of Figure 4-1 while varying a shunt capacitor across port one to change the resonant frequency of the network. Data was obtained so that the Q versus frequency curve could be plotted.

Of the methods available for measuring Q, only the transient pulse method is sufficiently accurate to measure the high Q's encountered with gyrator circuits. This method consists of exciting the gyrator circuit with a pulse and determining the exponential decrement rate of the resulting oscillation. Since this method has been fully described elsewhere [21,22], it will not be discussed in detail here.

The capacitor C across port two was changed and the previous test was performed again. After several tests had been performed with a range of capacitors on port two, the resistors R were changed to a different value and the tests repeated. The tests were repeated until data had been obtained with several combinations of values for R and C.

The value of the simulated inductance L is very nearly equal to R^2C, where R is the value of resistor used in the circuit and C is the capacitor across port two. This will be discussed in more detail later.

The next test performed was to evaluate the performance of the simulated inductance in a parallel tuned circuit.

4.3 Test Results

The test gyrator was constructed as shown in Figure 4-1 with RCA type CA741 operational amplifiers and RN55, ±1%, metal film resistors. The data taken in each test was then corrected for any shunt resistances that were external to the gyrator itself. The corrected Q-data was then used to plot Q versus frequency for each test.

The curves in Figure 4-2 were plotted for the case of R = 10 kΩ with various capacitors across port two to simulate different inductances. It may be observed that all of the curves have the same general shape with the peak Q occurring at a progressively lower frequency as the capacitance across port two is increased. Also note that at higher frequencies, the curves for the smaller inductances almost coincide, which is evidently a function of the operational amplifier gain-bandwidth product and also of the resistor R value. These curves show that all the simulated inductors have a high Q of 1000 or greater between 20 Hz and 2.5 kHz.

The curves in Figure 4-3 were plotted from the test data for the case R = 31.6 kΩ. The same comments apply here that were made in the previous paragraph except for a lower frequency range of approximately 10 Hz to 700 Hz.

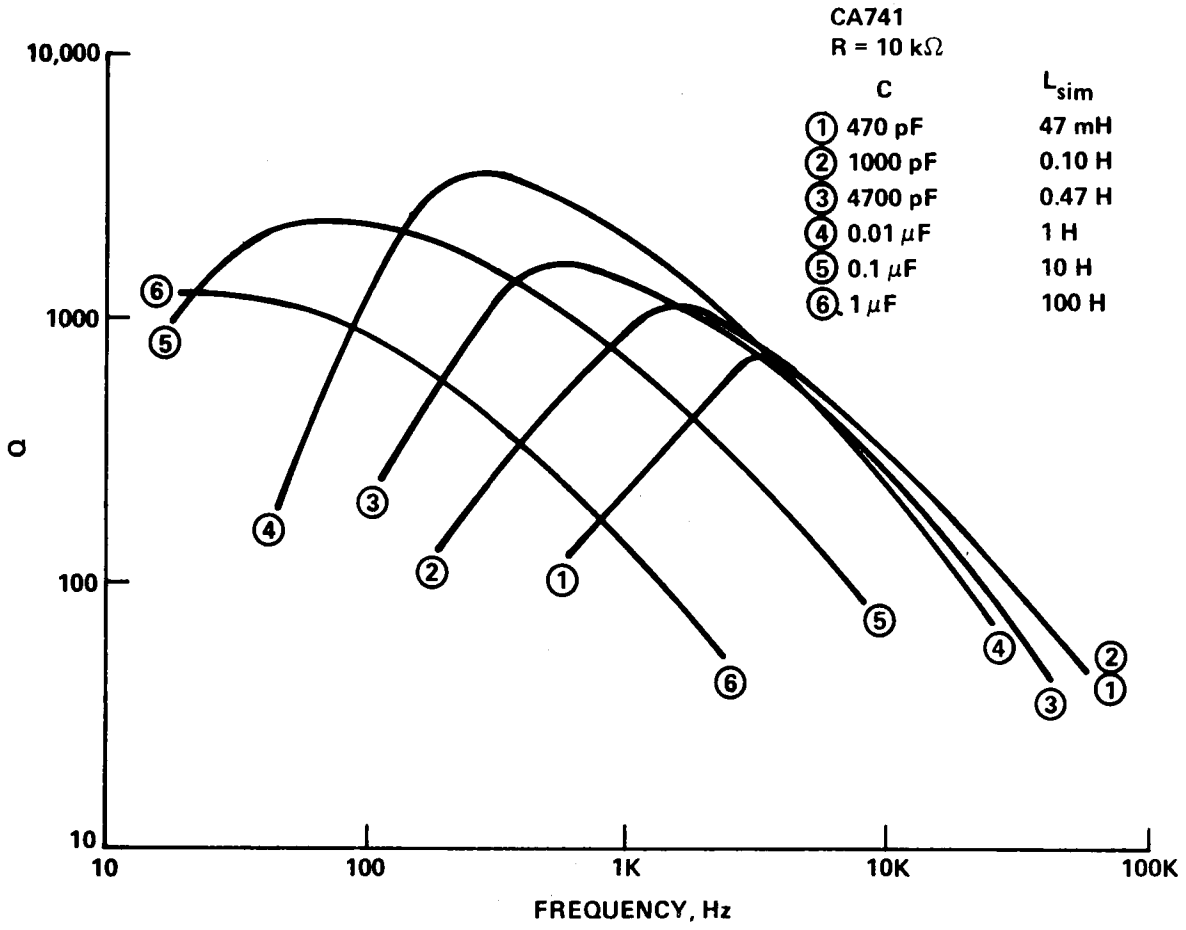


Figure 4-2. Curves of Q versus frequency for R = 10 kΩ .

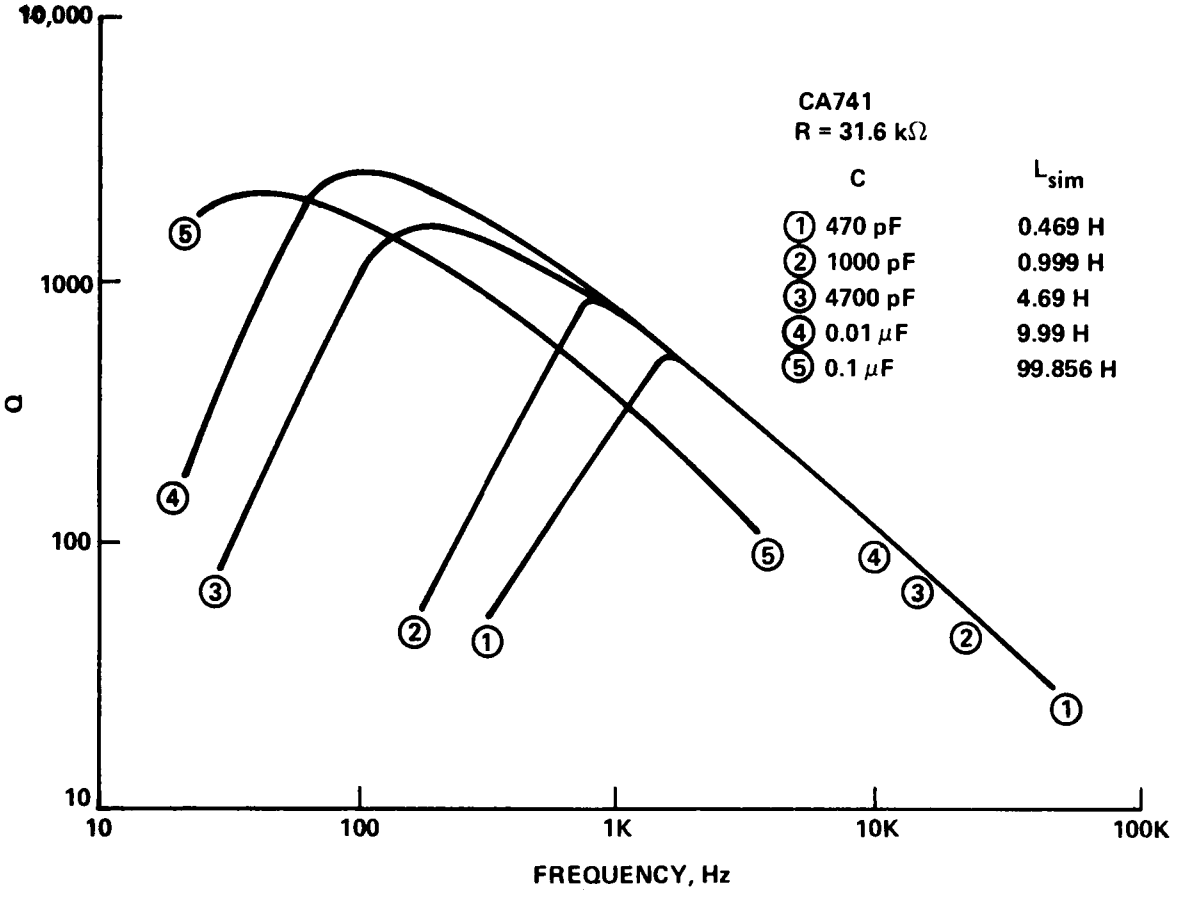


Figure 4-3. Curves of Q versus frequency for R = 31.6 kΩ.

The curves in Figure 4-4 were plotted from data for R = 100 kΩ. The same comments as before apply except that the frequency range is narrower, from approximately 20 Hz to 250 Hz. Also notice that the peak Q-values are not quite as high, but are still considerably higher than those of actual inductors.

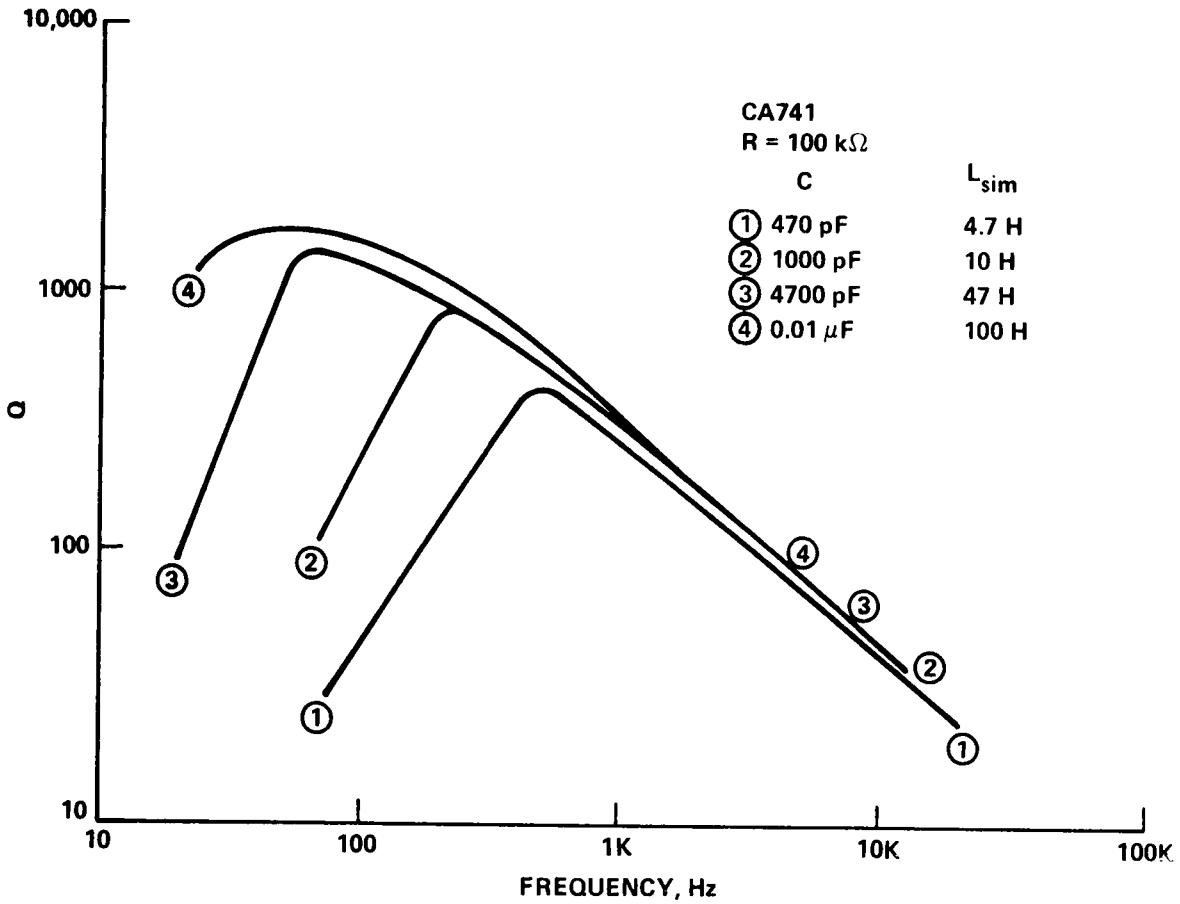


Figure 4-4. Curves of Q versus frequency for R = 100 kΩ.

The curves in Figure 4-5 were plotted for the case that R = 3.16 kΩ. The previous comments again apply except that the peak Q-values occur at a higher frequency. From Figure 4-5 a Q of 1000 can be obtained very nearly to 10 kHz.

Another test was performed on the circuit to determine the linearity for different input signal levels. This test was performed with R = 10 kΩ, C = 4700 pF, f = 10 kHz, and a ±14 V power supply. The input signal was

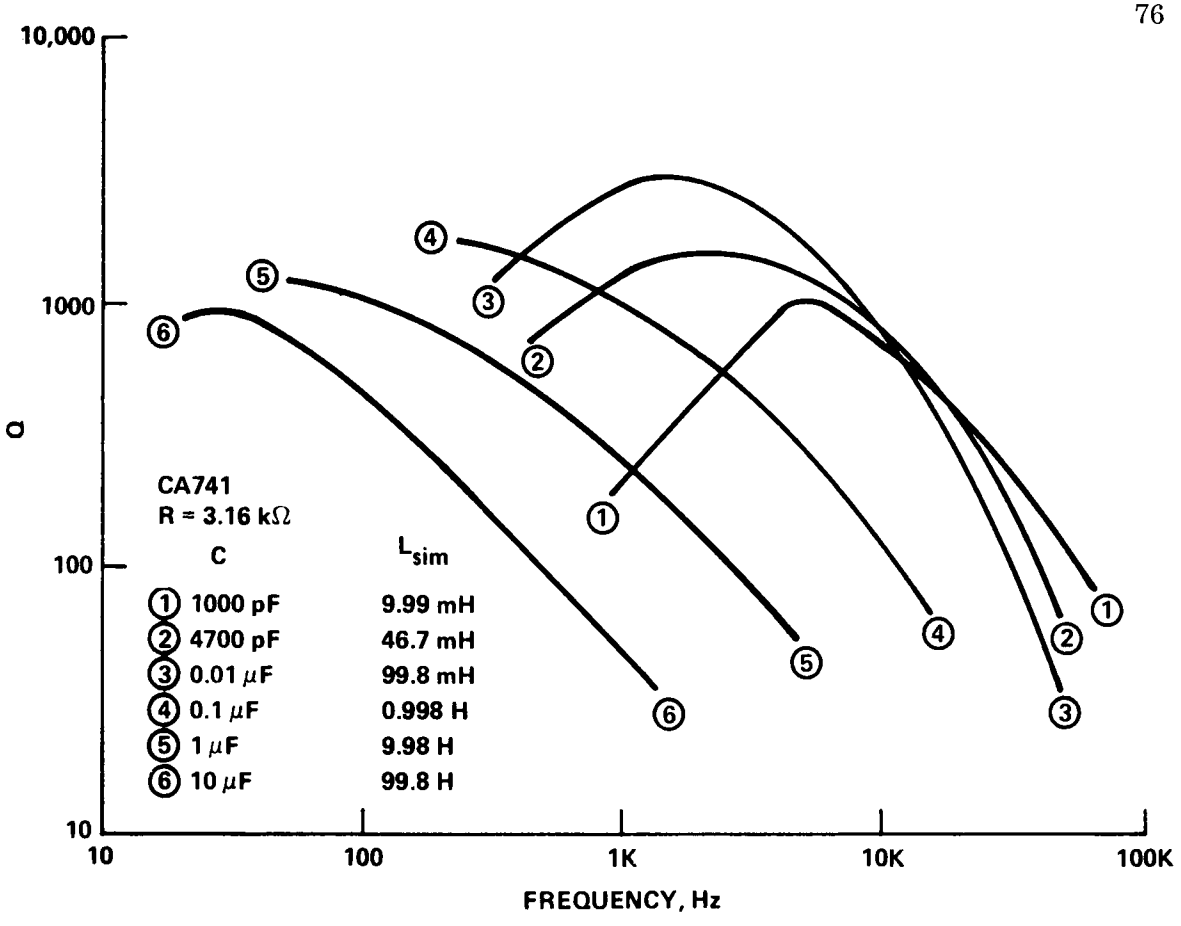


Figure 4-5. Curves of Q versus frequency for R = 3.16 kΩ.

varied from 10 mV rms to 7 V rms and test data recorded. The nonlinearity was found to be less than 0.2% up to 3 V rms. The nonlinearity then increased to 1.7% at 6 V rms and to 5% at 7 V rms. The sharp increase in nonlinearity at the higher voltage levels is a result of the voltage swing limitations of the operational amplifier.

4.4 Calculated Gyrator Z_{in}

The driving point impedance Z_{in} for this gyrator circuit can be readily determined by substituting the two-port impedance parameters into Equation (1-5). If the substitutions $R_1 = R_2 = R$ and $A_1 = A_2 = A$, as shown in Figure

4-1 (page 70), are made in Equation (2-28) for the gyrator in Figure 2-27 (page 41), Equation (2-28) reduces to

$$z_{11} = \frac{2R^2(A + 1)}{D_2}$$

$$z_{12} = \frac{-AR^2(A + 2)}{D_2}$$

$$z_{21} = \frac{AR^2(A + 2)}{D_2}$$

$$z_{22} = \frac{2R^2(A + 1)}{D_2}$$

$$D_2 = R(A^2 + 2A + 2) \quad . \tag{4-1}$$

It might be noted that these equations were obtained with the assumption that the operational amplifier bandwidth and input resistance R_i are infinite. The effect of these parameters will be developed later.

Substituting Equation (4-1) into Equation (1-5) to obtain Z_{in} gives

$$Z_{in} = \frac{R^2(A^2 + 2A + 2) + 2R(A + 1)Z_L}{2R(A + 1) + Z_L(A^2 + 2A + 2)} \quad . \tag{4-2}$$

The gyrator is normally loaded with a capacitor across port two so that $Z_L = 1/sC$. Making this substitution, Equation (4-2) becomes

$$Z_{in} = \frac{sR^2C(A^2 + 2A + 2) + 2R(A + 1)}{s2RC(A + 1) + (A^2 + 2A + 2)} \quad . \tag{4-3}$$

If the gain A of the operational amplifier in Equation (4-3) is allowed to approach infinity, the limit is given by

$$\lim_{A \to \infty} Z_{in} = sR^2C \quad . \tag{4-4}$$

This is the expression for an ideal inductor as shown in Figure 4-6.

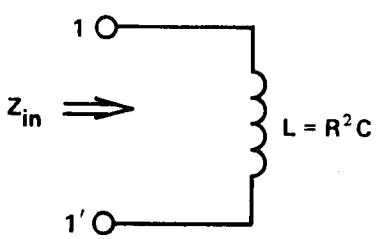


Figure 4-6. Ideal inductor obtained when A approaches infinity.

However, since a practical operational amplifier has a finite gain A, the expression for Z_{in} given by Equation (4-3) holds. As shown in Chapter 1, this Z_{in} may be realized as the passive network shown in Figure 4-7, where the component values are

$$R_1 = \frac{2R(A + 1)}{(A^2 + 2A + 2)}$$

$$L_1 = \frac{R^2C(A^2 + 2A - 2)}{(A^2 + 2A + 2)}$$

$$R_2 = \frac{R(A^2 + 2A - 2)}{2(A + 1)} \quad . \tag{4-5}$$

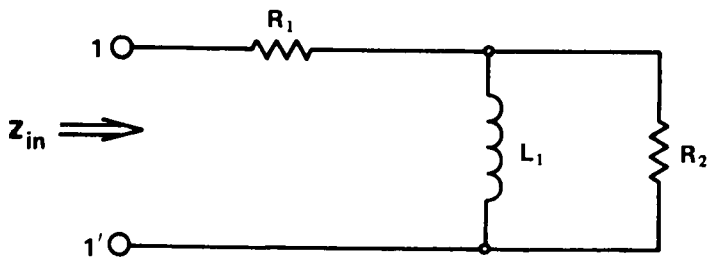


Figure 4-7. Network realized from Equation (4-3).

From this it can be seen that for the case A >> 1, Equation (4-5) reduces to

$$R_1 \approx \frac{2R}{A}$$

$$L_1 \approx R^2C$$

$$R_2 \approx \frac{RA}{2} \quad . \tag{4-6}$$

A practical operational amplifier may be represented by the gain expression as

$$A = A_0\omega_c/(s + \omega_c) \quad , \tag{4-7}$$

where A_0 is the dc open loop gain and ω_c is the frequency at which the gain A_0 is down 3 dB. When this equation is substituted into Equation (4-3) and the results are simplified, the expression for Z_{in} of the operational amplifier gyrator becomes

$$Z_{in} = \frac{s^3 2R^2C + s^2 2R[RC\omega_c(A_0 + 2) + 1] + sR\omega_c[RC\omega_c(A_0^2 + 2A_0 + 2) + 2(A_0 + 2)] + 2R\omega_c^2(A_0 + 1)}{s^3 2RC + s^2 2[RC\omega_c(A_0 + 2) + 1] + s2\omega_c[RC\omega_c(A_0 + 1) + A_0 + 2] + \omega_c^2(A_0^2 + 2A_0 + 2)} \quad . \quad (4\text{-}8)$$

This is the expression for the driving point impedance of the operational amplifier gyrator as shown in Figure 4-1 (page 70). Equation (4-8) will now be used to synthesize a better circuit model of the gyrator that can be used to account for its high frequency behavior.

4.5 Synthesis of Z_{in}

A network can be synthesized by the methods described by Van Valkenburg [5]. Beginning with the equation for Z_{in} given by Equation (4-8), the network of Figure 4-8 can be realized. The value of the components in the network of Figure 4-8 are given by the following equations:

$$R_1 = \frac{2R(A_0 + 1)}{(A_0^2 + 2A_0 + 2)} \quad (4\text{-}9)$$

$$L_1 = \frac{R[RC\omega_c(A_0^2 + 2A_0 - 2) + 2A_0]}{\omega_c(A_0^2 + 2A_0 + 2)} \quad (4\text{-}10)$$

$$R_2 = \frac{R[RC\omega_c(A_0^2 + 2A_0 - 2) + 2A_0]}{2[RC\omega_c(A_0 + 1) + 2]} \quad (4\text{-}11)$$

$$C_1 = \frac{2C(A_0 + 2)}{RC\omega_c(A_0^2 + 2A_0 - 2) + 2A_0} \quad (4\text{-}12)$$

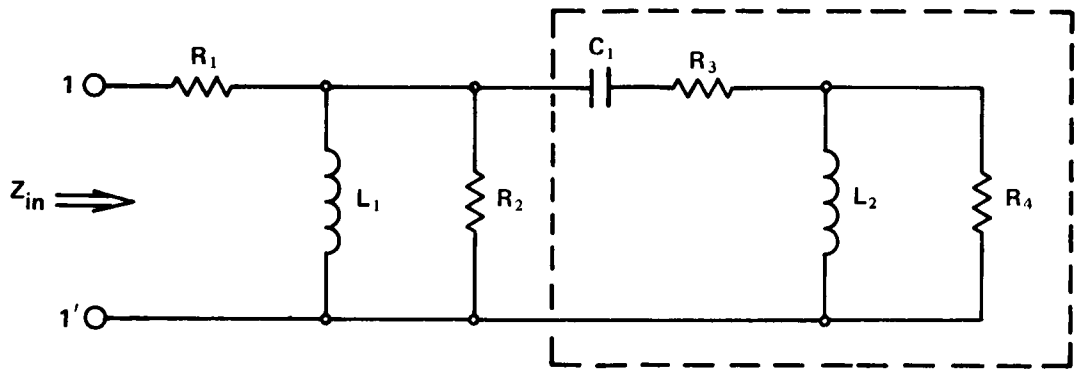


Figure 4-8. Network synthesized from Equation (4-8).

$$R_3 = \frac{RC\omega_c A_0 + 2}{2C\omega_c(A_0 + 2)} \tag{4-13}$$

$$L_2 = \frac{RC\omega_c A_0 + 4RC\omega_c - 2}{2C\omega_c{}^2(A_0 + 2)^2} \tag{4-14}$$

$$R_4 = \frac{RC\omega_c A_0 + 4RC\omega_c - 2}{2C\omega_c(A_0 + 2)} \tag{4-15}$$

Again, since $A_0 >> 1$, each of these expressions may be simplified to the following equations:

$$R_1 = \frac{2R}{A_0} \tag{4-16}$$

$$L_1 = R^2C + \frac{2R}{\omega_c A_0} \tag{4-17}$$

$$R_2 = \frac{RA_0}{2} \tag{4-18}$$

$$C_1 = \frac{2}{R\omega_c A_0} \tag{4-19}$$

$$R_3 = \frac{R}{2} \tag{4-20}$$

$$L_2 = \frac{R}{2\omega_c A_0} \tag{4-21}$$

$$R_4 = \frac{R}{2} \quad . \tag{4-22}$$

Each of Equations (4-16) through (4-22) is sufficiently accurate for most purposes except Equation (4-18) for R_2. These equations were derived under the assumption that the input resistance R_i of each operational amplifier was infinite. This assumption would be reasonable if a field effect transistor (FET) input operational amplifier was used; however, the effects of the finite input resistance R_i must be taken into consideration when a bipolar amplifier is used.

Now, if Figure 4-1 (page 70) is modified to include the effects of a finite R_i for each of the operational amplifiers, this circuit will be as shown in Figure 4-9.

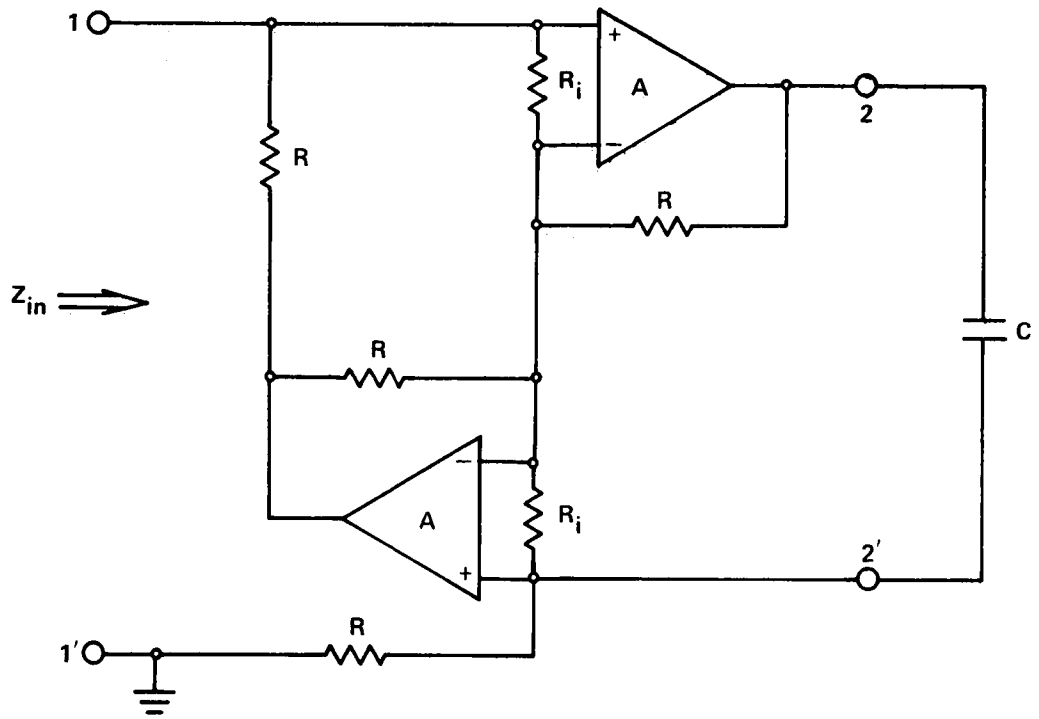


Figure 4-9. Gyrator circuit of Figure 4-1 (page 70) showing R_i.

The equation for Z_{in} including the effects of the finite resistance R_i is derived in the Appendix, but is too long and cumbersome to be shown here. However, it can be shown to be of the same form and degree as Equation (4-8). Likewise, it can be shown that R_i has a negligible effect on the component values shown in Equations (4-9) through (4-15) and in Equations (4-16) through (4-22) with the exception of R_2. The equation for R_2 including the effects of R_i is given by

$$R_2 \approx \frac{R^2 C \omega_c A_0}{2\omega_c RC + 2\frac{R}{R_i}} \quad . \tag{4-23}$$

This means that the Q-factor obtainable is directly dependent upon the operational amplifier input resistance R_i and on the gain bandwidth product $A_0\omega_c$.

The portion of the network of Figure 4-8 (page 81) enclosed within the dashed lines is attributable to the operational amplifier gain bandwidth characteristics. The resonant frequency of the C_1L_2 combination can be shown to be very closely approximated by

$$\omega_0 = \omega_c A_0 \quad , \tag{4-24}$$

which again is the operational amplifier gain bandwidth product. Observe that for frequencies much less than ω_0, the effects of L_2 become negligible and the L_2R_4 combination of Figure 4-8 may be omitted so that the remaining network is the same as Figure 3-3 (page 65).

4.6 Effects of Operational Amplifier Parameter Variations

The effect of parameter tolerance variations are examined briefly. The resistors and capacitor used in the test circuit are high quality components with a tolerance of 1%. However, the manufacturers data sheet for the CA741 operational amplifier shows a wide variation between the typical and minimum parameter values. For example the RCA data sheet [23] for the CA741 operational amplifier lists a typical gain of 200,000 compared to a minimum expected gain of 50,000. The same data sheet lists a typical R_i

of 2 MΩ to a minimum of 300 kΩ. The 3 dB frequency, f_c, may be determined from a curve to be of the order of 5 to 8 Hz.

Table 4-1 was constructed to illustrate the effect of the operational amplifier parameters on the values of components in Figure 4-8 (page 81). Equations (4-16) through (4-22) were used with the exception that Equation (4-23) was substituted for Equation (4-18). For all cases R = 10 kΩ and C = 4700 pF were used. Typical values, minimum values, and values between these were used for the operational amplifier parameter values. The table is

Table 4-1. Effect of Operational Amplifier Parameters on Components of Figure 4-8

Component	$A_0 = 50,000$ $\omega_c = 30$ $R_i = 300$ kΩ	$A_0 = 100,000$ $\omega_c = 40$ $R_i = 1$ MΩ	$A_0 = 200,000$ $\omega_c = 50$ $R_i = 2$ MΩ
R_1	0.4 Ω	0.2 Ω	0.1 Ω
L_1	0.4833 H	0.475 H	0.472 H
R_2	10.6 MΩ	93.8 MΩ	467.8 MΩ
C_1	133 pF	50 pF	20 pF
R_3	5 kΩ	5 kΩ	5 kΩ
L_2	3.28 mH	1.25 mH	0.5 mH
R_4	5 kΩ	5 kΩ	5 kΩ

intended to show that the operational amplifier parameters have a minimal effect on the value of the simulated inductance; however, the Q-factor is directly dependent upon the operational amplifier parameters. For most applications this performance is still very good; however, for certain high performance requirements, the operational amplifiers should be selected. From Table 4-1 it is apparent that the value of R_2 is directly affected by the gain-bandwidth product and the input resistance of the operational amplifier.

4.7 Gyrator Implementation in a Filter

To demonstrate the use of a capacitor loaded gyrator to simulate an inductance, the test gyrator was used in a simple narrow band parallel L-C bandpass filter network. The test filter network is shown in Figure 4-10. A buffer stage was used on the output to prevent a loading effect by the measuring instruments. Figure 4-11 is the equivalent circuit of Figure 4-10.

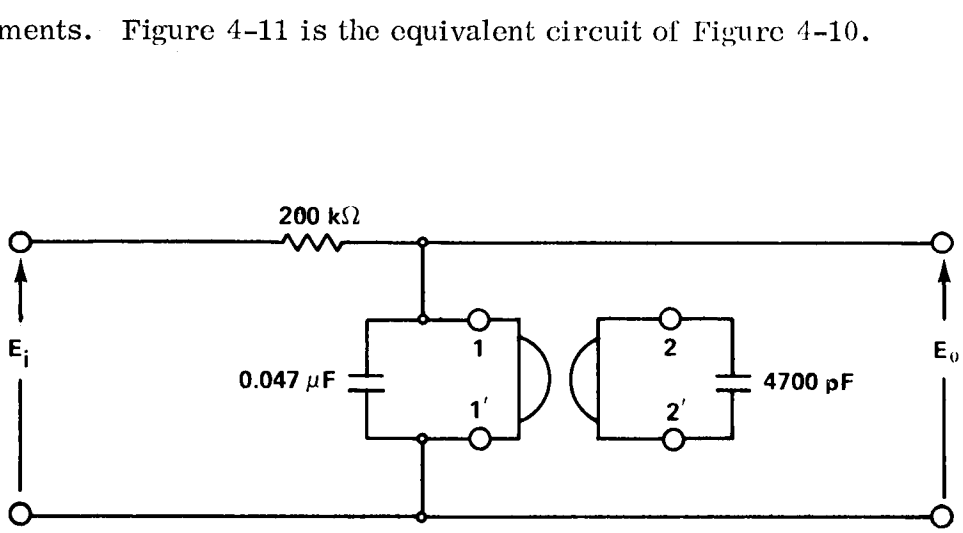


Figure 4-10. Test filter network.

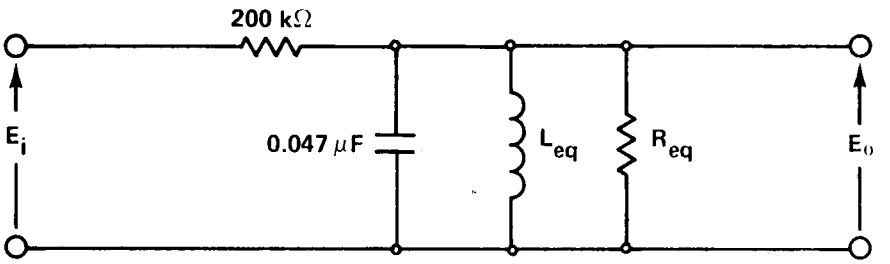


Figure 4-11. Equivalent circuit of Figure 4-10.

The experimental test data is plotted in Figures 4-12 and 4-13. Figure 4-12 shows the overall response of the filter. Figure 4-13 is an expanded scale plot of Figure 4-12 illustrating the region of the bandpass. This shows a bandpass of approximately 18 Hz with a center frequency of 1061 Hz.

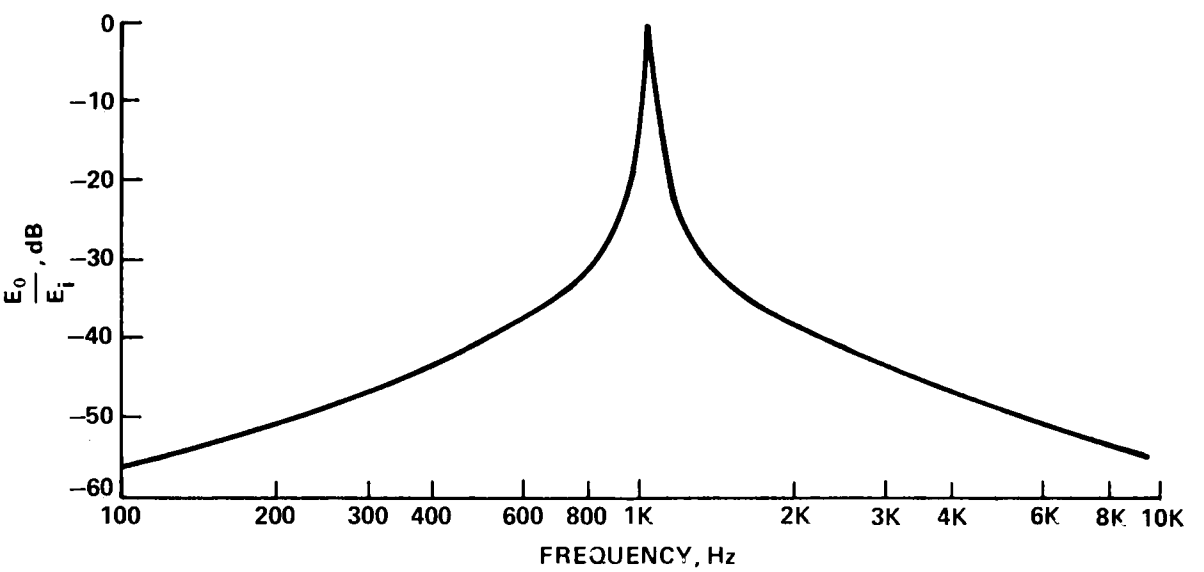


Figure 4-12. Frequency response of filter network.

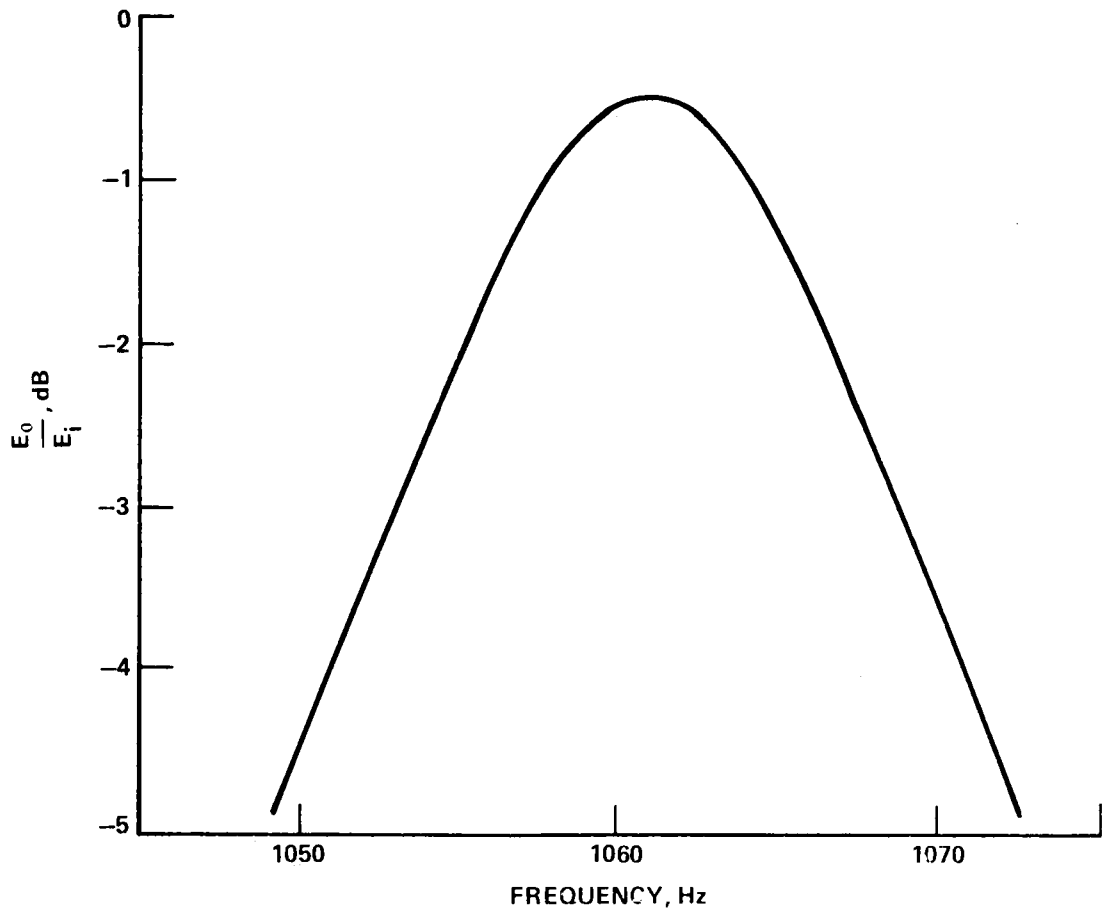


Figure 4-13. Expanded scale of Figure 4-12 bandpass.

The driving point impedance of the gyrator was used to obtain an expression for the transfer function of the filter in Figure 4-10. The typical and minimum parameters of the operational amplifier were substituted into this expression and it was solved on an HP9830A programmable calculator for the frequency response. These frequency responses are shown in Figures 4-14 and 4-15. Because of the scale of Figure 4-14, all the curves coincide.

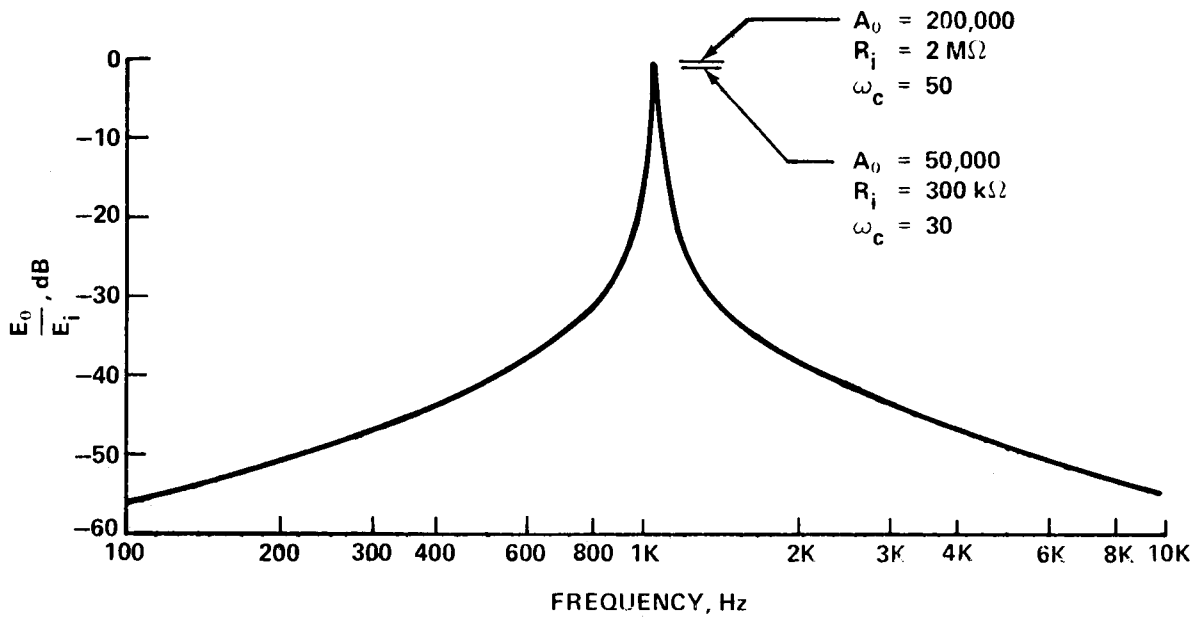


Figure 4-14. Calculated frequency response of transfer function.

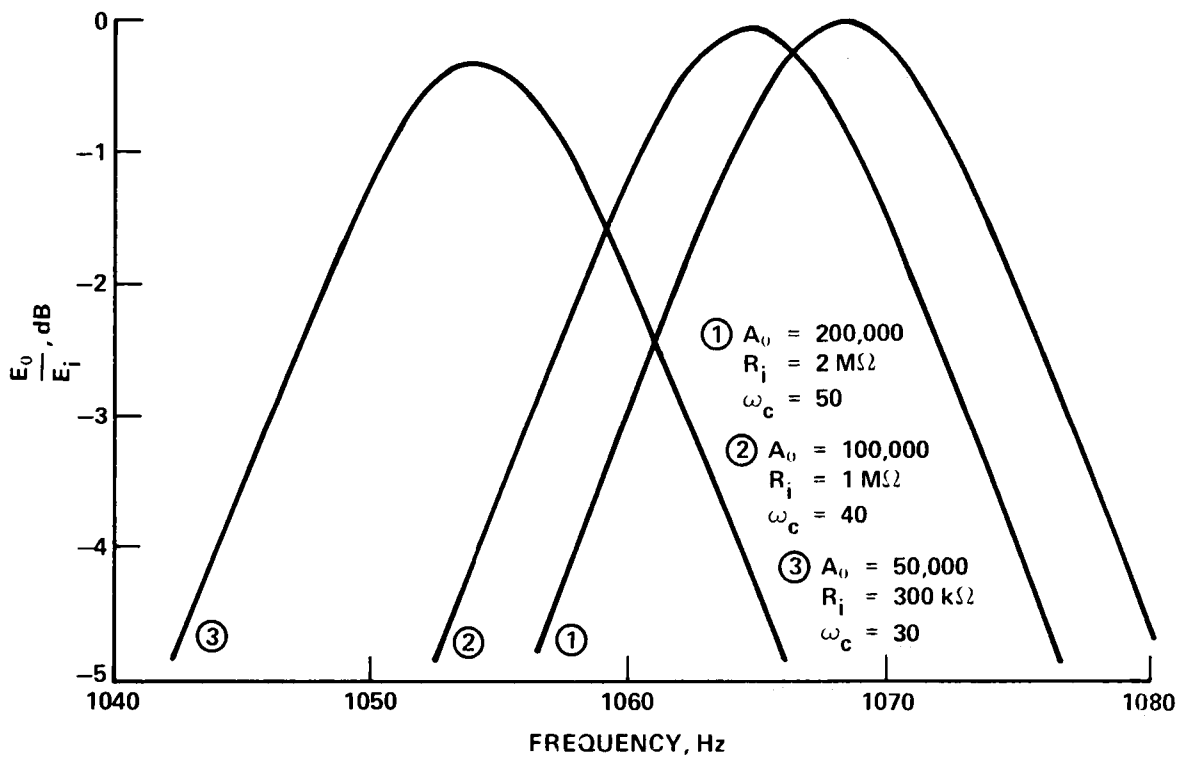


Figure 4-15. Expanded scale of calculated bandpass of Figure 4-14.

However, in Figure 4-15 which is an expanded scale plot of the bandpass of Figure 4-14, it may be observed that the effect of the operational amplifier parameters on frequency response is to shift the center frequency slightly. The shape of the curves are the same with an approximate bandwidth of 17.5 Hz. The center frequency shift could be predicted by observing the value of capacitor C_1 in Table 4-1 (page 85) with different operational amplifier parameters.

A comparison of Figures 4-12 and 4-14 shows very good agreement between the measured data and the calculated data. Likewise, a comparison of Figures 4-13 and 4-15 shows good agreement between the measured and calculated data in the bandpass. The bandwidth and curve shape are very close.

Lastly, a comparison to a theoretical filter was made. This circuit is shown in Figure 4-16. Again the frequency response was calculated on the HP9830A programmable calculator for two cases: (1) $Q = \infty$ and (2) $Q = 1000$. The results of these calculations are plotted in Figures 4-17 and 4-18. The curves in Figure 4-18 show that for $Q = 1000$, the peak amplitude is slightly less than for $Q = \infty$. Also at 3 dB down from the peak, the $Q = 1000$ curve bandwidth is greater by a small margin, as expected.

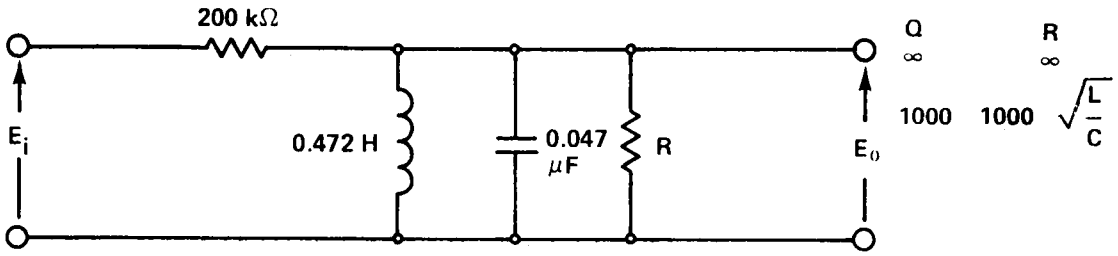


Figure 4-16. Theoretical filter.

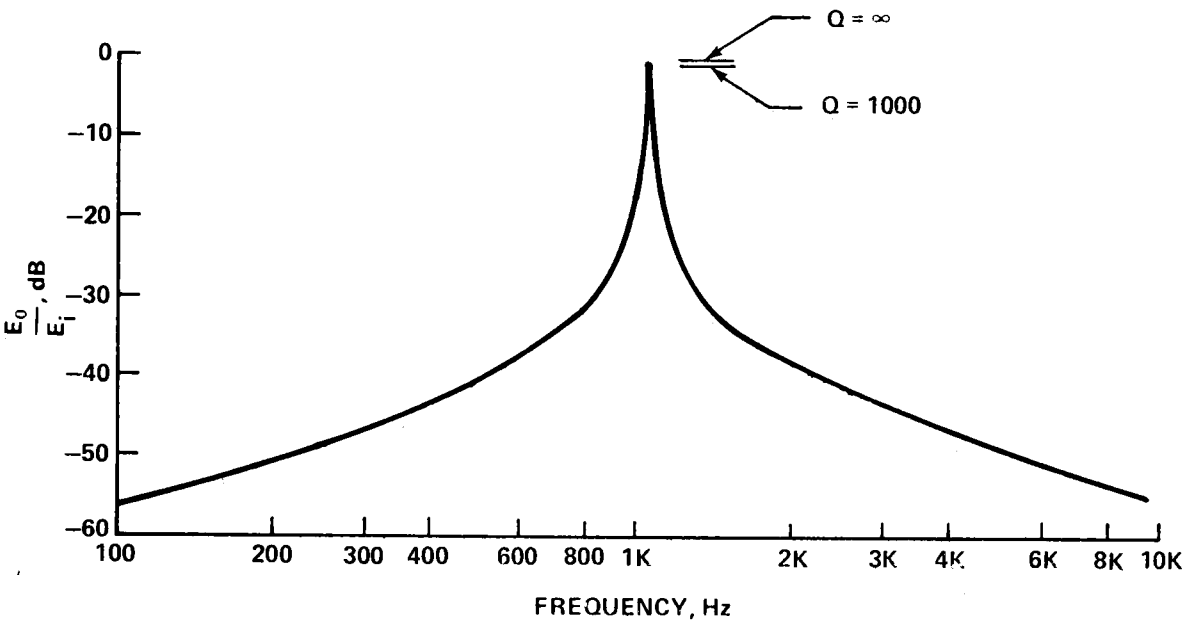


Figure 4-17. Response of theoretical LC filter.

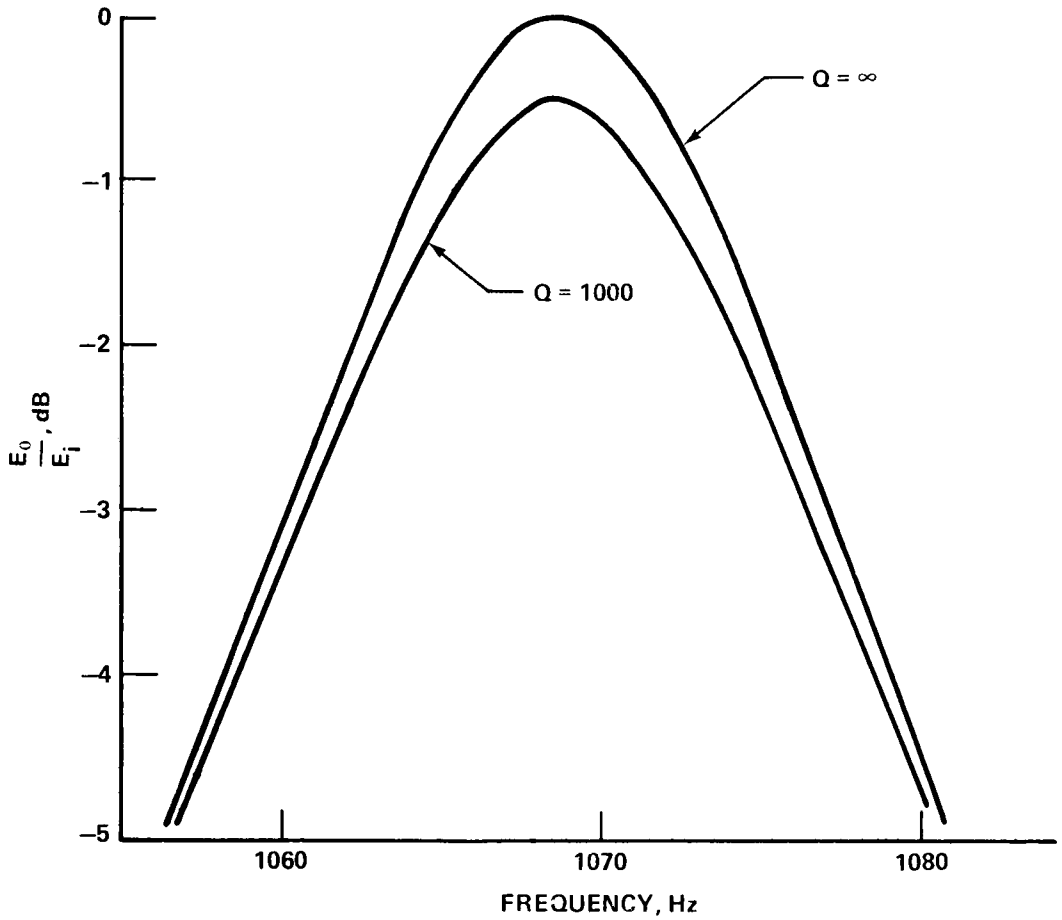


Figure 4-18. Expanded scale of bandpass of the theoretical filter.

A comparison of the curves in Figure 4-12 (page 87) with those of Figure 4-17 shows excellent agreement between the measured response and the theoretical response. Comparing Figure 4-13 (page 88) with Figure 4-18 shows very good agreement between measured and calculated results. The peak amplitude and bandwidth of the measured curve compares very well to the Q = 1000 curve. The center frequency can be made to agree by a slight tuning adjustment of the shunt capacitor.

4.8 Conclusions

Test data obtained from the experimental gyrator circuit was used to plot the Q versus frequency curves shown in part 4.3. Resistors used in the test circuit ranged from 3.16 kΩ to 100 kΩ and the load capacitors ranged from 470 pF to 10 μF. It is quite reasonable to expect that this range of resistors could be extended at least down to 1 kΩ; however, this has not been verified by testing. It seems feasible to use resistor values greater than 100 kΩ to obtain large inductors; however, a comparison of the curves indicates a trend of lower Q-factors at large resistor values.

The simulated inductance ranged from 10 mH to 100 H. This range could reasonably be extended down to 1 mH by using 1 kΩ resistors. A Q of 1000 or greater was obtained for the inductance range from 50 mH to 100 H with a frequency range from less than 10 Hz to 10 kHz. For Q-factors of a few hundred, this frequency range would possibly extend from less than 1 Hz to approximately 30 kHz. The high frequency performance of the gyrator is a function of the operational amplifier parameters.

The nonlinearity was measured to be less than 0.2% for signals of 3 V rms or less.

The equation for the input impedance of the modified Antoniou gyrator was derived in terms of the nonideal operational amplifier parameters. This equation was then used to synthesize an equivalent network that can be used to describe the frequency response of the gyrator.

Each of the circuit elements of the equivalent network was defined in terms of the gyrator circuit components, and the effects of the operational amplifier parameters upon each element were analyzed and compared in tabular form. From this the simulated inductance L was found to be very nearly equal to R^2C, where R and C are the resistance and capacitance values respectively used in the gyrator circuit, and L was found to be only minutely affected by the operational amplifier parameters. Experimental results show excellent agreement with the calculated inductance values.

The use of the gyrator in a narrow bandpass filter was demonstrated also. The experimental results were first compared to the analytical results obtained from using the equation for the input impedance of the gyrator, and the experimental results were compared to the response of a theoretical filter. Excellent agreement of results was obtained in both cases.

CHAPTER 5

SUMMARY

The purpose of this research on operational amplifier gyrators was to evaluate the performance of the gyrators using integrated operational amplifiers and to select the one gyrator with optimum performance for further analysis and evaluation and then to demonstrate its use in a filter network.

Chapter 1 introduces the gyrator and briefly describes the properties of a gyrator and their effect on the Q-factor.

In Chapter 2, a survey of the literature was performed to investigate the work performed thus far on gyrators utilizing operational amplifiers. The original work on each gyrator circuit was summarized.

In Chapter 3, each of the circuits listed in Chapter 2 were constructed and tested. The test results of each gyrator were summarized and compared on the basis of stability, Q-factor, and bandwidth. From this comparison the modified Antoniou circuit was selected for further testing.

In Chapter 4, the modified Antoniou gyrator was thoroughly tested and analyzed. This gyrator circuit was constructed using CA741 integrated operational amplifiers as shown in Figure 4-1 (page 70), and the experimental test results were used to develop the Q versus frequency curves. An

expression for the driving point impedance was developed and synthesized as an equivalent circuit model. The use of a gyrator in a filter network was demonstrated and shown to be in excellent agreement with the theoretically predicted results.

It is important to point out that when the quantities $R_1 = R_2 = R$ and $A_1 = A_2 = A$ were substituted into Equation (2-27) for the other modified Antoniou gyrator shown in Figure 2-26 (page 40), these equations also reduced to give Equation (4-1). This shows that the mathematical models of both gyrators are the same if the operational amplifier input resistance R_i is neglected. The experimental test results obtained in Chapter 3 showed the two circuits to be very similar with the gyrator circuit of Figure 2-27 (page 41) having only a moderately superior performance. This means that the difference in the experimental results was caused by differences in the operational amplifier parameters. Also all the equations developed up to and including Equation (4-22) in Chapter 4 apply to both modified Antoniou gyrators.

The usefulness of this gyrator circuit is limited to simulating only grounded inductors. None of the operational amplifier gyrator circuits found during the course of literature search was suitable for simulating a floating inductor. Only Deboo's [15] three-terminal operational amplifier gyrator circuit shown in Figure 2-14 (page 29) was originally developed to realize a

floating inductor. Two circuits that were tested were derived from Deboo' s circuit and had severe stability problems; therefore, no further effort was expended on this circuit. Riordan [16] also proposed a method of simulating a floating inductor that involved using two of his circuits interconnected. One method of simulating a floating inductor that is used quite extensively with all transistor gyrator circuits and involves two gyrators connected in series is shown in Figure 5-1. This method requires a gyrator circuit with one side of port two connected to common. Possibly the modified Brugler or Deboo circuits could be used here to simulate a floating inductor if optimum performance is not a requirement. Another method proposed involves the use of a floating power supply for each floating inductor and is therefore considered uneconomical except in the simplest cases. An operational amplifier gyrator to simulate a floating inductor with optimum properties could appropriately be used as the subject of another study.

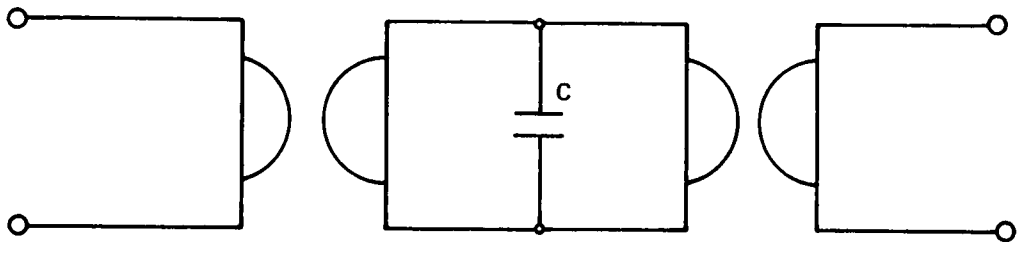


Figure 5-1. One method of realizing a floating inductor.

The effect of the nonideal operational amplifier parameters on the gyrator performance was considered also. The circuit model shown in Figure 4-8 (page 81) is used for this discussion. The effect of the finite input resistance R_i of the operational amplifier was considered first. From Equation (4-23) resistor R_2 is directly proportional to R_i, and since R_2 shunts the simulated inductance L_1, the Q-factor is directly affected by R_i. Therefore, the use of an FET input operational amplifier with its inherently high R_i would result in an optimum Q-inductor.

The effect of the gain-bandwidth product was considered next. This product appears in each of Equations (4-17), (4-19), and (4-21). L_1 in Equation (4-17) represents the simulated inductance where the theoretical value is increased by a term inversely proportional to this product. Also, both the parasitic elements C_1 and L_2, given in Equations (4-19) and (4-21) respectively, are inversely proportional to this product. The high frequency behavior of the gyrator is primarily determined by these two elements. The self-resonant frequency of the simulated inductance is determined by the L_1C_1 combination and, therefore, is directly proportional to this product.

LIST OF REFERENCES

LIST OF REFERENCES

1. Tellegen, B. D. H., "The Gyrator: A New Network Element," Phillips Research Report, Vol. 3, No. 2, pp. 81-101, April 1948.

2. Mitra, S. K., Analysis and Synthesis of Linear Active Networks, Wiley 1969, p. 45.

3. Mitra, S. K., Analysis and Synthesis of Linear Active Networks, Wiley 1969, pp. 46-51.

4. Mitra, S. K., Analysis and Synthesis of Linear Active Networks, Wiley 1969, pp. 404-405.

5. Van Valkenburg, M. E., Introduction to Modern Network Synthesis, Wiley 1960, pp. 140-188.

6. Yengst, W. C., Procedures of Modern Network Synthesis, MacMillian 1964, p. 344.

7. Su, K. L., Active Network Synthesis, McGraw-Hill, 1965, p. 208.

8. Morse, A. S. and Huelsman, L. P., "A Gyrator Realization Using Operational Amplifiers," IEEE Transactions on Circuit Theory, Vol. CT-11, No. 2, pp. 277-278, June 1964.

9. Huelsman, L. P., Theory and Design of Active RC Circuits, McGraw-Hill 1968, pp. 176-177.

10. Brugler, J. S., "RC Synthesis with Differential-Input Operational Amplifiers," in "Papers on Integrated Circuit Synthesis," compiled by Newcomb, R. W. and Rao, T. N., Stanford University, Palo Alto, California, Technical Report 6560-4, pp. 116-130, June 1966.

11. Antoniou, A., "3-Terminal Gyrator Circuits Using Operational Amplifiers," Electronics Letters, Vol. 4, No. 26, pp. 591-592, December 1968.

12. Hawley, I. H., "A Gyrator Realization Using Operational Amplifiers," in "Papers on Integrated Circuit Synthesis," compiled by Newcomb, R. W. and Rao, T. N., Stanford University, Palo Alto, California, Technical Report 6560-4, pp. 61-92, June 1966.

13. Sheingold, D. H., "Constant Current Source for Analog Computer Use," IEEE Transactions on Electronic Computers, EC-12, p. 324, June 1963.

14. Prescott, A. J., "Loss-Compensated Active Gyrator Using Differential-Input Operational Amplifiers," Electronics Letters, Vol. 2, No. 7, pp. 283-284, July 1966.

15. Deboo, G. J., "Application of a Gyrator-Type Circuit to Realize Ungrounded Inductors," IEEE Transactions on Circuit Theory, Vol. CT-14, No. 1, pp. 101-102, March 1967.

16. Riordan, R. H. S., "Simulated Inductors Using Differential Amplifiers," Electronics Letters, Vol. 3, No. 2, pp. 50-51, February 1967.

17. Antoniou, A., "Stability Properties of Some Gyrator Circuits," Electronics Letters, Vol. 4, No. 23, pp. 510-512, November 1968.

18. Llewellyn, F. B., "Some Fundamental Properties of Transmission Systems," Procedure Inst. Radio Engrs., Vol. 40, pp. 271-283, 1952.

19. Antoniou, A., "Gyrators Using Operational Amplifiers," Electronics Letters, Vol. 3, No. 8, pp. 350-352, August 1967.

20. Antoniou, A., "New Gyrator Circuits Obtained by Using Nullors," Electronics Letters, Vol. 4, No. 5, pp. 87-88, March 1968.

21. May, J. T., Jr., "A Study of the Non-Ideal Properties of the Grounded Capacitor-Loaded Gyrator," Ph. D. Dissertation, University of Tennessee, pp. 108-115, June 1960.

22. Gary, Paul A., "An Integrable Direct-Coupled Gyrator," in "Papers on Integrated Circuit Synthesis," compiled by Newcomb, R. W. and Rao, T. N., Stanford University, Palo Alto, California, Technical Report 6560-4, pp. 52-57, June 1966.

23. Linear Integrated Operational Amplifier CA741, RCA, Somerville, New Jersey, 1974.

APPENDIXES

APPENDIX A

DERIVATION OF THE GYRATOR INPUT IMPEDANCE

FOR FIGURE 4-9 (PAGE 83)

The gyrator input impedance Z_{in} is derived for an operational amplifier with finite input resistance R_i. Figure 4-9 is repreated here as Figure A-1 with the nodes numbered as shown.

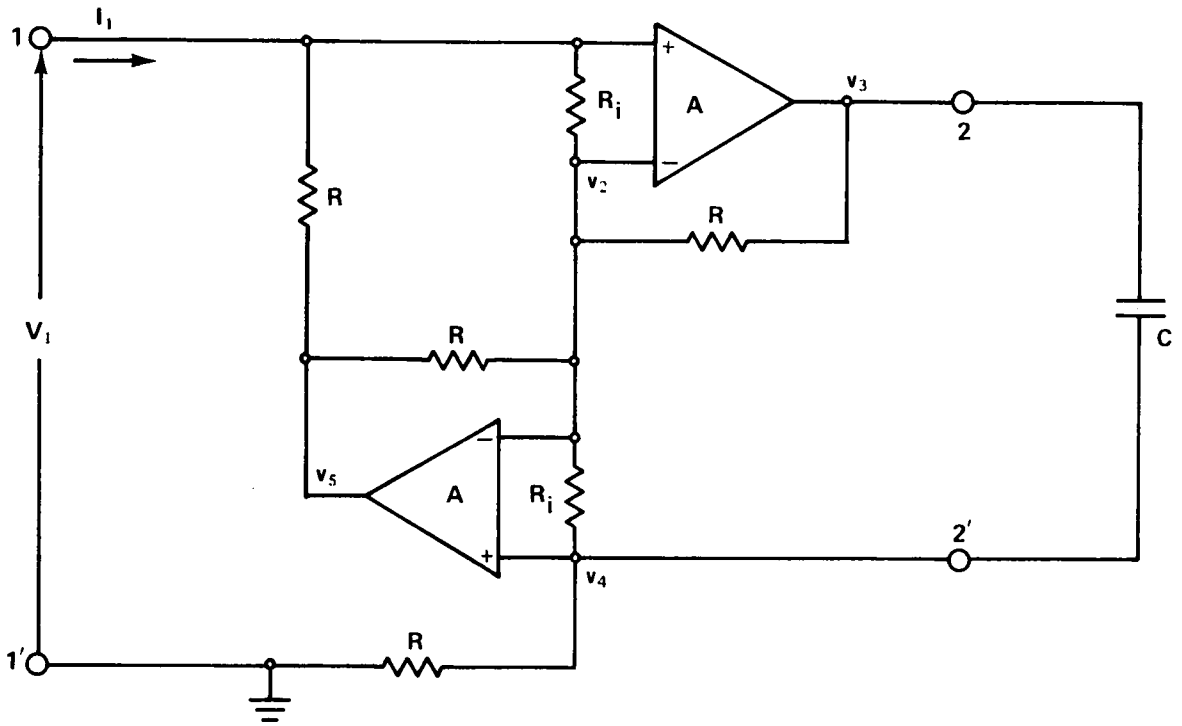


Figure A-1. Gyrator circuit of Figure 4-9 with nodes numbered.

From Figure A-1, the node equations are written as follows:

$$I_1 = \frac{V_1 - v_5}{R} + \frac{V_1 - v_2}{R_i} \tag{A-1}$$

$$\frac{V_1 - v_2}{R_i} + \frac{v_3 - v_2}{R} = \frac{v_2 - v_4}{R_i} + \frac{v_2 - v_5}{R} \tag{A-2}$$

$$\frac{v_2 - v_4}{R_i} + sC(v_3 - v_4) = \frac{v_4}{R} \tag{A-3}$$

$$v_3 = A(V_1 - v_2) \tag{A-4}$$

$$v_5 = A(v_4 - v_2) \tag{A-5}$$

Solving these simultaneous equations for the input impedance Z_{in} where

$$Z_{in} = \frac{V_1}{I_1} \tag{A-6}$$

gives the following relation:

$$Z_{in} = \frac{sR^2C\left[(A^2+2A+2) + \frac{R}{R_i}(A+2)\right] + R\left[2(A+1) + \frac{R}{R_i}(A+4) + \frac{R^2}{R_i^2}\right]}{sRC\left[2(A+1) + \frac{R}{R_i}(3A+4) + \frac{R^2}{R_i^2}\right] + \left[(A^2+2A+2) + 3\frac{R}{R_i}(A+2) + 4\frac{R^2}{R_i^2}\right]} \tag{A-7}$$

Substituting

$$A = \frac{A_0\omega_c}{s + \omega_c} = \frac{K}{s + \omega_c} \quad , \tag{A-8}$$

where K is defined as the gain-bandwidth product, into Equation (A-7) gives the following:

$$Z_{in} = \frac{N_3s^3 + N_2s^2 + N_1s + N_0}{D_3s^3 + D_2s^2 + D_1s + D_0} \quad , \tag{A-9}$$

where

$$N_3 = 2R^2C\left(1 + \frac{R}{R_i}\right) \tag{A-10}$$

$$N_2 = \left(2KR^2C + 4\omega_c R^2C + K\frac{R^3}{R_i}C + 4\omega_c\frac{R^3}{R_i}C + 2R + 4\frac{R^2}{R_i} + \frac{R^3}{R_i^2}\right) \tag{A-11}$$

$$N_1 = \left(K^2R^2C + 2K\omega_c R^2C + 2\omega_c{}^2R^2C + 2\omega_c{}^2\frac{R^3}{R_i}C + K\omega_c\frac{R^3}{R_i}C\right.$$

$$\left. + 2KR + 4\omega_c R + K\frac{R^2}{R_i} + 8\omega_c\frac{R^2}{R_i} + 2\omega_c\frac{R^3}{R_i^2}\right) \tag{A-12}$$

$$N_0 = \left(2K\omega_c R + 2\omega_c{}^2R + K\omega_c\frac{R^2}{R_i} + 4\omega_c{}^2\frac{R^2}{R_i} + \omega_c{}^2\frac{R^3}{R_i^2}\right) \tag{A-13}$$

$$D_3 = RC\left(2 + 4\frac{R}{R_i} + \frac{R^2}{R_i^2}\right) \tag{A-14}$$

$$D_2 = \left(2KRC + 4\omega_c RC + 3K\frac{R^2}{R_i}C + 8\omega_c\frac{R^2}{R_i}C + 6\frac{R}{R_i} + 4\frac{R^2}{R_i^2} + 2\omega_c\frac{R^3}{R_i^2}C + 2\right) \tag{A-15}$$

$$D_1 = \left(2K\omega_c RC + 2\omega_c^2 RC + 3K\omega_c\frac{R^2}{R_i}C + 4\omega_c^2\frac{R^2}{R_i}C + 3K\frac{R}{R_i} + 12\omega_c\frac{R}{R_i} + 8\omega_c\frac{R^2}{R_i^2} + \omega_c^2\frac{R^3}{R_i^2}C + 2K + 4\omega_c\right) \tag{A-16}$$

$$D_0 = \left(6\omega_c^2\frac{R}{R_i} + 3K\omega_c\frac{R}{R_i} + 4\omega_c^2\frac{R^2}{R_i^2} + K^2 + 2K\omega_c + 2\omega_c^2\right) . \tag{A-17}$$

Equations (A-9) through (A-17) give the input impedance Z_{in} of the gyrator in terms of all the operational amplifier parameters.

APPENDIX B

IMPORTANT DESIGN EQUATIONS

The applicable design equations of Chapter 4 are grouped together here to provide a ready reference in using the operational amplifier gyrator.

The network of Figure 4-8 (page 81) can be simplified to provide a useful model of the gyrator up to its self-resonant frequency (SRF). This is shown in Figure B-1.

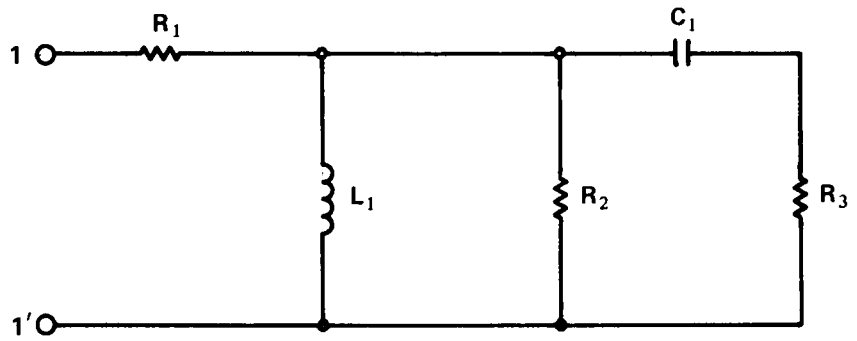


Figure B-1. Equivalent circuit model of a gyrator useful up to the self-resonant frequency.

A good approximation of the SRF is given by the relation

$$SRF \approx \frac{1}{2\pi\sqrt{L_1C_1}} \quad . \tag{B-1}$$

Each element of Figure B-1 can be determined by the following relations.

$$R_1 = \frac{2R}{A_0} \tag{B-2}$$

$$L_1 = R^2C + \frac{2R}{\omega_c A_0} \tag{B-3}$$

$$R_2 \approx \frac{R R_i C \omega_c A_0}{2(\omega_c R_i C + 1)} \tag{B-4}$$

$$C_1 = \frac{2}{R\omega_c A_0} \tag{B-5}$$

$$R_3 = \frac{R}{2} \tag{B-6}$$

where A_0, ω_c, and R_i are operational amplifier parameters defined as follows:

A_0 — open loop gain

ω_c — break frequency of the open loop gain

R_i — input resistance.

Values of R and C are obtained from Figure 4-1 (page 70) which is repeated here as Figure B-2 for convenience.

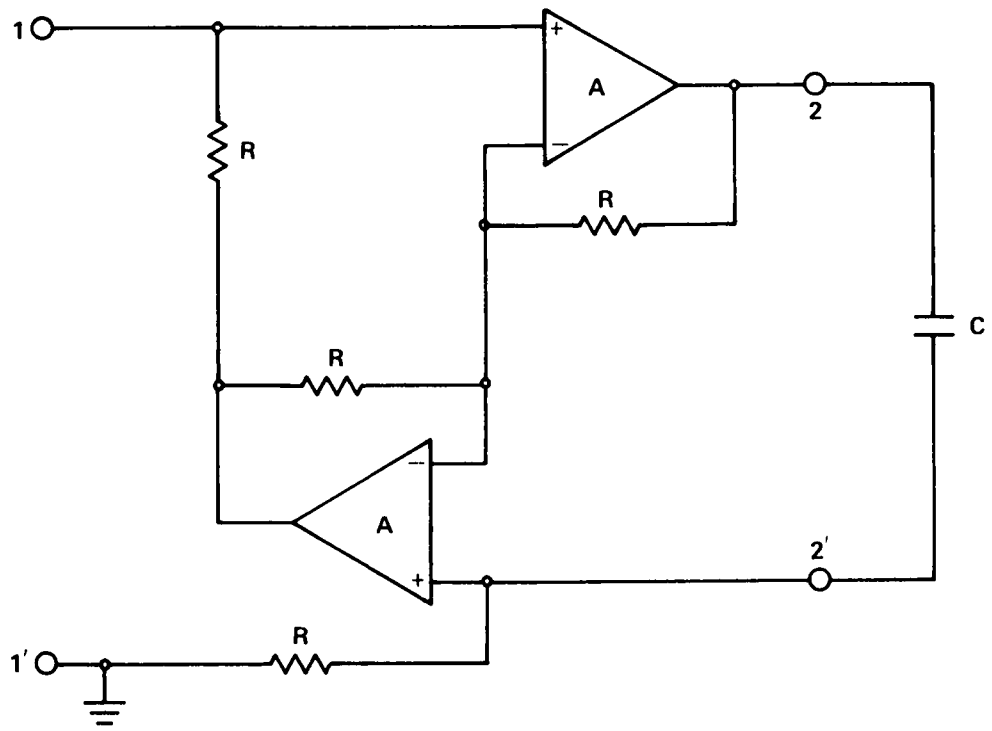


Figure B-2. Antoniou gyrator circuit.

VITA

William C. Sutherland was born in Columbia, Tennessee, in 1935. He attended the elementary schools there and graduated from Central High School in 1954. He enrolled in Tennessee Polytechnic Institute the following September and graduated with a B.S. degree in Electrical Engineering in December, 1958.

Immediately after graduation, he was employed by NASA's Langley Research Center in Hampton, Virginia. Later he transferred to NASA's Marshall Space Flight Center in Huntsville, Alabama, where he is currently employed.

He entered the Graduate School at The University of Tennessee in Knoxville in September, 1970, and received the M.S. degree in Electrical Engineering in March, 1976.

He is married to the former Dorothy Jewell Goodwin of Williamsport, Tennessee. Their three children are Billy and twins Dennis and Denise.